Faculty of Science and Engineering

School of Molecular and Life Sciences

Synthesis, Growth Mechanism and Optical Properties of Colloidal Wurtzite ZTe (Z=Zn, Cd) Nanoplatelets

Fei Wang

This thesis is presented for the degree of

Doctor of Philosophy

of

Curtin University

October 2019

Declaration

To the best of my knowledge and belief this thesis contains no material previously published by any other person except where due acknowledgement has been made.

This thesis contains no material which has been accepted for the award of any other degree or diploma in any university.

Signature:

Date: 20/10/2019

Abstract

This study explores the colloidal synthesis, growth mechanism and optical properties of colloidal wurtzite ZTe (Z=Zn, Cd) nanoplatelets.

Chapter 1 introduces the necessary research background of this study. The definitions of colloidal semiconductor nanocrystals (CSNCs) and magic-sized nanoclusters (MSNCs), the brief history of developing the colloidal synthetic methods for semiconductor nanocrystals, surface chemistry of CSNCs, photophysical properties of CSNCs, the previous investigations on two-dimensional CSNCs were given in the following subsections of Chapter 1. The thesis organization section in Chapter 1 explains the structure of this thesis.

In chapter 2, the material characterization techniques and analysis methods such as spectroscopy techniques and density functional theory calculations employed in this study were explained.

Chapter 3 reports the colloidal synthesis, growth mechanism and optical properties of colloidal wurtzite ZnTe nanoplatelets. In this work, we successfully synthesized 2D wurtzite ZnTe NPLs with a thickness of about 1.5 nm by using polytellurides as tellurium precursor. Mechanistic studies, both experimentally and theoretically, reveal that the step-wise transition of metastable ZnTe F323 MSNCs produces metastable ZnTe F398 MSNCs that then form wurtzite ZnTe NPLs via oriented attachment along [100] and [002] directions.

Chapter 4 reports the colloidal synthesis, growth mechanism and optical properties of colloidal wurtzite CdTe nanoplatelets. In this work, we investigated the shape-controllable synthesis of 2D wurtzite CdTe nanoplatelets by simply tuning Te precursor reactivity. We have successfully prepared ribbon-, shield- and bullet-like NPLs from a step-wise conversion of CdTe MSNCs by using Te_3^{2-}, Te_2^{2-} and Te^{2-} polytellurides as tellurium precursor, respectively. X-ray photoelectron spectroscopy and Fourier-transform infrared spectroscopy techniques were used to investigate the surface chemical environment and composition of as-prepared CdTe NPLs.

In Chapter 5, the conclusions of this thesis were summarized and outlook was given for following research project.

Acknowledgements

First of all, I would like to sincerely thank my kind supervisors Dr. Guohua Jia and Prof. Mark Buntine for their endless support and continuous guidance for my PhD study at Curtin University. Dr. Guohua Jia taught me a lot such as how to use the fumehood and set up the Schlenk line. I had regular meetings and constructive discussions with him, and good suggestions from him when I was not sure what to do next. He showed me how to select a good and meaningful research topic and narrow down the research aims. Also, he spent lots of time and efforts to revise the paper manuscripts and gave very insightful feedbacks to me. In addition, we had wonderful time at the exciting group outings to the Swan Valley and the Tomato Lake Park.

Secondly, I express my sincere thanks to Assoc. Prof. Martin Saunders and Dr. Alexandra Suvorova from Centre for Microscopy, Characterisation and Analysis at The University of Western Australia for their continuous technical help in use JEOL and Titan transmission electron microscopy. I appreciate Peter Chapman for his patient technical support with Raman spectrometer, differential thermal analysis, infrared spectrometer and IT service. His humors also made me laugh and brought me a lot of happiness. During the PhD study, I had very good friendship with Chao Shen, Wei Hu and Dechao Chen. We had many walks along the beautiful and quiet Canning River as well as the fantastic beaches in Perth, and dined out to relax and refresh up. In addition, I would like to thank the other group members Shaghraf Javid, Wei Chen and Yingping Pang. We spent a lot of good time together and discuss our dreams and future plans. Best luck to your future!

Thirdly, I feel very grateful to Curtin University and China Scholarship Council, who provide me the joint PhD scholarship to cover the tuition and living expenses. I want to thank the Graduate Research School to fund me the conference travel at the 6th Nano Today conference in Lisbon, Portugal.

Last but not least important, I would like to greatly appreciate my family for their continuous love, support and encouragement during my PhD study as well as those who ever helped me.

Symbols and Abbreviations

CSNCs	colloidal semiconductor nanocrystals
QDs	quantum dots
SDs	spherical dots
NRs	nanorods
NPLs	nanoplatelets
MSNCs	magic-sized nanoclusters
TOP	trioctylphosphine
TOPO	trioctylphosphine oxide
PL	photoluminescence
Cd-TDPA	cadmium tetradecylphosphonic acid salt
$CdSt_2$	cadmium sterate
Se-TPP	selenium-triphenylphosphite
Se-DPP	selenium-diphenylpropyl phosphine
Se-TBP	selenium-tributylphosphine
Se-TOP	selenium-trioctylphosphine
ODE	1-octadecene
0D	zero-dimensional
1D	one-dimensional
2D	two-dimensional
WZ	wurtzite
ZB	zinc-blende
RS	rock-salt
CBC	the covalent bond classification
$R\text{-}NH_2$	primary amines
R_3P	trialkylphosphines
DDA	dodecylamine
DOS	density of electronic states

E	energy
OA	oriented attachment
UV-vis	ultra-violet-visible
IR	infrared
NMR	nuclear magnetic resonance
FTIR	Fourier transform infrared
TEM	transmission electron microscopy
HRTEM	high-resolution TEM
FFT	fast Fourier transform
STEM	scanning transmission electron microscopy
HAADF-STEM	high angle annular dark field-STEM
STEM-EDX	STEM-energy-dispersive X-ray spectroscopy
XRD	X-ray diffraction
SAED	selected area electron diffraction
def2-SVP	def2-Split valence polarization
DFT	density functional theory
VASP	Vienna *Ab Initio* Simulation Package
PAW	projector-augmented wave
PBE	Perdew-Burke-Ernzerhof
B3LYP	Becke, 3-parameter, Lee–Yang–Parr
XC	exchange-correlation
LDA	local-density approximation
GGA	generalized gradient approximations
LSDA	local spin density approximation
UHF	unrestricted Hartree–Fock
HF	Hartree-Fock
TDDFT	time-dependent density functional theory
PCM	polarized continuum model
LEDs	light-emitting diodes

Table of Contents

Chapter 1 Introduction

1.1 Colloidal semiconductor nanocrystals and magic-sized nanoclusters

Quantum dots (QDs) are also termed as colloidal semiconductor nanocrystals (CSNCs) that contain but are not limited to spherical dots (SDs),[1-6] nanorods (NRs),[7-15] nanowires,[16-21] and nanoplatelets (NPLs).[22-29] They are fragments in nanometer scale of their corresponding bulk materials and approximately compose of 100 to 100,000 atoms as shown in Figure 1.1.[30] As an intermediate between molecules and nanocrystals, magic-sized nanoclusters (MSNCs) are well-defined structures with only tens of atoms. Currently, metal nanoclusters[31-35] and colloidal semiconductor MSNCs[36-37] have been found. Owing to the similar size scale (1-2 nm) between MSNCs and crystal nuclei,[38-41] a better understanding of MSNCs can provide more insights to the formation of crystal nuclei. Interestingly, MSNCs have been used as crystal seeds to grow larger nanocrystals and as monomer reservoirs to modulate the growth kinetics of colloidal nanocrystals.[42-43] In addition, colloidal semiconductor MSNCs may provide ideal hosts for doping of metal ions such as Co^{2+} and Mn^{2+}.[44-45] As an emerging research field, colloidal semiconductor MSNCs are attracting great attention in the community. Compared with MSNCs, CSNCs have been well investigated. Colloidal SDs, NRs and NPLs have been synthesized where their excitons are confined in three-, two- and one-dimensions in nanometer size scale, respectively.[46] To increase the photoluminescence (PL) quantum yield or modify the bandgap structure, core-shell nanocrystals were prepared and studied. In addition, hybrid metal-CSNCs heteronanostructures[47-54] and doped CSNCs[55-62] have attracted great attention because of their potential applications in photocatalysis,[47, 63-66] microelectronics[67-70] and optoelectronics.[71-78]

As the synthetic chemistry of CSNCs is extensively investigated, the precise size and shape control of CSNCs have been successfully achieved. Monodispersed CSNCs with high photoluminescence quantum yield have been produced and used to fabricate various commercialized products such as quantum dot lighting emitting diodes (QLED) TV, Qdot® probes, and CFQQD® lighting as shown in Figure 1.2.

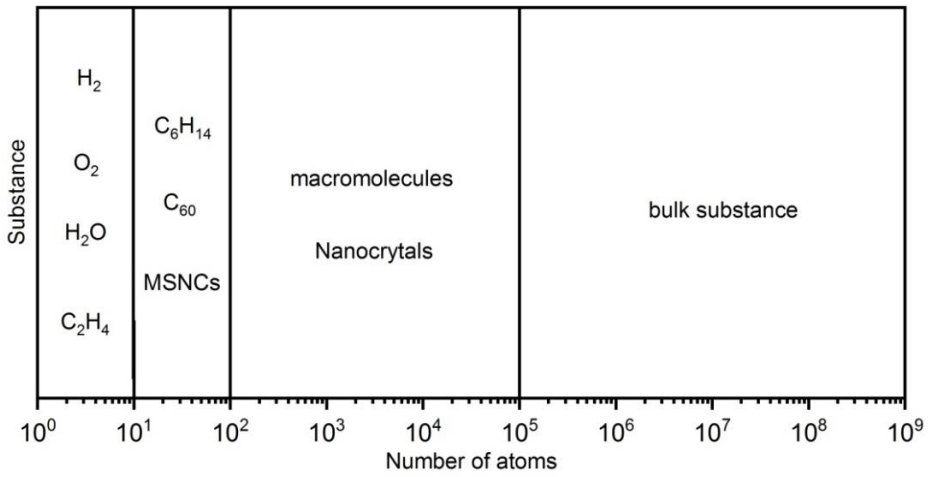

Figure 1.1 Number of atoms as a scale of representative substance.

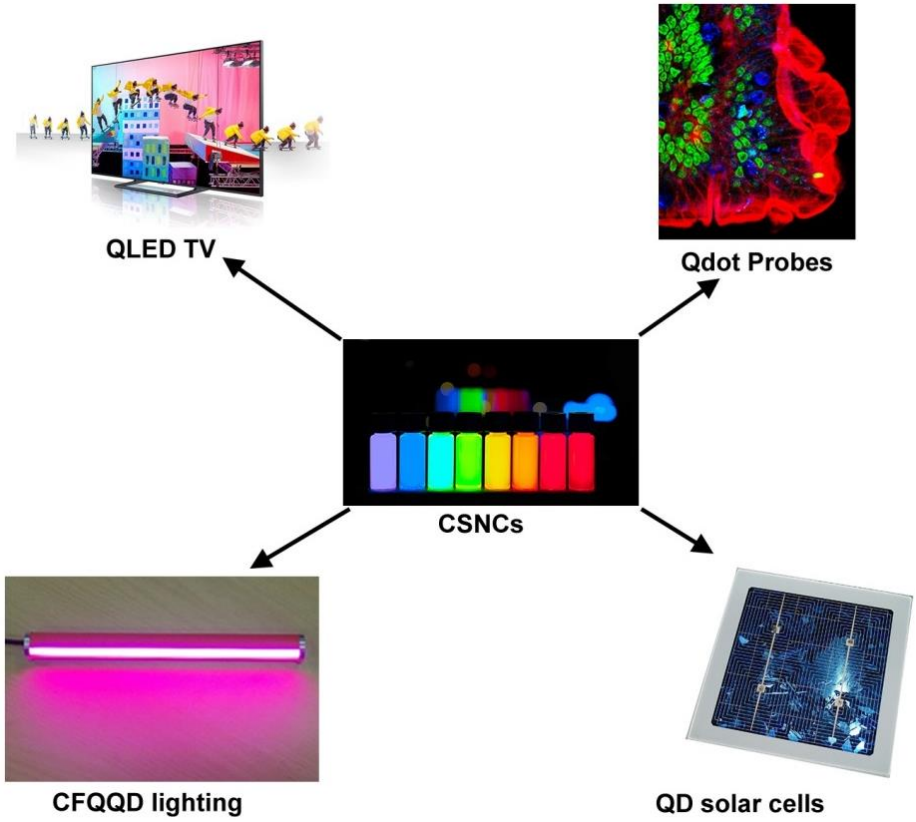

Figure 1.2 Representative commercialized products using CSNCs.

1.2 Colloidal synthesis of semiconductor nanocrystals

1.2.1 A brief history

In the early 1990s, the organometallic syntheses in coordinating solvent was firstly introduced to prepare colloidal CdSe nanocrystals with narrow size distribution by Bawendi *et al*.[79] However, this synthetic approach possesses several intrinsic disadvantages such as the extreme toxic, expensive, explosive and pyrophoric materials along with the sophisticated equipment. This synthetic method was replaced by the safe, simple, reproducible, versatile alternative route (the CdO approach) proposed by Peng *et al.* in 2001.[80] Due to the relatively simple nucleation and growth approach, the alternative route can produce nearly monodisperse nanocrystals with the PL quantum efficiency reaching close to 85%. In addition, the single-molecule precursor synthetic method has also been developed as another approach.[81] Nevertheless, this method is investigated rarely in the following years due to complicated preparation of single-molecule precursors. In 2006, Hyeon *et al.* investigated the synthesis of two-dimension CdSe nanoribbons assisted by bilayer mesophase templates comprised of $CdCl_2$-alkylamines complex.[82]

Table 1.1 Events of the colloidal synthesis of semiconductor nanocrystals

Time	Events
1993	organometallic syntheses[79]
1997	single-molecule precursor synthetic method[81]
2001	the CdO approach[80]
2006	soft colloidal template syntheses[82]

1.2.2 Precursor chemistry

The precursor chemistry of the colloidal synthesis of CSNCs plays the key role in achieving the shape and size control of produced nanocrystals as well as the processes of nucleating and crystal growth. Generally, the chemistry reactivity of the cation and anion precursors are required to be balanced to prepare monodispersed nanocrystals. Organometallic precursors such as $Zn(CH_3)_2$ and $Cd(CH_3)_2$ were first introduced as cation precursors in organometallic synthetic route.[83-87] As mentioned above, these organometallic precursors are extreme toxic and expensive along with high reactivity, which is replaced by metal oxides and fatty acid salts in the an alternative synthetic route. The precursor reactivity can

be further tuned by adding activation agent.[88-94] In addition, the selection of precursors and the molar ratio between cation and anion precursors have impacts on the PL quantum yield and the crystal phase.[95] Figure 1.3 presents the relations between factors in precursor chemistry.

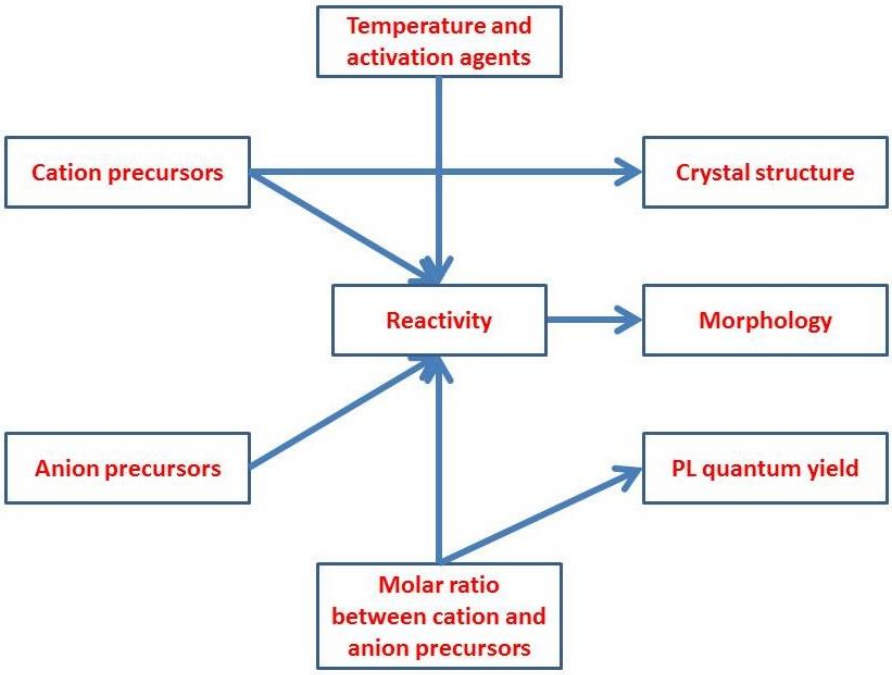

Figure 1.3 Relations between factors in precursor chemistry.

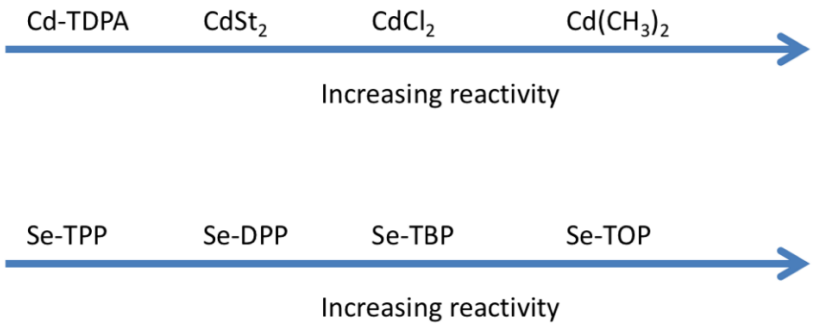

Figure 1.4 Comparison of reactivities of selected cation and anion precursors.

1.2.3 Coordinating solvents and non-coordinating solvents

Coordinating solvents such as fatty acids, alkylamines, phosphonic acids, trioctylphosphine oxide (TOPO) were firstly used in the colloidal syntheses of semiconductor nanocrystals.[40, 79, 96-99] Meanwhile, these solvents act as ligands for both the monomers and nanocrystals in the reaction. In contrast, non-coordinating solvents neither participate in the reaction nor act as ligands for the

monomers and nanocrystals. They act as the reaction medium that help to tune the reactivity of the monomers by changing the ligand concentrations in the reaction process. Furthermore, the tunable chemistry reactivity of monomers controlled by the ligand strength and concentration can provide a necessary balance between the processes of nucleation and nanocrystal growth, and thus acting as a key factor in the colloidal synthesis of high quality nanocrystals with a narrow size distribution. Long chain alkanes and alkenes are used as typical non-coordinating solvents without participating the reaction due to their liquid state at elevated temperatures and good stability to withstand the reaction temperatures of semiconductor nanocrystal syntheses. Non-coordinating organic solvents, such as 1-octadecene (ODE),[100] tetradecane,[101] tetracosane,[91] and 1-eicosene[102] have been used in the colloidal synthesis of CSNCs. Nevertheless, ODE is most widely used owing to its liquid state at the room temperature and capability in acting as a reaction medium at elevated temperatures above 300 ^{o}C. In addition, ODE is easy to be removed after syntheses because of its liquid state at the room temperature and extremely non-polar structure. ODE can also be removed from the reaction mixture by using methanol and hexanes. Nanocrystals will stay at the hexane layer while the excess unreacted monomers and ligands are staying at the methanol layer. Nanocrystals can be precipitated out with further additions of methanol or acetone in the hexane layer, which prove to be gentler for nanocrystals and more effective than directly using excess acetone to precipitate the nanocrystal from the mixture. In addition, it was found that tetradecane is an excellent solvent at a reaction temperature below 200 °C due to its availability as a high-purity reagent and lower viscosity compared with ODE at the operational temperature.[101]

Table 1.2 Selected solvents for the colloidal syntheses of CSNCs.

Solvents	Function
oleic acid	ligands
oleylamine	ligands
TOPO	ligands
ODE	reaction media

1.2.4 Nucleation and growth mechanism of CSNCs

A thorough understanding of the processes of nucleation and growth mechanism of CSNCs is vitally important for synthesizing size-, shape- and

composition-controlled CSNCs. As shown in Figure 1.5, the formation of CSNCs includes three distinct stages: pre-nucleation (stage I), nucleation (stage II) and nanocrystal growth (stage III) according to the LaMer diagram established in 1950.[103] The seminal work of LaMer studied the various stages of the formation processes of CSNCs from homogeneous reaction solution, which shows the necessity to temporally separate the nucleation and growth process for obtaining monodispersed CSNCs. Generally, the "hot-injection" method is used to achieve the temporal separation of the rapid burst of self-nucleation and the growth period. In the pre-nucleation stage, the precursors will convert to the monomers and the concentration of the monomers will exceed the concentration of the critical concentration C_c, triggering the burst of nucleation. Subsequently, the growth stage occurs as the concentration of the monomers drops down to C_c. Currently, the "hot-injection" method is the most widely employed synthetic method to synthesize monodisperse CSNCs.[104-106] Another synthetic approach is the "heat-up" method, in which the reaction mixture is increased from room temperature (RT) to an elevated reaction temperature.[107-110] Compared with the "hot-injection" method, the pre-nucleation and nucleation period in the "heat-up" method are much longer.

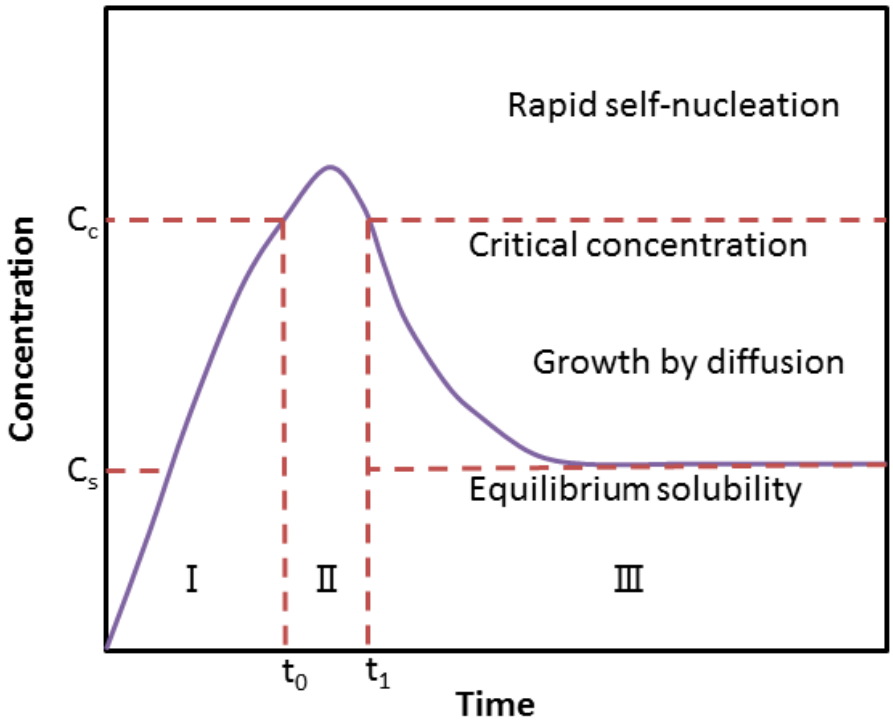

Figure 1.5 LaMer diagram: stage I, the processes of the precursor conversion and the increase of the monomer concentration above the critical concentration C_c (pre-nucleation); stage II, nucleation; stage III, the process of nanocrystals growth from the reaction solution while the monomer concentration C is in the range from C_s to C_c.

In 2009, Hyeon *et al.* reported that $CdCl_2$-alkylamines complexes can act as soft colloidal template to synthesize two-dimensional (2D) wurtzite nanosheets.[111] Cation precursors with bilayer template structure are prepared by mixing cadmium chloride with octylamine and oleylamine, then anion precursors were injected into the cation precursors. Subsequently, Buhro *et al.* found that two families of MSNCs can be synthesized using the soft colloidal template method and the MSNCs can act as nuclei to evolve into 2D nanocrystals such as quantum platelets.[38, 112]

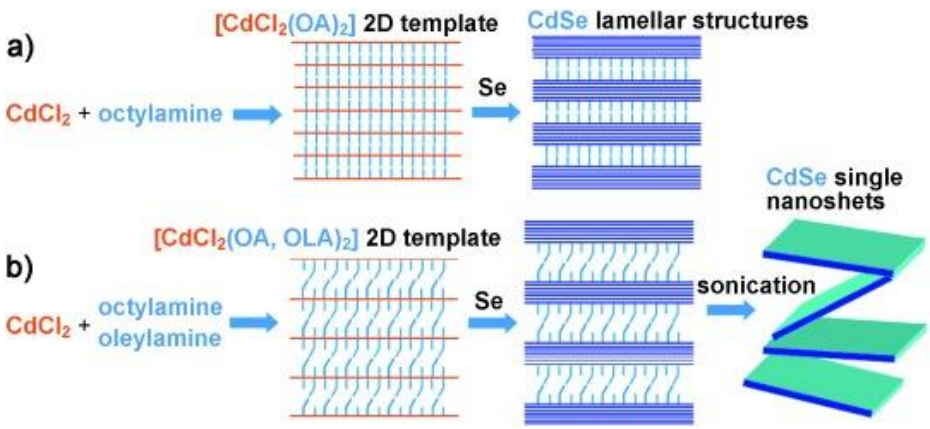

Scheme 1.1 Schematic illustration of the synthetic process of a) lamellar-structured CdSe nanosheets and b) separated single-layered CdSe nanosheets. Reprinted with permission from ref. 111. Copyright 2009 John Wiley and Sons.[111]

It was found that the injection of anion precursors at a low temperature ranging from room temperature to 100 °C is the key to form the soft colloidal template and MSNCs. Also, it was observed that the $(CdSe)_{13}$ MSNCs will evolve into $(CdSe)_{34}$ as the reaction temperature increases,[41] which verifies the thermal stability of MSNCs is closly related to temperature.

1.2.5 "Focusing of size distribution" and "Defocusing of size distribution"

The formation of colloidal monodisperse high-quality nanocrystals depends on the so-called "focusing of size distribution" principle.[86] Generally, a controllable synthesis requires a swift injection of precursor providing a quick and short nucleation formation and followed by a relatively slow and long crystal growth process. Initially, crystal nucleus with a relatively narrow size distribution will be formed, and then the slow growth stage will provide enough time to easily tune the resulting nanocrystals. At a given monomer concentration, there is a critical size vaule at equilibrium. In addition, nanocrystals with size smaller than the critical size value will possess negative growth rates whereas larger nanocrystals grow at rates that strongly depend on their size. The relatively small nanocrystals with the size larger than the critical size value will grow much faster than larger nanocrystals due to their greater chemical reactivity for either reaction-controlled

or diffusion-controlled growth processes, resulting in narrow size distribution. When the monomer concentration decreases because of the consumption of crystal growth, the critical size value will become larger than the mean size value of present nanocrystals; the size distribution will broaden as smaller nanocrystals will dissolve and then disappear but larger nanocrystals will still grow, which is called "defocusing of size ditribution" or Ostwald ripening. However, the size distribution will be refocused by additional injections of monomers at growth temperature. Thus, the focusing time and the focused size can be tuned by changing the initial monomer concentration due to the time for depletion of the monomer concentration changes.

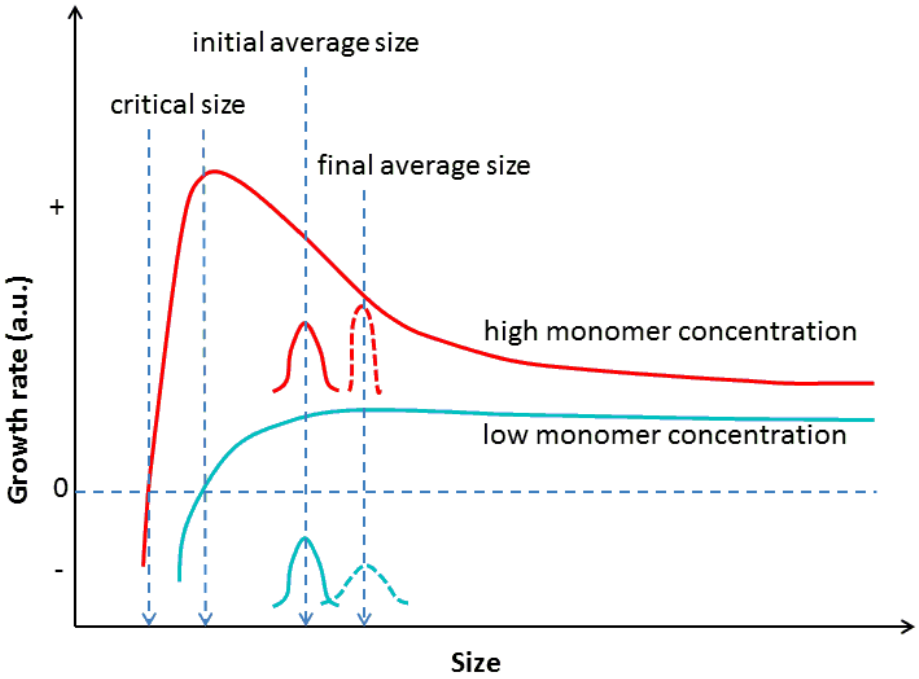

Figure 1.6 Size-distribution focusing.

1.2.6 Oriented attachment growth of nanocrystals

Oriented attachment (OA) was widely observed in different syntheses of two-dimensional (2D) and one-dimensional (1D) CSNCs such as CdSe nanoplatelets,[113] PbS nanosheets,[114] CdSe nanorods,[115] and ZnSe nanowires.[116] The oriented attachment occurs due to the high surface energy of certain crystal planes and the dipole-dipole interaction of nanocrystals along certain crystal direction. Banfield *et al.* investigated the oriented attachment and asymmetric crystal formation of nanoparticles using molecular energetic calculations.[117] It was found that the

orientation-specific long-range interatomic interactions along with surface energy reduction could predict the crystal morphology development and explain how oriented attachment produces crystals with lower symmetry than the initial material. In addition, the results show that the Coulombic interactions instead of van der Waals interactions control the oriented attachment growth of ionic nanocrystals.[117]

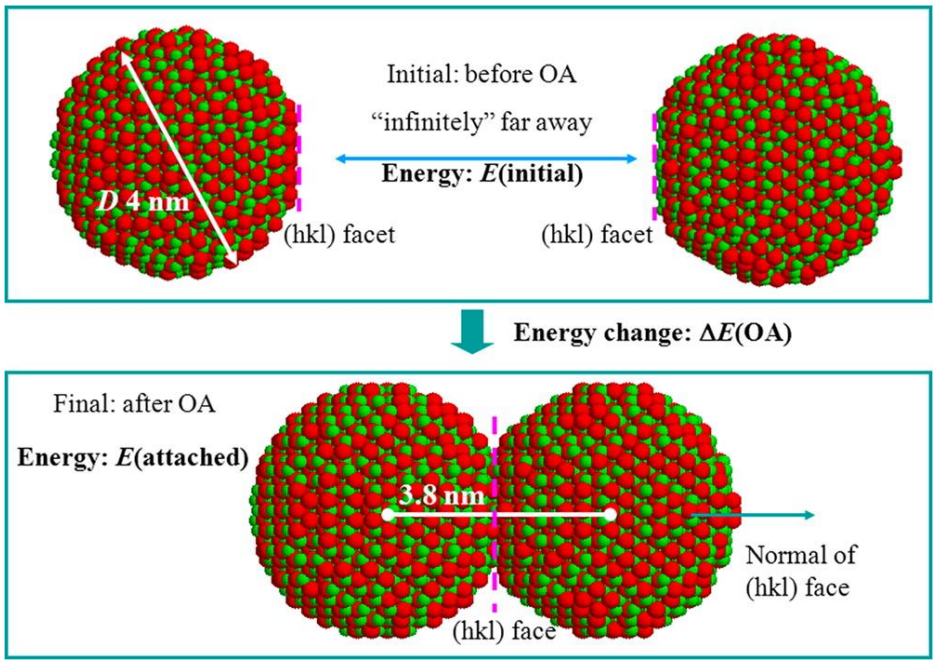

Figure 1.7 Diagram showing an oriented attachment (OA) process in which two 4 nm particles are attached on an (*hkl*) surface. Reprinted with permission from ref. 117. Copyright 2012 American Chemical Society.[117]

1.2.7 Seed-mediated growth

Seed-mediated growth was observed in colloidal syntheses of CSNCs. Both MSNCs and nanocrystals can be used as crystal seeds. Buhro *et al.* investigated the synthesis of 2D CdSe wurtzite quantum platelets converting from $(CdSe)_{34}$ MSNCs.[41] Recently, Peng *et al.* reported that CdSe nanocrystals with a diameter between 1.7 nm to 2.2 nm was used as crystal seeds to produce 2D CdSe zinc-blende nanocrystals assisted by cadmium acetate to form single-dot intermediates and followed by oriented attachment.[113] First, crystal seeds grow into single-dot intermediates via intra-particle ripening, then those single-dot intermediates become 2D crystal embryo through attachment. Next, 2D nanocrystals are formed

by oriented attachment and intra-particle ripening of 2D crystal embryo. The schematic illustration of the synthetic process is depicted in Figure 1.8.

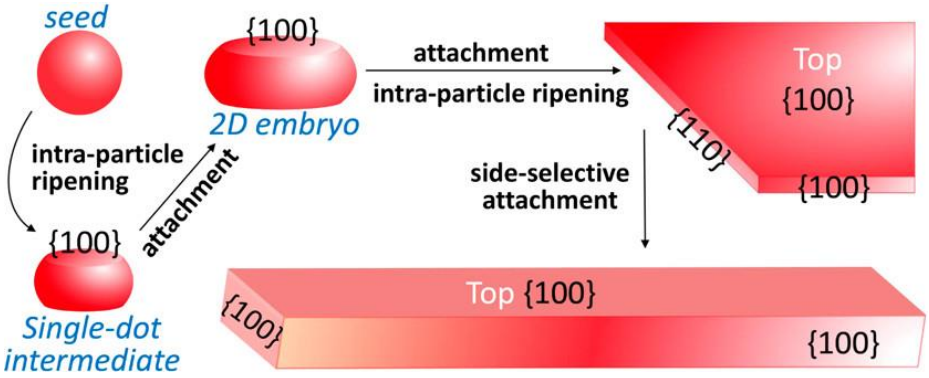

Figure 1.8 Schematic illustration of the seed-mediated growth of zinc-blende CdSe nanoplatelets. Reprinted with permission from ref. 113. Copyright 2017 American Chemical Society.[113]

1.2.8 Crystal structure of CSNCs

There are three representative types of crystal structure of CSNCs such as wurtzite (WZ), zinc-blende (ZB) and rock-salt (RS), as shown in Figure 1.9. Wurtzite structure (space group:P63mc) is also called hexagonal structure. Crystals with a wurtzite structure belong to AB covalent bond crystals with A atoms in hexagonal close packing and B atoms filled in the tetrahedral void formed by the nearest A atoms. The lattice parameters for a wurtzite structure is $a=b\neq c$ and $\alpha=\beta=90^{o}$, $\gamma=120^{o}$. Zinc-blende structure (space group:F-43m) is also termed as cubic structure. Crystals with a zinc-blende structure belong to AB covalent bond crystals with B atoms in cubic close packing and A atoms filled in the tetrahedral void formed by the nearest B atoms. The lattice parameters for a zinc-blende structure is $a=b=c$ and $\alpha=\beta=\gamma=90^{o}$. Rock-salt structure (space group:Fm3m) is commonly known as cubic structure. Crystals with a rock-salt structure belong to AB-type crystals with a face-centered cubic array of B atoms with A atoms inside the octahedral holes. The lattice parameters for a rock-salt structure is $a=b=c$ and $\alpha=\beta=\gamma=90^{o}$. For some substance, the stability of their crystal structure depends on temperature if crystal phase transition exists. The WZ ZnSe and ZnTe nanocrystals are thermodynamically metastable at low temperatures.[118-119] In addition, the ligand-surface interaction affects the crystal structure. Peng *et al.* reported that

the formation of zinc-blende and wurtzite CdSe nanocrystals was determined by the interactions between ligands and crystal surfaces instead of the interior crystal structure difference.[95] Phosphonate ligands promoted the formation of CdSe nanocrystal with wurtzite structure while carboxylate ligands promoted the formation of CdSe nanocrystals with zinc-blende structure during both the processes of nucleation and growth. In contrast, phosphines, phosphonic acids and fatty amines did not show determinant effects. Interestingly, fatty amines are a secondary factor for the determination of crystal structure likely owing to their highly dynamic nature and weak bonding to the crystal surface.

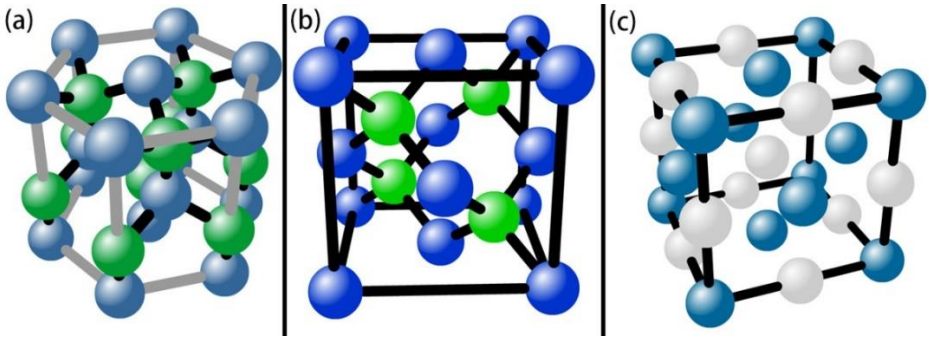

Figure 1.9 Three representative crystal structures of CSNCs (a) wurtzite, (b) zinc-blende, (c) rock-salt.

1.3 Surface chemistry of CSNCs

1.3.1 The covalent bond classification (CBC) method

The surface chemistry of CSNCs influences their electronic structure, the PL quantum yield and colloidal stability due to the interactions between the surface inorganic or organic ligands coordinated to the surface atoms of the CSNCs and the surface atoms or solvents. In conformity with the covalent bond classification (CBC) method proposed by Green,[120] there are three basic types of interaction by which a ligand may bond to a metal centre and the ligand is classified by the nature and the number of these interactions. The symbols Z, X and L represent the three types of interaction, corresponding to 0-electron neutral, 1-electron and 2-electron ligands respectively and are clearly distinguished according to a molecular orbital representation of the bonding as shown in Figure 1.10. An L-type ligand is one interacting with a metal centre via a dative covalent bond in which both electrons are donated by the L-type ligands. Those L-type ligands are

Lewis bases that have lone pairs of electrons such as primary amines (R-NH_2) and trialkylphosphines (R_3P trialkylphosphines). An X-type ligand is one interacting with a metal centre via a normal 2-electron covalent bond, composed of one electron donated from the metal and one electron from the X-type ligand. Simple examples of X-type ligands are Cl and H. For a Z-type ligand, they also interact with a metal centre via a dative covalent bond with two electrons donated from the metal. Z-type ligands are Lewis acids with a vacant orbital to accept a pair of electron from the metal.

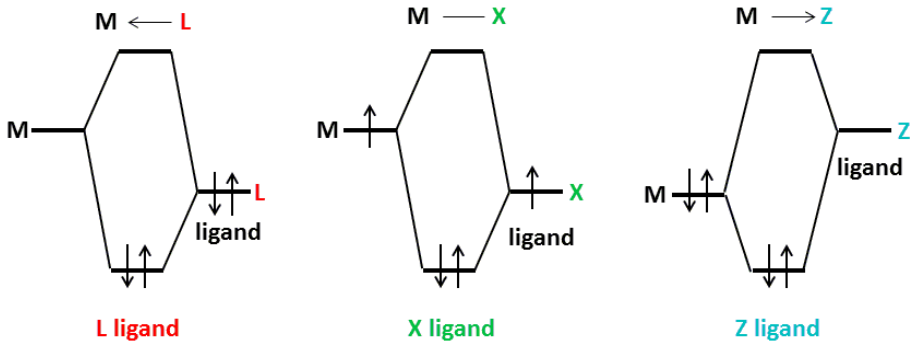

Figure 1.10 Molecular orbitals of three basic types of interactions between a metal centre and a ligand.

Owen *et al.* employed the CBC method to explain the surface chemistry of CSNCs and gave a schematic illustration of nanocrystal ligand binding motifs as depict in Scheme 1.2. They further investigated the stoichiometry of metal chalcogenide nanocrystals and the ligand exchange by NMR spectroscopy. It was found that the relative displacement potency mainly depends on geometric factors such as steric effect, chelation and the hard/soft match with cadmium ion.[121] In addition, they shows that most under-coordinated "dangling" atoms do not form surface traps and the X- and L-type ligands are favorable to the electronic structure stability of CSNCs. Nevertheless, the Z-type ligands will induce mid-gap states which localize on the 4p lone pair of 2-coordinated chalcogenide surface atoms.[122]

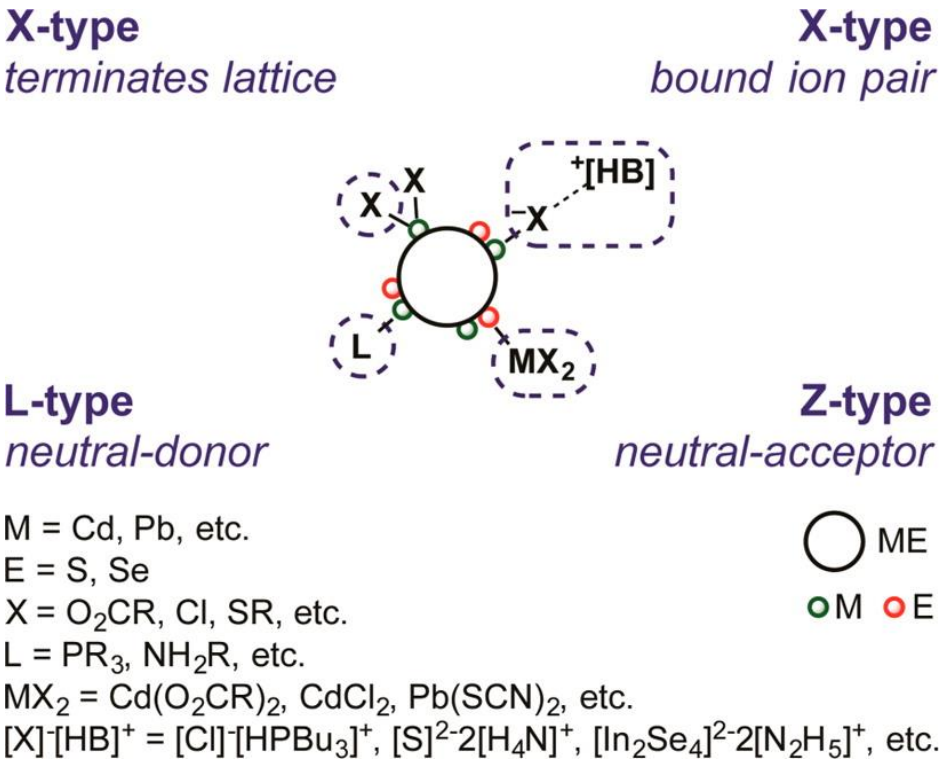

Scheme 1.2 Nanocrystal ligand binding motifs according to the covalent bond classification method. Reprinted with permission from ref. 121. Copyright 2013 American Chemical Society. [121]

1.3.2 Core/shell heterostructures

Because the surface atoms of CSNCs cannot be fully passivated by organic ligands, another approach to remove the surface traps of nanocrystals, improve the PL quantum yield and tune the electronic structure of CSNCs is to grow an inorganic passivation layer epitaxially on the surface of CSNCs to form a core/shell heterostructures.[104, 123-131] In addition, an inorganic shell of another semiconductor on the core CSNCs can intentionally manipulate the charge carrier spatially due to bandgap alignment.[58, 132-137] The electronic structures of core, type I and type II core/shell heterostructure CSNCs are depicted in Figure 1.11.

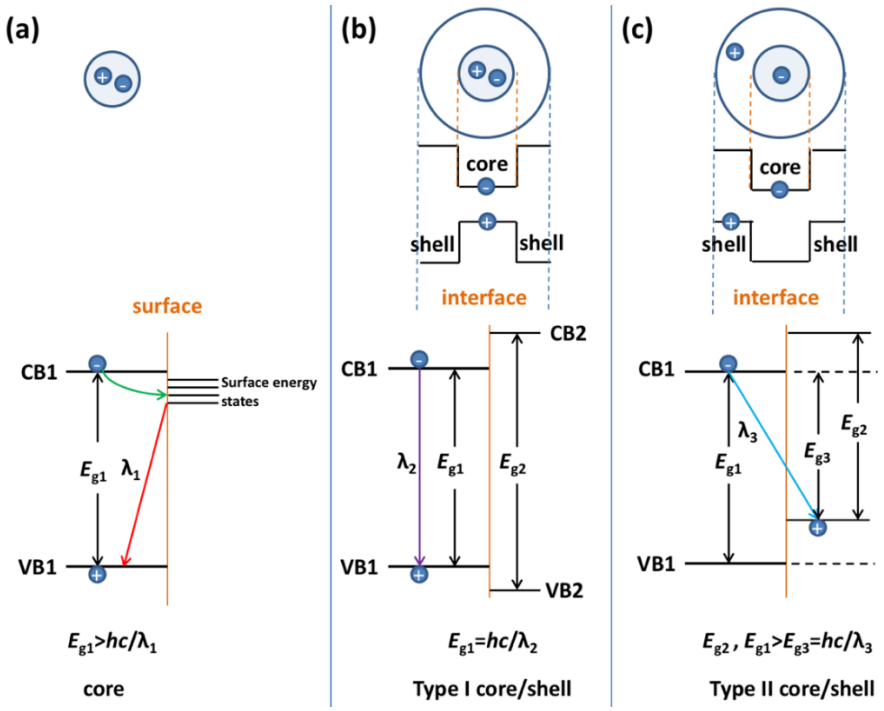

Figure 1.11 The electronic structure of core (a), type I (b) and type II (c) core/shell heterostructure of CSNCs.

For the bare core CSNCs without a shell of another semiconductor, there could be some surface traps, which makes the energy of the emitted light smaller than the bandgap energy of the core CSNCs. For type I core/shell CSNCs, both holes and electrons are confined in the core CSNCs due to the lower valence and conduction band energy of the core CSNCs than that of the shell CSNCs. Therefore, the energy of the emitted light equals to the energy of the bandgap of the core CSNCs. In contrast, the electrons and the holes are respectively confined in core and shell CSNCs, which makes the bandgap energy of type II core/shell CSNCs smaller than that of both bare core and type I core/shell CSNCs. Figure 1.12 presents the band alignment of representative CSNCs. Simple examples of type I core/shell CSNCs include ZnTe/ZnS, ZnSe/ZnS, CdTe/CdS, and CdSe/CdS. Simple examples of type II core-shell comprise ZnSe/ZnTe and CdSe/CdTe.

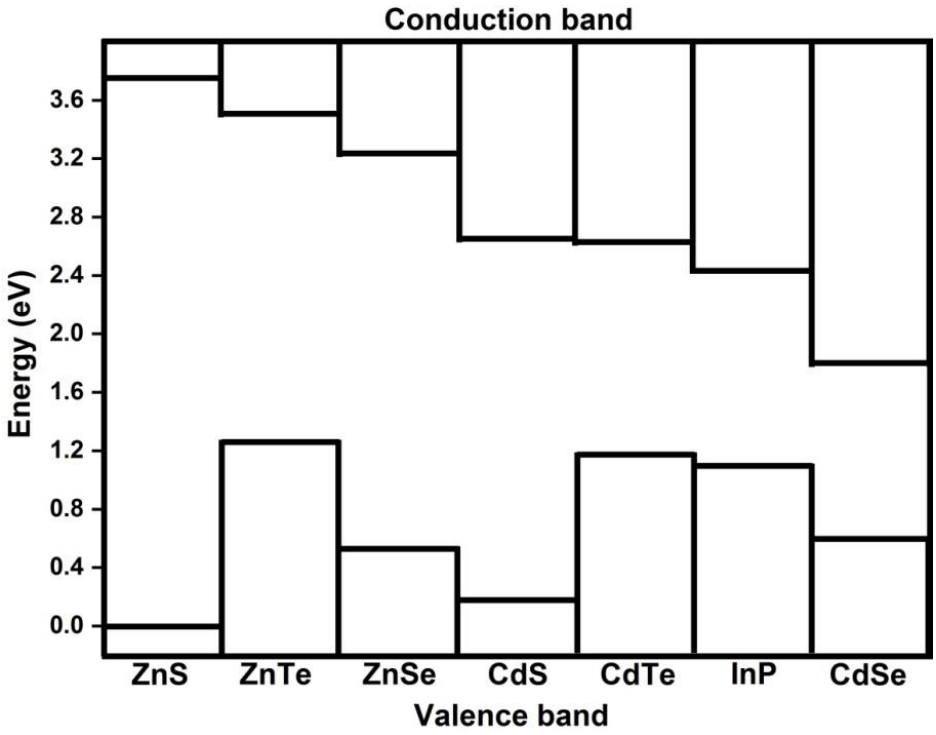

Figure 1.12 Band alignments of selected semiconductor materials at room temperature (the top of the valence band of ZnS in vacuum is set to 0 eV).

Generally, it is easy to grow an inorganic passivation layer on the surface of CSNCs if the lattice mismatch between the shell and the core CSNCs is below 10%. Figure 1.13 shows the lattice mismatch of representative core-shell CSNCs. For most of the II-VI CSNCs, the lattice mismatch is below or close to 10%.

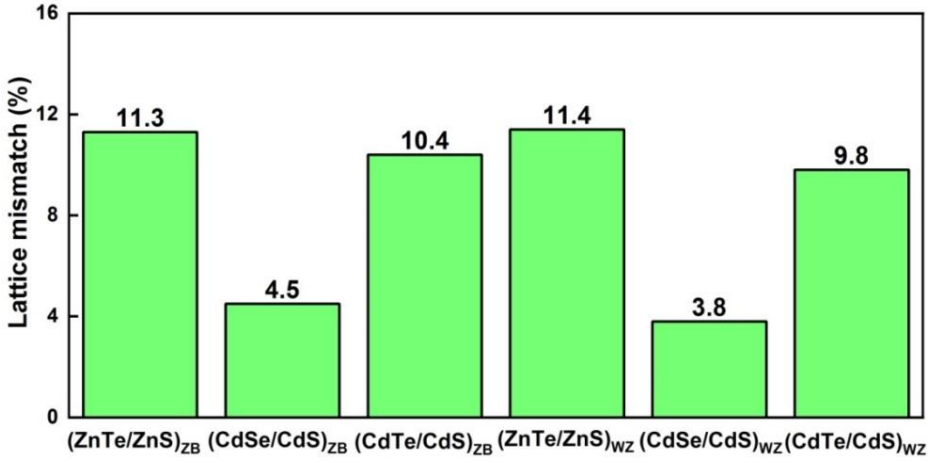

Figure 1.13 Lattice mismatch of representative core-shell CSNCs.

1.3.3 Purification

The as-synthesized CSNCs need to be purified for material characterization such as TEM and XRD. Herein, a pair of non-polar solvent and polar solvent is used for size selective precipitation.[138] The hydrophobic stabilizing molecules on the surface of as-prepared CSNCs make them soluble in non-polar solvents due to the hydrophobic interactions between the solvent molecules and the tails of the surfactant molecules on the surface of CSNCs. The solvent-surfactant interactions are progressively disrupted if a polar solvent is added to the solution gradually, leading to the aggregation of CSNCs. Then, the CSNCs can be collected using a centrifuge. Usually, the pair of non-polar solvent and polar solvent includes toluene and methanol, toluene and acetone, chloroform and acetone, chloroform and methanol. The schematic illustration of the purification of as-synthesized CSNCs is shown in Figure 1.14.

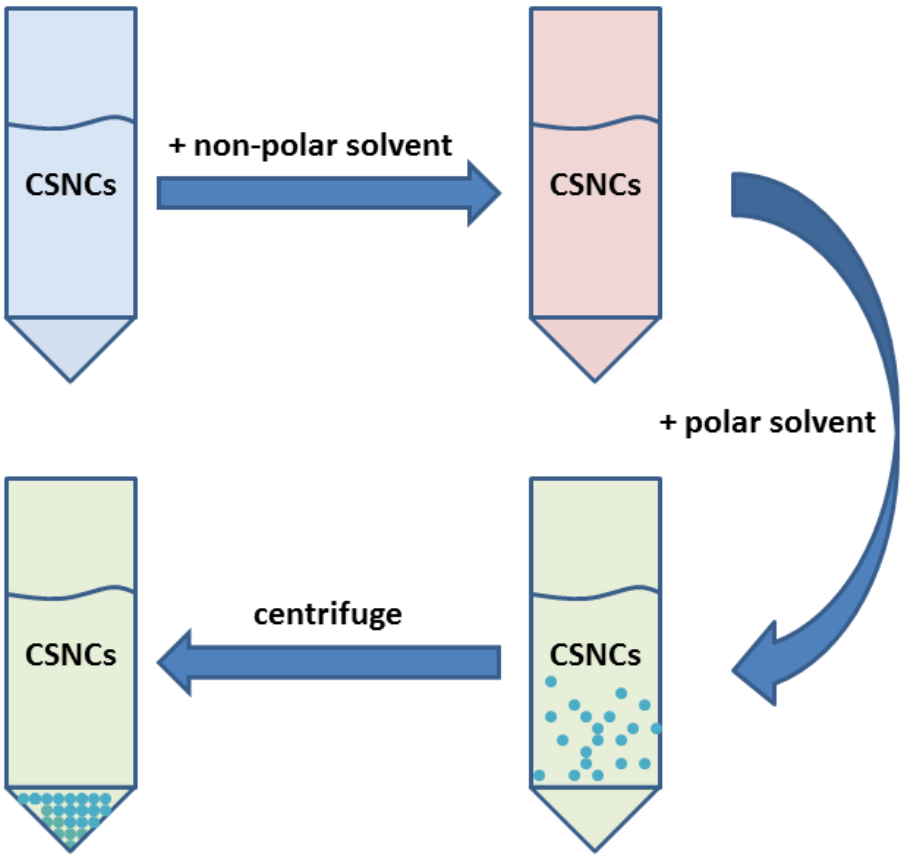

Figure 1.14 Schematic illustration of the purification of as-synthesized CSNCs.

1.3.4 Entropic ligands

The solution processability of CSNCS is the key for solution-processed optoelectronics, biomedical labeling and printable electronics etc. Peng *et al.* proposed a concept "entropic ligands" to represent a class of ligands that make the CSNCs with outstanding solubility.[123, 139-140] "Entropic ligands" can maximize the intramolecular entropic effects due to the bending and rotation entropy of the C-C σ bonds within organic ligands, increasing the solubility of various CSNCs by 10^2-10^6 times. Figure 1.15 shows the schematic illustration of the solubility of entropic ligands coated CdSe nanocrystals.

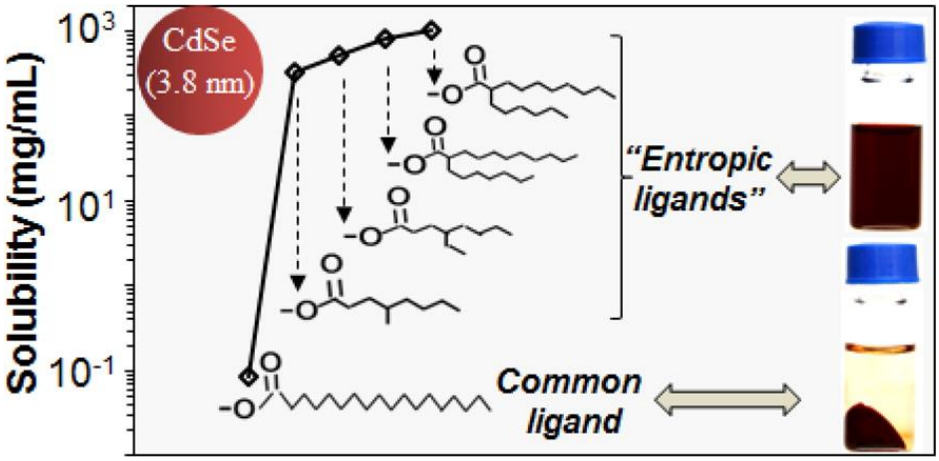

Figure 1.15 The solubility of entropic ligands coated CSNCs. Reprinted with permission from ref. 139. Copyright 2016 American Chemical Society.[139]

1.4 Photophysical properties of CSNCs

CSNCs have aroused great scientific interest owing to their tunable and size-dependent bandgap, which is the so-called quantum size confinement effect. Binary II-VI and III-V CSNCs are most extensively investigated as their bandgaps are close to or in the range of the visible spectral range.[141-146] This makes them hold great promise for developing novel light sources such as QLED. Figure 1.16 highlights the size-dependent bandgap of CdSe CSNCs.[147]

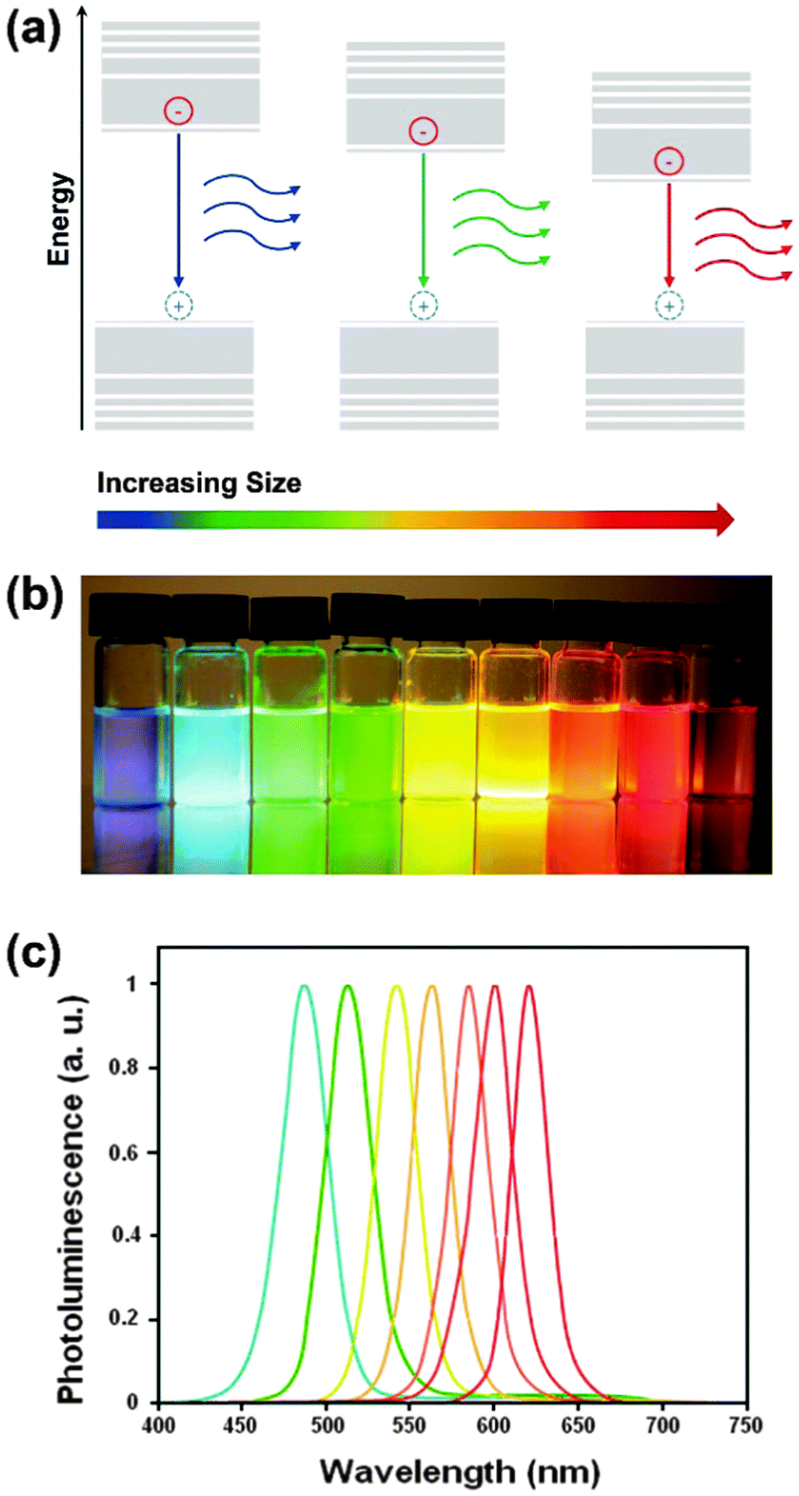

Figure 1.16 (a) Sketch of the effect of band-gap narrowing by increasing the size of NCs. (b) Suspensions of colloidal CdSe/ZnS core/shell HNCs of different sizes under UV excitation and (c) Relative size-dependent emission spectra. Reprinted with permission from ref. 147. Copyright 2016 Royal Society of Chemistry.[147]

The electronic structure of CSNCs was first explained by Brus using effective mass approximation model.[148] In his model, the excited states are a strong function as the size of CSNCs and the bandgap shift is approximately expressed as

$$E = \frac{\hbar^2\pi^2}{2R^2}\left[\frac{1}{m_e} + \frac{1}{m_h}\right] - \frac{1.8e^2}{R\epsilon},$$

where *E* is the energy shift regarding the bulk bandgap; $\hbar$ is the reduced Planck constant; m_e and m_h are the effective masses of electron and hole of the semiconductor in units of m_0, respectively; *R* is the size of CSNCs; ϵ is the dielectric constant of the semiconductor. When the exciton Bohr radius of the semiconductor is larger than the size of CSNCs, the size of the exciton depends on the shape of the NC instead of the strength of the electron-hole Coulombic interaction.[149] The exciton Bohr radius a_e is expressed as

$$a_e = \frac{4\pi\varepsilon_0\hbar^2}{m_0e^2}\varepsilon_\infty\left[\frac{1}{m_e} + \frac{1}{m_h}\right] = a_0\varepsilon_\infty\left[\frac{1}{m_e} + \frac{1}{m_h}\right],$$

where a_0 is the Bohr radius of a hydrogen atom (0.529 Å); ε_∞ is the high frequency dielectric constant of the medium; $\hbar$ is the reduced Planck constant; m_h and m_e are the effective masses of hole and electron of the semiconductor in units of m_0, respectively.

The electronic energy states of a semiconductor become discrete when its size is smaller than its exciton Bohr radius. Figure 1.17 shows the electronic energy states of semiconductor in the transition from discrete molecules to CSNCs and bulk semiconductors.

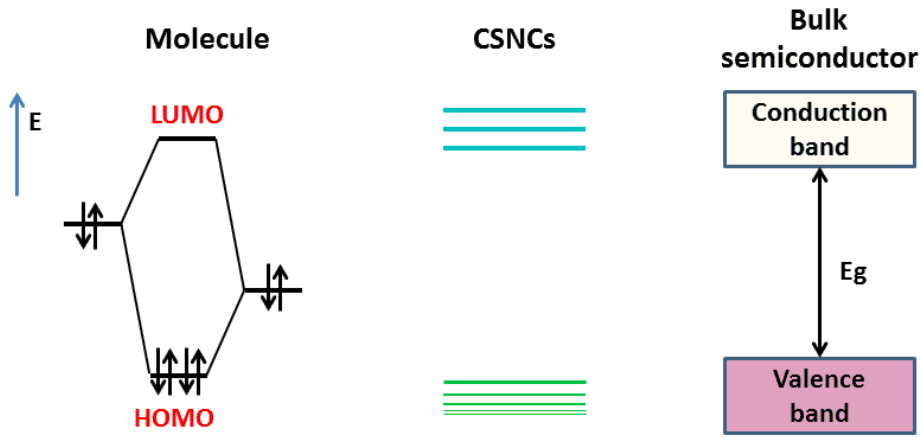

Figure 1.17 The electronic energy states of semiconductor in the transition from discrete molecules to CSNCs and bulk semiconductors.

Figure 1.18 depicts the schematic illustration of the energy level structures of bulk semiconductor and semiconductor nanostructures with excitons confined in different dimensions, i.e. 0D (excitons are confined in all directions), 1D (excitons are confined in the diameter direction) and 2D (excitons are confined only in the thickness dimension), as well as their densities of electronic states (DOS) as a function of energy.

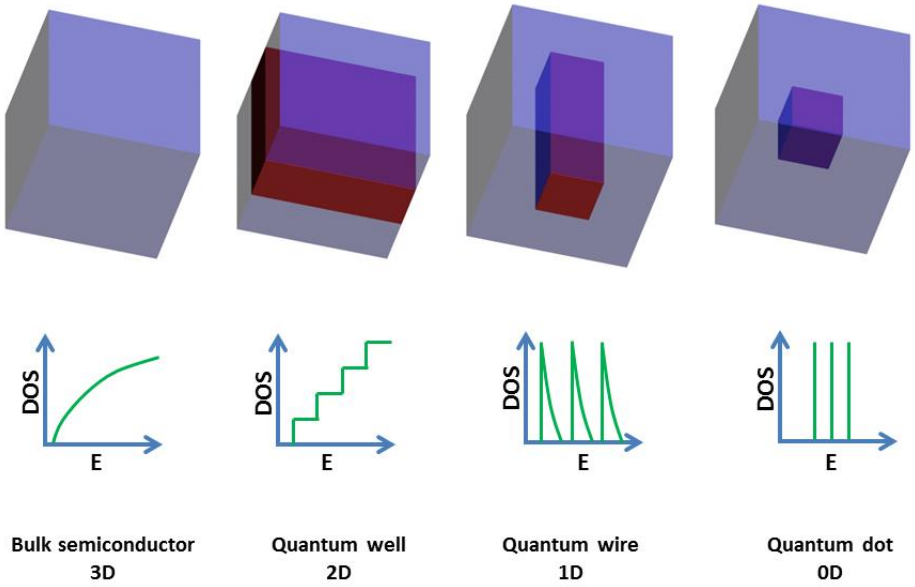

Figure 1.18 The schematic illustration of the energy level structures of bulk semiconductor and semiconductor nanostructures with excitons confined in different dimensions and their densities of electronic states as a function of energy.

1.5 Two-dimensional colloidal semiconductor nanocrystals

Two-dimensional (2D) CSNCs have aroused great interest recently. These nanocrystals with flat basal planes and atomic-thickness are called as nanoribbons (quantum belts) or nanosheets,[82, 150-152] nanoplatelets (quantum platelets),[97, 153-157] or quantum disks[158-159] due to different lateral dimensions and aspect ratio. Their remarkable optical properties such as sharp and intense absorption and PL spectra, nearly zero stoke shift, and shorter fluorescence lifetime gradually have attracted intense interest in the scientific community.

1.5.1 A brief history of wurtzite nanoplatelets

In 2006, Hyeon *et al.* first reported the solution-phase synthesis of wurtzite CdSe nanoribbons with a uniform thickness of 1.4 nm at low temperature.[82] The CdSe QBs were synthesized from the mixture of $CdCl_2$(octylamine)$_2$ complex and octylammonium selenocarbamate at 70 °C. Both their absorption and PL spectra with extremely sharp peaks and the nearly zero stoke shift confirm the formation of 2D nanostructure. The full width at half maximum (FWHM) of the PL spectrum is about ~70 meV.

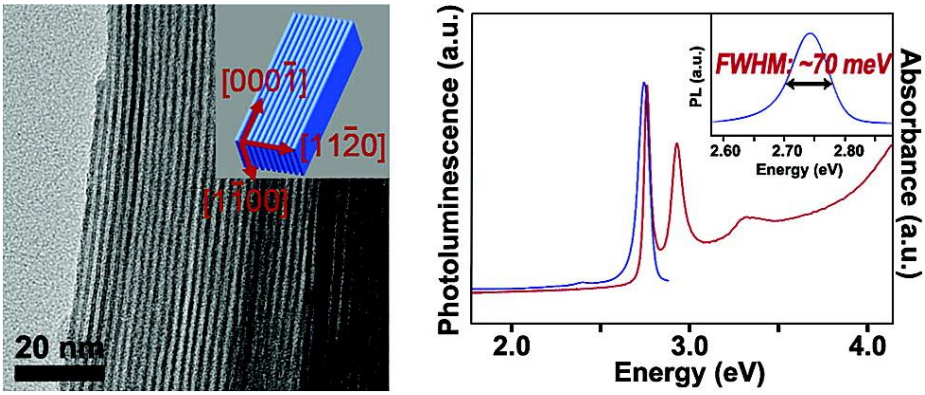

Figure 1.19 The standing on CdSe QBs and their absorption and PL spectra. Reprinted with permission from ref. 82. Copyright 2009 American Chemical Society.[82]

In 2009, the same group reported the synthesis of lamellar-structured CdSe nanosheets from the reaction of $CdCl_2$(octylamine)$_2$ complex and selenium (Se) powder in octylamine at 100 °C. By replacing the $CdCl_2$(octylamine)$_2$ complex with $CdCl_2$(octylamine)$_2$(oleylamine)$_2$ complex, single-layered CdSe nanosheets were produced after the sonication of reaction mixture.[111]

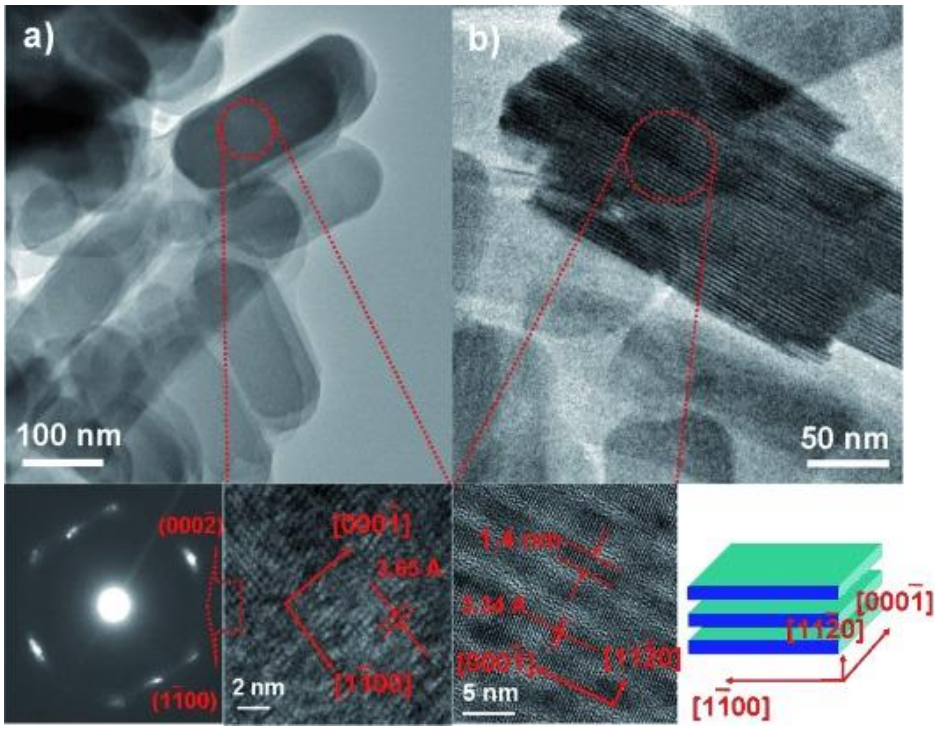

Figure 1.20 Characterization of the lamellar-structured CdSe nanosheets. a) TEM image (top), SAED pattern (bottom left), and HRTEM image (bottom right). b) TEM image (top) and HRTEM image (bottom left) of the edges of CdSe nanosheets; bottom right image illustrates the crystallographic nature of the nanosheets. Reprinted with permission from ref. 111. Copyright 2009 John Wiley and Sons.[111]

Followed by the work of Hyeon *et al.*, the isolation of $[(CdSe)_{13}$(n-octylamine)$_{13}]$ and $[(CdSe)_{13}$(oleylamine)$_{13}]$ magic-sized CdSe nanoclusters were reported by Buhro *et al.* in 2012.[160] The magic size number was determined to be 13 by LDI (Laser Desorption/Ionization) mass spectrum. Two years later, the same group reported the isolation of II-IV semiconductor MSNCs such as $(ZnSe)_{13}$(n-butylamine)$_{13}$, $(ZnTe)_{13}$(n-butylamine)$_{13}$, $(ZnS)_{34}$(n-butylamine)$_{34}$, $(CdS)_{34}$(n-butylamine)$_{18}$ and the syntheses of CdS, ZnS, CdSe, ZnSe quantum platelets and CdTe quantum belts.[38] Recently, the same group reported the isolation of $(ZnSe)_{34}$ and $(CdTe)_{34}$ MSNCs.[112] The characteristic absorption peaks of the II-VI MSNCs, quantum platelets (QPs) and quantum belts (QBs) were listed in Table 1.3.

Table 1.3 Characteristic absorption peaks of II-VI MSNCs, quantum platelets (QPs) and quantum belts (QBs).[38, 161]

MSNCs/QPs	Max absorption peak (nm)		
	1st	2nd	3rd
$(CdS)_{34}$(n-butylamine)$_{18}$	361	326	
$(ZnS)_{34}$(n-butylamine)$_{34}$	258		
$(ZnSe)_{13}$(n-butylamine)$_{13}$	289	279	
$(CdTe)_{13}$(n-octylamine)$_{13}$	373	353	
$(ZnTe)_{13}$(n-butylamine)$_{13}$	323	302	
CdS QPs	375	337	
ZnS QPs	282		
ZnSe nanosheets	347	329	
ZnSe QPs	347	329	304
CdTe QBs	491	444	

In 2014, Buhro *et al.* reported that these 2D nanocrystals were converted from MSNCs that were characterized by mass spectrometry.[41] These $(CdSe)_{34}$ MSNCs were first formed in the soft templates, then converted to quantum platelets by annealing at a temperature of 25 ^{o}C or >40 ^{o}C by first-order kinetics with no induction period. The control of the thickness (1.4, 1.8 and 2.2 nm) of CdSe QPs was achieved by using different alkylamine or dialkylamine in combination of the control of the reaction temperature.

1.5.2 A brief history of zinc-blende nanoplatelets

In 2008, Ithurria and Dubertret *et al.* first reported the colloidal synthesis of zinc-blende CdSe nanoplatelets with controllable thickness at the atomic level.[162] Cadmium myristate and selenium powder are used as cadmium and selenium precursor, respectively. The colloidal synthesis is based on the solution-phase reaction of the precursors in presence of ODE and acetate salt. By changing the injection temperature of selenium precursor, the thickness of the CdSe nanoplatelets can be tuned at 1.9 or 2.2 or 2.5 nm, respectively, which is derived from the PL excitation spectra and theoretical calculation. Although Dubertret *et al.* proposed a growth mechanism as shown in Figure 1.21, no direct evidence of the growth of zinc blend CdSe nanoplatelets was given in that work.

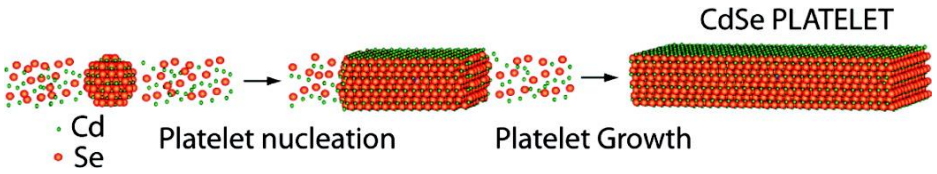

Figure 1.21 The schematic illustration of the formation of zinc-blende CdSe nanoplatelets. Reprinted with permission from ref. 162. Copyright 2008 American Chemical Society.[162]

Figure 1.22 presents the TEM images of zinc-blende CdSe colloidal nanoplatelets synthesized at different injection temperatures of selenium precursor and reaction time. The lateral size of these nanoplatelets ranges from 15 to 50 nm. Interestingly, rolled-up CdSe nanobelts were produced if cadmium acetate is injected at the room temperature with the other precursors prior to heating.

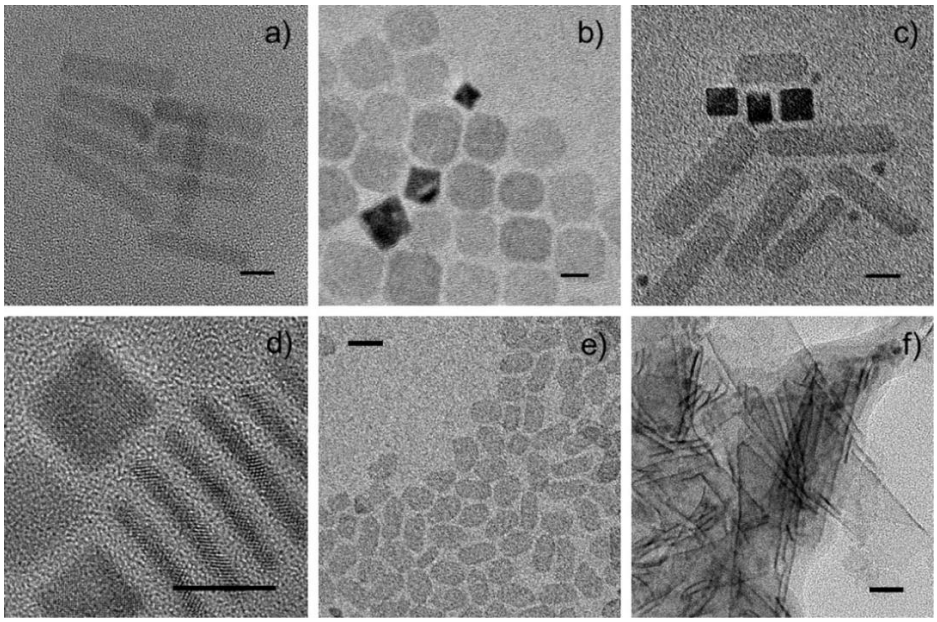

Figure 1.22 TEM images of zinc-blende CdSe colloidal nanoplatelets synthesized at different injection temperatures of selenium precursor. (a) Injection of cadmium acetate at 195 °C and heating at 240 °C for 10 min. (b and c) Same as in (a) with a second precursor injection at 240 °C and heating for 20 min. (d) High resolution TEM of (b). (e) Same as (a) using manganese acetate in place of cadmium acetate. (f) Cadmium acetate is injected at room temperature with the other precursors prior to heating. Scale bars: (a−d) 10 nm, (e, f) 20 nm. Reprinted with permission from ref. 162. Copyright 2008 American Chemical Society.[162]

Figure 1.23 shows the room temperature PL (dash line) and PLE (solid line) spectra of CdSe nanoplatelets synthesized at different injection temperatures of selenium precursor. The PLE spectra exhibit an absorption doublet which are transitions from heavy hole and light hole at valence band to electron at conduction band. The first exciton absorption peak at a longer wavelength has near-zero shift with the PL emission peak, which is a characteristic of colloidal semiconductor nanoplatelets. These CdSe nanoplatelets with the first exciton absorption peak at 462, 512 and 550 nm, respectively, is deduced to be with a thickness of 1.9 or 2.2 or 2.5 nm.

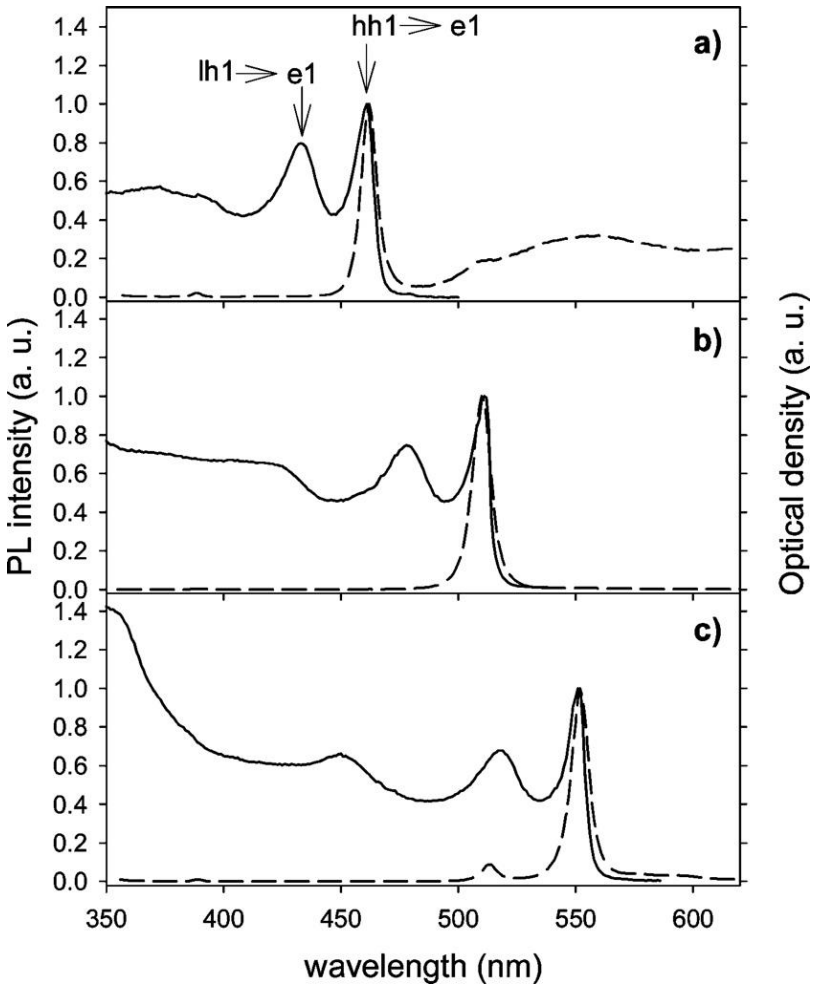

Figure 1.23 Room temperature PL (dash line) and PLE (solid line) spectra of CdSe nanoplatelets synthesized under different reaction conditions. (a) Cadmium acetate injected at a low temperature, (b) Cadmium acetate injected at 195 °C. (c) Same as in (b) with one additional injection of precursors at 240 °C. Reprinted with permission from ref. 162. Copyright 2008 American Chemical Society.[162]

Although there are many reports about the colloidal synthesis of zinc-blende II-VI NPLs, the growth mechanism is yet still debated. Peng *et al.* reported that the formation of zinc-blende nanoplatelets included the conversion of 0D seeds to 2D nanocrystals and two symmetry-breaking of events as shown in Figure 1.24.[113] The symmetry breaking between the thickness and lateral directions took place in the early stage via the rapid formation of dot intermediates with the appearance of flat polar [110] basal planes and of the desired thickness from the seeds via intra-particle ripening. The first symmetry breaking between the thickness and lateral directions of NPLs was achieved due to the rapid formation of single intermediate 0D nanocrystals via intra-particle ripening of the seeds whereas the second symmetry breaking between two lateral dimensions occurred from the unequal growth of the polar and well-passivated [100] side crystal facets during the process of oriented attachment. It was found that the addition of cadmium salts of short-chain carboxylic acids such as cadmium acetate can assist both the formation of single-dot intermediate and their oriented attachment. However, cadmium alkanoates with a long hydrocarbon chain can promote the conversion of the 0D seeds to 2D nanocrystals and transport insoluble acetate to the surface of the nanocrystals.

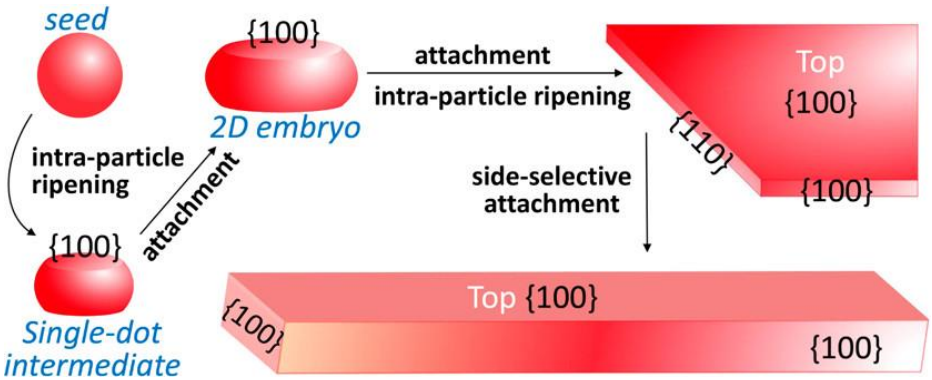

Figure 1.24 The schematic illustration of the formation of zinc-blende CdSe nanoplatelets. Reprinted with permission from ref. 113. Copyright 2017 American Chemical Society.[113]

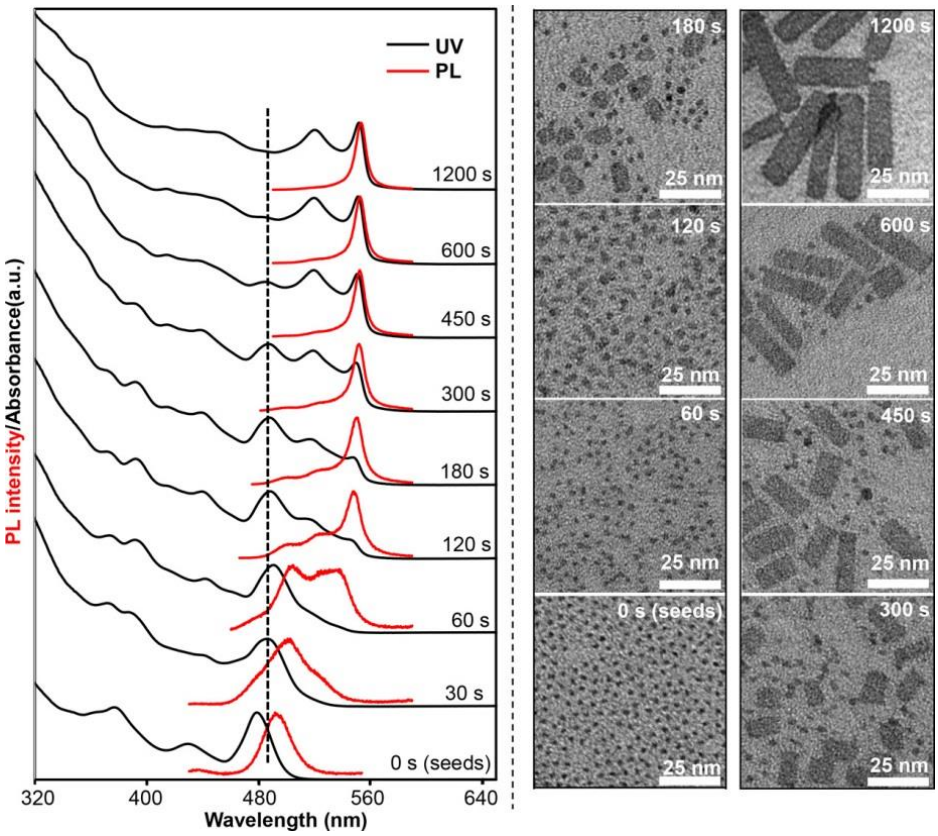

Figure 1.25 Temporal evolutions of UV−Vis/PL (left) and TEM images (right) of CdSe nanocrystals at 250 °C. The dashed line (left panel) indicates the absorption peak position of the persistent 0D nanocrystals. Reprinted with permission from ref. 113. Copyright 2017 American Chemical Society.[113]

The temporal evolutions of UV-vis/PL and TEM images of CdSe nanocrystals in Figure 1.25 clearly show the formation of zinc-blende CdSe nanoplatelets from the conversion of 0D seeds to 2D nanocrystals. The absorption peak redshifted from 480 to 490 nm at the first 30s of the reaction (Figure 1.25, left panel), which means the size growth of 0D seeds. The corresponding PL peak evolved from a symmetric and sharp peak to a peak with two shoulders on both sides. This was verified by the TEM images (Figure 1.25, right panel) which show the size of the nanocrystals increases slightly from 1.8 to 2.0 nm. When the reaction proceeded beyond 300s, the population of 0D nanocrystal seeds decreased and gradually disappeared. After the reaction proceeded for 180s, irregular 2D CdSe NPLs appeared, accompanied by the appearance of sharp absorption peak shown in the left panel of Figure 1.25. 0D nanocrystals fully are converted to 2D regular CdSe

NPLs after 1200s of the reaction time.

Compared with the oriented-attachment mechanism, Norris *et al.* reported the theory of the intrinsic growth instability for the growth mechanism of zinc-blende nanoplatelets in 2017.[163] They applied the general theory of 2D nucleation and crystal growth to CdSe nanocrystals with the assumption of an existing zinc-blende CdSe crystallite bounded by Cd-terminated (001) facets. By DFT calculation of the energy changes for different crystal facet dimensions when an island nucleates and expands to cover the facet, they evaluated the energy difference in wide and narrow facet regimes. For large facets, a nucleated island will grow isotropically to minimize its energy and the critical island size determines the corresponding nucleation barrier. For narrow facets with thickness less than the critical size, the nucleated island swiftly expands the whole facet and grows along the facet. Therefore, the corresponding nucleation barrier significantly decreased, resulting in a faster growth rate at reaction temperatures. The red and blue areas in Figure 1.26(a) show new edges and surfaces formed by the nucleated islands, respectively.

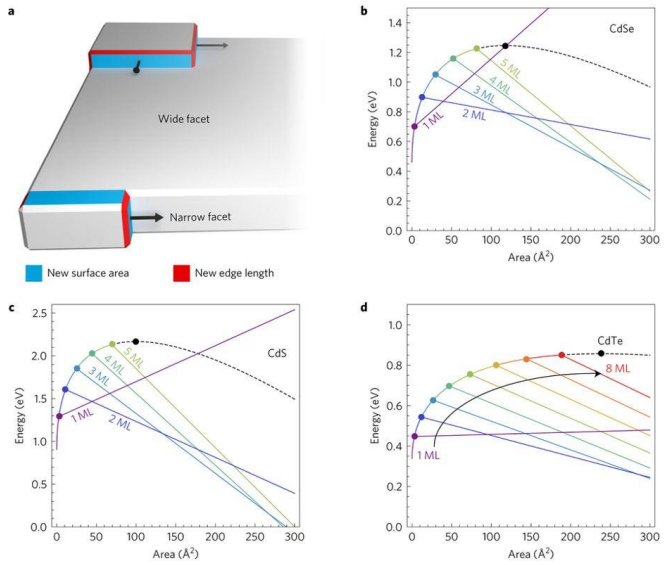

Figure 1.26 Theory of the intrinsic growth instability for the growth mechanism of zinc-blende NPLs. a: Qualitatively different growth modes on wide and narrow facets of a nanocrystal. b–d, Calculated energy versus island size on facets of different thicknesses based on parameters obtained from DFT calculations for CdSe (b), CdS (c) and CdTe (d). Reprinted with permission from ref. 163. Copyright 2017 Springer Nature.[163]

Figure 1.26(b-d) presents the calculated formation energy versus island size on facets with different thicknesses according to parameters derived from DFT calculations for CdSe (b), CdS (c) and CdTe (d). The black dashed line in each figure symbolizes the wide-facet limit while the coloured lines embodies various thicknesses of the narrow facets in monolayers (MLs) of NPLs as labelled. Circles in each figure represents the corresponding nucleation barriers. From the results, the model predicts that CdSe or CdS or CdTe NPLs with one monolayer thickness are thermodynamically unstable because their island energy expands continually with island area. For NPLs with thickness thicker than one monolayer, the growth of NPLs is suppressed because the nucleation barrier reaches the wide-facet limit.

1.6 Thesis organization

The first chapter of this thesis, i.e. introduction, provides the basic research background of colloidal semiconductor nanocrystals such as the colloidal chemical synthetic approaches, the surface chemistry, photophysical properties, and especially the history of 2D colloidal semiconductor nanocrystals, which lays the foundation to help the readers better understand this thesis. The second chapter describes the material characterization techniques and analysis methods employed in this PhD thesis such as UV-vis spectroscopy, PL spectroscopy, infrared spectroscopy, NMR spectroscopy, transmission electron microscopy, XRD and density function theory calculation. The third and fourth chapter introduces the colloidal synthesis, growth mechanism and optical properties of colloidal wurtzite ZnTe and CdTe nanoplatelets, respectively. Conclusions and outlook will be included in the final chapter.

1.7 References

1. Alivisatos, A. P., Semiconductor clusters, nanocrystals, and quantum dots. *Science* **1996,** *271* (5251), 933-937.
2. Empedocles, S. A.; Bawendi, M. G., Quantum-confined stark effect in single CdSe nanocrystallite quantum dots. *Science* **1997,** *278* (5346), 2114-2117.
3. H. Sargent, E., Infrared quantum dots. *Advanced Materials* **2005,** *17* (5), 515-522.
4. Moreels, I.; Lambert, K.; Smeets, D.; De Muynck, D.; Nollet, T.; Martins, J.

C.; Vanhaecke, F.; Vantomme, A.; Delerue, C.; Allan, G., Size-dependent optical properties of colloidal PbS quantum dots. *ACS Nano* **2009,** *3* (10), 3023-3030.

5. Micic, O. I.; Curtis, C. J.; Jones, K. M.; Sprague, J. R.; Nozik, A. J., Synthesis and characterization of InP quantum dots. *The Journal of Physical Chemistry* **1994,** *98* (19), 4966-4969.

6. Murphy, J. E.; Beard, M. C.; Norman, A. G.; Ahrenkiel, S. P.; Johnson, J. C.; Yu, P.; Mićić, O. I.; Ellingson, R. J.; Nozik, A. J., PbTe colloidal nanocrystals: synthesis, characterization, and multiple exciton generation. *Journal of the American Chemical Society* **2006,** *128* (10), 3241-3247.

7. Hu, J.; Li, L.-s.; Yang, W.; Manna, L.; Wang, L.-w.; Alivisatos, A. P., Linearly polarized emission from colloidal semiconductor quantum rods. *Science* **2001,** *292* (5524), 2060-2063.

8. Ahrenkiel, S.; Mićić, O.; Miedaner, A.; Curtis, C.; Nedeljković, J.; Nozik, A., Synthesis and characterization of colloidal InP quantum rods. *Nano Letters* **2003,** *3* (6), 833-837.

9. Shieh, F.; Saunders, A. E.; Korgel, B. A., General shape control of colloidal CdS, CdSe, CdTe quantum rods and quantum rod heterostructures. *The Journal of Physical Chemistry B* **2005,** *109* (18), 8538-8542.

10. Kan, S.; Mokari, T.; Rothenberg, E.; Banin, U., Synthesis and size-dependent properties of zinc-blende semiconductor quantum rods. *Nature Materials* **2003,** *2* (3), 155.

11. Li, L.-s.; Hu, J.; Yang, W.; Alivisatos, A. P., Band gap variation of size-and shape-controlled colloidal CdSe quantum rods. *Nano Letters* **2001,** *1* (7), 349-351.

12. Panda, A. B.; Acharya, S.; Efrima, S., Ultranarrow ZnSe nanorods and nanowires: structure, spectroscopy, and one-dimensional properties. *Advanced Materials* **2005,** *17* (20), 2471-2474.

13. Zavelani-Rossi, M.; Lupo, M. G.; Krahne, R.; Manna, L.; Lanzani, G., Lasing in self-assembled microcavities of CdSe/CdS core/shell colloidal quantum rods. *Nanoscale* **2010,** *2* (6), 931-935.

14. Xi, L.; Lam, Y. M., Controlling growth of CdSe nanowires through ligand optimization. *Chemistry of Materials* **2009,** *21* (15), 3710-3718.

15. Acharya, S.; Gautam, U. K.; Sasaki, T.; Bando, Y.; Golan, Y.; Ariga, K., Ultra

narrow PbS nanorods with intense fluorescence. *Journal of the American Chemical Society* **2008,** *130* (14), 4594-4595.

16. Chen, G.-H.; Ho, S.-J.; Chen, H.-S., Cubic zincblende ZnSe nanowires with an entangling structure grown via oriented attachment and their application in organic–inorganic heterojunction light-emitting diodes. *The Journal of Physical Chemistry C* **2014,** *118* (44), 25816-25822.

17. Tang, K. B.; Qian, Y. T.; Zeng, J. H.; Yang, X. G., Solvothermal route to semiconductor nanowires. *Advanced Materials* **2003,** *15* (5), 448-450.

18. Wisniewski, D.; Byrne, K.; Fernandes, C.; Stewart, C.; de Souza, C. F.; Ruda, H. E., Fingerprinting electronic structure in nanomaterials: a methodology illustrated by ZnSe nanowires. *Nano Letters* **2019**.

19. Ning, J.; Liu, J.; Levi-Kalisman, Y.; Frenkel, A. I.; Banin, U., Controlling anisotropic growth of colloidal ZnSe nanostructures. *Journal of the American Chemical Society* **2018,** *140* (44), 14627-14637.

20. Zhang, D.; Yu, Y.; Bekenstein, Y.; Wong, A. B.; Alivisatos, A. P.; Yang, P., Ultrathin colloidal cesium lead halide perovskite nanowires. *Journal of the American Chemical Society* **2016,** *138* (40), 13155-13158.

21. Zhang, D.; Eaton, S. W.; Yu, Y.; Dou, L.; Yang, P., Solution-phase synthesis of cesium lead halide perovskite nanowires. *Journal of the American Chemical Society* **2015,** *137* (29), 9230-9233.

22. Davis, A. H.; Hofman, E.; Chen, K.; Li, Z.-J.; Khammang, A.; Zamani, H.; Franck, J. M.; Maye, M. M.; Meulenberg, R. W.; Zheng, W., Exciton energy shifts and tunable dopant emission in manganese doped two-dimensional CdS/ZnS core/shell nanoplatelets. *Chemistry of Materials* **2019,** *140* (43), 14097-14111.

23. Riedinger, A.; Mule, A. S.; Knüsel, P. N.; Ott, F. D.; Rossinelli, A. A.; Norris, D. J., Identifying reactive organo-selenium precursors in the synthesis of CdSe nanoplatelets. *Chemical Communications* **2018,** *54* (83), 11789-11792.

24. Guzelturk, B.; Pelton, M.; Olutas, M.; Demir, H. V., Giant modal gain coefficients in colloidal II–VI nanoplatelets. *Nano Letters* **2018,** *19* (1), 277-282.

25. Feng, F.; NGuyen, L. T.; Nasilowski, M.; Nadal, B.; Dubertret, B.; Coolen, L.; Maitre, A., Consequence of shape elongation on emission asymmetry for colloidal CdSe/CdS nanoplatelets. *Nano Research* **2018**, 1-10.

26. Bouet, C.; Mahler, B.; Nadal, B.; Abecassis, B.; Tessier, M. D.; Ithurria, S.; Xu, X. Z.; Dubertret, B., Two-dimensional growth of CdSe nanocrystals, from nanoplatelets to nanosheets. *Chemistry of Materials* **2013,** *25* (4), 639-645.

27. Rowland, C. E.; Fedin, I.; Diroll, B. T.; Liu, Y.; Talapin, D. V.; Schaller, R. D., Elevated temperature photophysical properties and morphological stability of CdSe and CdSe/CdS nanoplatelets. *The Journal of Physical Chemistry Letters* **2018,** *9* (2), 286-293.

28. Yeltik, A.; Olutas, M.; Sharma, M.; Gungor, K.; Demir, H. V., Nonradiative energy transfer between doped and undoped flat semiconductor nanocrystals of colloidal quasi-2D nanoplatelets. *The Journal of Physical Chemistry C* **2018,** *123* (2), 1470-1476.

29. Khan, A. H.; Brescia, R.; Polovitsyn, A.; Angeloni, I.; Martín-García, B.; Moreels, I., Near-infrared emitting colloidal PbS nanoplatelets: lateral size control and optical spectroscopy. *Chemistry of Materials* **2017,** *29* (7), 2883-2889.

30. Peng, X., Green chemical approaches toward high-quality semiconductor nanocrystals. *Chemistry–A European Journal* **2002,** *8* (2), 334-339.

31. Du, Y.; Sheng, H.; Astruc, D.; Zhu, M., Atomically precise noble metal nanoclusters as efficient catalysts: a bridge between structure and properties. *Chemical Reviews* **2019,** *ASAP*.

32. Tao, Y.; Li, M.; Ren, J.; Qu, X., Metal nanoclusters: novel probes for diagnostic and therapeutic applications. *Chemical Society Reviews* **2015,** *44* (23), 8636-8663.

33. Ishida, Y.; Corpuz, R. D.; Yonezawa, T., Matrix sputtering method: a novel physical approach for photoluminescent noble metal nanoclusters. *Accounts of Chemical Research* **2017,** *50* (12), 2986-2995.

34. Jin, R.; Zeng, C.; Zhou, M.; Chen, Y., Atomically precise colloidal metal nanoclusters and nanoparticles: fundamentals and opportunities. *Chemical Reviews* **2016,** *116* (18), 10346-10413.

35. Jin, R., Atomically precise metal nanoclusters: stable sizes and optical properties. *Nanoscale* **2015,** *7* (5), 1549-1565.

36. Yang, J.; Muckel, F.; Baek, W.; Fainblat, R.; Chang, H.; Bacher, G.; Hyeon, T., Chemical synthesis, doping, and transformation of magic-sized semiconductor alloy nanoclusters. *Journal of the American Chemical Society*

2017, *139* (19), 6761-6770.

37. Wang, F.; Wang, Y.; Liu, Y.-H.; Morrison, P. J.; Loomis, R. A.; Buhro, W. E., Two-dimensional semiconductor nanocrystals: properties, templated formation, and magic-size nanocluster intermediates. *Accounts of Chemical Research* **2014,** *48* (1), 13-21.

38. Wang, Y.; Zhou, Y.; Zhang, Y.; Buhro, W. E., Magic-size II–VI nanoclusters as synthons for flat colloidal nanocrystals. *Inorganic Chemistry* **2015,** *54* (3), 1165-1177.

39. Cossairt, B. M.; Owen, J. S., CdSe clusters: at the interface of small molecules and quantum dots. *Chemistry of Materials* **2011,** *23* (12), 3114-3119.

40. Peng, Z. A.; Peng, X., Nearly monodisperse and shape-controlled CdSe nanocrystals via alternative routes: nucleation and growth. *Journal of the American Chemical Society* **2002,** *124* (13), 3343-3353.

41. Wang, Y.; Zhang, Y.; Wang, F.; Giblin, D. E.; Hoy, J.; Rohrs, H. W.; Loomis, R. A.; Buhro, W. E., The magic-size nanocluster $(CdSe)_{34}$ as a low-temperature nucleant for cadmium selenide nanocrystals; room-temperature growth of crystalline quantum platelets. *Chemistry of Materials* **2014,** *26* (7), 2233-2243.

42. Jiang, Z.-J.; Kelley, D. F., Role of magic-sized clusters in the synthesis of CdSe nanorods. *ACS Nano* **2010,** *4* (3), 1561-1572.

43. Yu, K., CdSe magic-sized nuclei, magic-sized nanoclusters and regular nanocrystals: monomer effects on nucleation and growth. *Advanced Materials* **2012,** *24* (8), 1123-1132.

44. Yang, J.; Muckel, F.; Choi, B. K.; Lorenz, S.; Kim, I. Y.; Ackermann, J.; Chang, H.; Czerney, T.; Kale, V. S.; Hwang, S.-J.; Bacher, G.; Hyeon, T., Co^{2+}-doping of magic-sized CdSe clusters: structural insights via ligand field transitions. *Nano Letters* **2018,** *18* (11), 7350-7357.

45. Muckel, F.; Yang, J.; Lorenz, S.; Baek, W.; Chang, H.; Hyeon, T.; Bacher, G.; Fainblat, R., Digital doping in magic-sized CdSe clusters. *ACS Nano* **2016,** *10* (7), 7135-7141.

46. Acharya, S.; Sarma, D.; Golan, Y.; Sengupta, S.; Ariga, K., Shape-dependent confinement in ultrasmall zero-, one-, and two-dimensional PbS nanostructures. *Journal of the American Chemical Society* **2009,** *131* (32),

11282-11283.

47. Hong, J. W.; Wi, D. H.; Lee, S.-U.; Han, S. W., Metal–semiconductor heteronanocrystals with desired configurations for plasmonic photocatalysis. *Journal of the American Chemical Society* **2016,** *138* (48), 15766-15773.

48. Dutta, S. K.; Mehetor, S. K.; Pradhan, N., Metal semiconductor heterostructures for photocatalytic conversion of light energy. *The Journal of Physical Chemistry Letters* **2015,** *6* (6), 936-944.

49. Zhang, L.; Blom, D. A.; Wang, H., Au–Cu_2O core–shell nanoparticles: a hybrid metal-semiconductor heteronanostructure with geometrically tunable optical properties. *Chemistry of Materials* **2011,** *23* (20), 4587-4598.

50. Vaneski, A.; Susha, A. S.; Rodríguez-Fernández, J.; Berr, M.; Jäckel, F.; Feldmann, J.; Rogach, A. L., Hybrid colloidal heterostructures of anisotropic semiconductor nanocrystals decorated with noble metals: synthesis and function. *Advanced Functional Materials* **2011,** *21* (9), 1547-1556.

51. Wang, W.; Ding, T.; Chen, G.; Zhang, L.; Yu, Y.; Yang, Q., Synthesis of Cu_2SnSe_3–Au heteronanostructures with optoelectronic and photocatalytic properties. *Nanoscale* **2015,** *7* (37), 15106-15110.

52. Li, M.; Yu, X. F.; Liang, S.; Peng, X. N.; Yang, Z. J.; Wang, Y. L.; Wang, Q. Q., Synthesis of Au–CdS core–shell hetero-nanorods with efficient exciton–plasmon interactions. *Advanced Functional Materials* **2011,** *21* (10), 1788-1794.

53. Liu, D.-Y.; Ding, S.-Y.; Lin, H.-X.; Liu, B.-J.; Ye, Z.-Z.; Fan, F.-R.; Ren, B.; Tian, Z.-Q., Distinctive enhanced and tunable plasmon resonant absorption from controllable Au@ Cu2O nanoparticles: experimental and theoretical modeling. *The Journal of Physical Chemistry C* **2012,** *116* (7), 4477-4483.

54. Wu, K.; Li, Q.; Du, Y.; Chen, Z.; Lian, T., Ultrafast exciton quenching by energy and electron transfer in colloidal CdSe nanosheet–Pt heterostructures. *Chemical Science* **2015,** *6* (2), 1049-1054.

55. Shen, S.; Zhang, Y.; Liu, Y.; Peng, L.; Chen, X.; Wang, Q., Manganese-doped Ag_2S-ZnS heteronanostructures. *Chemistry of Materials* **2012,** *24* (12), 2407-2413.

56. Pradhan, N.; Das Adhikari, S.; Nag, A.; Sarma, D., Luminescence, plasmonic, and magnetic properties of doped semiconductor nanocrystals. *Angewandte Chemie International Edition* **2017,** *56* (25), 7038-7054.

57. Sharma, M.; Gungor, K.; Yeltik, A.; Olutas, M.; Guzelturk, B.; Kelestemur, Y.; Erdem, T.; Delikanli, S.; McBride, J. R.; Demir, H. V., Near-unity emitting copper-doped colloidal semiconductor quantum wells for luminescent solar concentrators. *Advanced Materials* **2017,** *29* (30), 1700821.

58. Delikanli, S.; Akgul, M. Z.; Murphy, J. R.; Barman, B.; Tsai, Y.; Scrace, T.; Zhang, P.; Bozok, B.; Hernández-Martínez, P. L.; Christodoulides, J., Mn^{2+}-doped CdSe/CdS core/multishell colloidal quantum wells enabling tunable carrier–dopant exchange interactions. *ACS Nano* **2015,** *9* (12), 12473-12479.

59. Thompson, M. J.; Blakeney, K. J.; Cady, S. D.; Reichert, M. D.; Pilar-Albaladejo, J. D.; White, S. T.; Vela, J., Cu_2ZnSnS_4 nanorods doped with tetrahedral, high spin transition metal ions: Mn^{2+}, Co^{2+}, and Ni^{2+}. *Chemistry of Materials* **2016,** *28* (6), 1668-1677.

60. Fainblat, R.; Muckel, F.; Barrows, C. J.; Vlaskin, V. A.; Gamelin, D. R.; Bacher, G., Valence-band mixing effects in the upper-excited-state magneto-optical responses of colloidal Mn^{2+}-doped CdSe quantum dots. *ACS Nano* **2014,** *8* (12), 12669-12675.

61. Santra, P. K.; Kamat, P. V., Mn-doped quantum dot sensitized solar cells: a strategy to boost efficiency over 5%. *Journal of the American Chemical Society* **2012,** *134* (5), 2508-2511.

62. Sharma, M.; Olutas, M.; Yeltik, A.; Kelestemur, Y.; Sharma, A.; Delikanli, S.; Guzelturk, B.; Gungor, K.; McBride, J. R.; Demir, H. V., Understanding the journey of dopant copper ions in atomically flat colloidal nanocrystals of CdSe nanoplatelets using partial cation exchange reactions. *Chemistry of Materials* **2018,** *30* (10), 3265-3275.

63. Shi, R.; Cao, Y.; Bao, Y.; Zhao, Y.; Waterhouse, G. I.; Fang, Z.; Wu, L. Z.; Tung, C. H.; Yin, Y.; Zhang, T., Self-assembled Au/CdSe nanocrystal clusters for plasmon-mediated photocatalytic hydrogen evolution. *Advanced Materials* **2017,** *29* (27), 1700803.

64. Regulacio, M. D.; Han, M.-Y., Multinary I-III-VI_2 and I_2-II-IV-VI_4 semiconductor nanostructures for photocatalytic applications. *Accounts of Chemical Research* **2016,** *49* (3), 511-519.

65. Ben-Shahar, Y.; Scotognella, F.; Kriegel, I.; Moretti, L.; Cerullo, G.; Rabani, E.; Banin, U., Optimal metal domain size for photocatalysis with hybrid semiconductor-metal nanorods. *Nature Communications* **2016,** *7*, 10413.

66. Qiu, F.; Han, Z.; Peterson, J. J.; Odoi, M. Y.; Sowers, K. L.; Krauss, T. D., Photocatalytic hydrogen generation by CdSe/CdS nanoparticles. *Nano Letters* **2016,** *16* (9), 5347-5352.

67. Hu, L.; Zhao, Y. L.; Ryu, K.; Zhou, C.; Stoddart, J. F.; Grüner, G., Light-induced charge transfer in pyrene/CdSe-SWNT hybrids. *Advanced Materials* **2008,** *20* (5), 939-946.

68. Chen, T.; Liu, Y., *Semiconductor nanocrystals and metal nanoparticles: physical properties and device applications*. CRC Press: 2016.

69. Capitani, C.; Pinchetti, V.; Gariano, G.; Santiago-González, B.; Santambrogio, C.; Prato, M.; Brescia, R.; Camellini, A.; Bellato, F.; Carulli, F., Quantized electronic doping towards atomically controlled 'charge-engineered' semiconductor nanocrystals. *Nano Letters* **2019**.

70. Efros, A. L.; Lockwood, D. J.; Tsybeskov, L., *Semiconductor nanocrystals: from basic principles to applications*. Springer Science & Business Media: 2013.

71. Polavarapu, L.; Nickel, B.; Feldmann, J.; Urban, A. S., Advances in quantum-confined perovskite nanocrystals for optoelectronics. *Advanced Energy Materials* **2017,** *7* (16), 1700267.

72. Erwin, S. C.; Zu, L.; Haftel, M. I.; Efros, A. L.; Kennedy, T. A.; Norris, D. J., Doping semiconductor nanocrystals. *Nature* **2005,** *436* (7047), 91.

73. Mocatta, D.; Cohen, G.; Schattner, J.; Millo, O.; Rabani, E.; Banin, U., Heavily doped semiconductor nanocrystal quantum dots. *Science* **2011,** *332* (6025), 77-81.

74. Kershaw, S. V.; Jing, L.; Huang, X.; Gao, M.; Rogach, A. L., Materials aspects of semiconductor nanocrystals for optoelectronic applications. *Materials Horizons* **2017,** *4* (2), 155-205.

75. Guo, Q.; Yao, Y.; Luo, Z.-C.; Qin, Z.; Xie, G.; Liu, M.; Kang, J.; Zhang, S.; Bi, G.; Liu, X., Universal near-infrared and mid-infrared optical modulation for ultrafast pulse generation enabled by colloidal plasmonic semiconductor nanocrystals. *ACS Nano* **2016,** *10* (10), 9463-9469.

76. Baimuratov, A. S.; Pereziabova, T. P.; Zhu, W.; Leonov, M. Y.; Baranov, A. V.; Fedorov, A. V.; Rukhlenko, I. D., Optical anisotropy of topologically distorted semiconductor nanocrystals. *Nano Letters* **2017,** *17* (9), 5514-5520.

77. Zhong, H.; Bai, Z.; Zou, B., Tuning the luminescence properties of

colloidal I–III–VI semiconductor nanocrystals for optoelectronics and biotechnology applications. *The Journal of Physical Chemistry Letters* **2012,** *3* (21), 3167-3175.

78. Konstantatos, G.; Sargent, E. H., *Colloidal quantum dot optoelectronics and photovoltaics*. Cambridge University Press: 2013.

79. Murray, C.; Norris, D. J.; Bawendi, M. G., Synthesis and characterization of nearly monodisperse CdE (E=sulfur, selenium, tellurium) semiconductor nanocrystallites. *Journal of the American Chemical Society* **1993,** *115* (19), 8706-8715.

80. Peng, Z. A.; Peng, X., Formation of high-quality CdTe, CdSe, and CdS nanocrystals using CdO as precursor. *Journal of the American Chemical Society* **2001,** *123* (1), 183-184.

81. Trindade, T.; O'Brien, P.; Zhang, X.-m., Synthesis of CdS and CdSe nanocrystallites using a novel single-molecule precursors approach. *Chemistry of Materials* **1997,** *9* (2), 523-530.

82. Joo, J.; Son, J. S.; Kwon, S. G.; Yu, J. H.; Hyeon, T., Low-temperature solution-phase synthesis of quantum well structured CdSe nanoribbons. *Journal of the American Chemical Society* **2006,** *128* (17), 5632-3.

83. Katari, J. B.; Colvin, V. L.; Alivisatos, A. P., X-ray photoelectron spectroscopy of CdSe nanocrystals with applications to studies of the nanocrystal surface. *The Journal of Physical Chemistry* **1994,** *98* (15), 4109-4117.

84. Manna, L.; Scher, E. C.; Alivisatos, A. P., Synthesis of soluble and processable rod-, arrow-, teardrop-, and tetrapod-shaped CdSe nanocrystals. *Journal of the American Chemical Society* **2000,** *122* (51), 12700-12706.

85. Hines, M. A.; Guyot-Sionnest, P., Bright UV-blue luminescent colloidal ZnSe nanocrystals. *The Journal of Physical Chemistry B* **1998,** *102* (19), 3655-3657.

86. Peng, X.; Wickham, J.; Alivisatos, A., Kinetics of II-VI and III-V colloidal semiconductor nanocrystal growth:“focusing” of size distributions. *Journal of the American Chemical Society* **1998,** *120* (21), 5343-5344.

87. Peng, X.; Manna, L.; Yang, W.; Wickham, J.; Scher, E.; Kadavanich, A.; Alivisatos, A. P., Shape control of CdSe nanocrystals. *Nature* **2000,** *404* (6773), 59.

88. Pan, D.; An, L.; Sun, Z.; Hou, W.; Yang, Y.; Yang, Z.; Lu, Y., Synthesis of Cu−In−S ternary nanocrystals with tunable structure and composition. *Journal of the American Chemical Society* **2008,** *130* (17), 5620-5621.

89. Shen, H.; Wang, H.; Li, X.; Niu, J. Z.; Wang, H.; Chen, X.; Li, L. S., Phosphine-free synthesis of high quality ZnSe, ZnSe/ZnS, and Cu-, Mn-doped ZnSe nanocrystals. *Dalton Transactions* **2009,** (47), 10534-10540.

90. García-Rodríguez, R. l.; Liu, H., Mechanistic insights into the role of alkylamine in the synthesis of CdSe nanocrystals. *Journal of the American Chemical Society* **2014,** *136* (5), 1968-1975.

91. Li, L. S.; Pradhan, N.; Wang, Y.; Peng, X., High quality ZnSe and ZnS nanocrystals formed by activating zinc carboxylate precursors. *Nano Letters* **2004,** *4* (11), 2261-2264.

92. Xie, R.; Battaglia, D.; Peng, X., Colloidal InP nanocrystals as efficient emitters covering blue to near-infrared. *Journal of the American Chemical Society* **2007,** *129* (50), 15432-15433.

93. Sun, M.; Yang, X., Phosphine-free synthesis of high-quality CdSe nanocrystals in noncoordination solvents:“activating agent” and “nucleating agent” controlled nucleation and growth. *The Journal of Physical Chemistry C* **2009,** *113* (20), 8701-8709.

94. Gao, Y.; Yang, H.; Zhang, Y.; Li, J.; Zhao, H.; Feng, J.; Sun, J.; Zheng, Z., Facile non-injection synthesis of high quality CZTS nanocrystals. *RSC Advances* **2014,** *4* (34), 17667-17670.

95. Gao, Y.; Peng, X., Crystal structure control of CdSe nanocrystals in growth and nucleation: dominating effects of surface versus interior structure. *Journal of the American Chemical Society* **2014,** *136* (18), 6724-6732.

96. Reiss, P.; Bleuse, J.; Pron, A., Highly luminescent CdSe/ZnSe core/shell nanocrystals of low size dispersion. *Nano Letters* **2002,** *2* (7), 781-784.

97. Lim, S. J.; Kim, W.; Shin, S. K., Surface-dependent, ligand-mediated photochemical etching of CdSe nanoplatelets. *Journal of the American Chemical Society* **2012,** *134* (18), 7576-7579.

98. Joo, J.; Na, H. B.; Yu, T.; Yu, J. H.; Kim, Y. W.; Wu, F.; Zhang, J. Z.; Hyeon, T., Generalized and facile synthesis of semiconducting metal sulfide nanocrystals. *Journal of the American Chemical Society* **2003,** *125* (36), 11100-11105.

99. Sun, Z.; Oyanagi, H.; Nakamura, H.; Jiang, Y.; Zhang, L.; Uehara, M.; Yamashita, K.; Fukano, A.; Maeda, H., Ligand effects of amine on the initial nucleation and growth processes of CdSe nanocrystals. *The Journal of Physical Chemistry C* **2010,** *114* (22), 10126-10131.

100. Bullen, C. R.; Mulvaney, P., Nucleation and growth kinetics of CdSe nanocrystals in octadecene. *Nano Letters* **2004,** *4* (12), 2303-2307.

101. Li, Y.; Pu, C.; Peng, X., Surface activation of colloidal indium phosphide nanocrystals. *Nano Research* **2017,** *10* (3), 941-958.

102. Park, J.; An, K.; Hwang, Y.; Park, J.-G.; Noh, H.-J.; Kim, J.-Y.; Park, J.-H.; Hwang, N.-M.; Hyeon, T., Ultra-large-scale syntheses of monodisperse nanocrystals. *Nature Materials* **2004,** *3* (12), 891.

103. LaMer, V. K.; Dinegar, R. H., Theory, production and mechanism of formation of monodispersed hydrosols. *Journal of the American Chemical Society* **1950,** *72* (11), 4847-4854.

104. Zhou, J.; Pu, C.; Jiao, T.; Hou, X.; Peng, X., A two-step synthetic strategy toward monodisperse colloidal CdSe and CdSe/CdS core/shell nanocrystals. *Journal of the American Chemical Society* **2016,** *138* (20), 6475-6483.

105. Tan, R.; Yuan, Y.; Nagaoka, Y.; Eggert, D.; Wang, X.; Thota, S.; Guo, P.; Yang, H.; Zhao, J.; Chen, O., Monodisperse hexagonal pyramidal and bipyramidal wurtzite CdSe-CdS core–shell nanocrystals. *Chemistry of Materials* **2017,** *29* (9), 4097-4108.

106. Li, J.; Wang, H.; Lin, L.; Fang, Q.; Peng, X., Quantitative identification of basic growth channels for formation of monodisperse nanocrystals. *Journal of the American Chemical Society* **2018,** *140* (16), 5474-5484.

107. van Embden, J.; Chesman, A. S.; Jasieniak, J. J., The heat-up synthesis of colloidal nanocrystals. *Chemistry of Materials* **2015,** *27* (7), 2246-2285.

108. Kwon, S. G.; Hyeon, T., Formation mechanisms of uniform nanocrystals via hot-injection and heat-up methods. *Small* **2011,** *7* (19), 2685-2702.

109. Dias, S.; Kumawat, K. L.; Biswas, S.; Krupanidhi, S., Heat-up synthesis of Cu_2SnS_3 quantum dots for near infrared photodetection. *RSC Advances* **2017,** *7* (38), 23301-23308.

110. Gong, F.; Tian, S.; Liu, B.; Xiong, D.; Zhao, X., Oleic acid assisted formation mechanism of $CuInS_2$ nanocrystals with tunable structures. *RSC Advances* **2014,** *4* (69), 36875-36881.

111. Son, J. S.; Wen, X. D.; Joo, J.; Chae, J.; Baek, S. I.; Park, K.; Kim, J. H.; An, K.; Yu, J. H.; Kwon, S. G.; Choi, S. H.; Wang, Z.; Kim, Y. W.; Kuk, Y.; Hoffmann, R.; Hyeon, T., Large-scale soft colloidal template synthesis of 1.4 nm thick CdSe nanosheets. *Angewandte Chemie International Edition* **2009,** *48* (37), 6861-6864.

112. Zhou, Y.; Jiang, R.; Wang, Y.; Rohrs, H. W.; Rath, N. P.; Buhro, W. E., Isolation of amine derivatives of $(ZnSe)_{34}$ and $(CdTe)_{34}$. Spectroscopic comparisons of the $(II–VI)_{13}$ and $(II–VI)_{34}$ magic-size nanoclusters. *Inorganic Chemistry* **2019,** *58* (3), 1815-1825.

113. Chen, Y.; Chen, D.; Li, Z.; Peng, X., Symmetry-breaking for formation of rectangular CdSe two-dimensional nanocrystals in zinc-blende structure. *Journal of the American Chemical Society* **2017,** *139* (29), 10009-10019.

114. Schliehe, C.; Juarez, B. H.; Pelletier, M.; Jander, S.; Greshnykh, D.; Nagel, M.; Meyer, A.; Foerster, S.; Kornowski, A.; Klinke, C., Ultrathin PbS sheets by two-dimensional oriented attachment. *Science* **2010,** *329* (5991), 550-553.

115. Pradhan, N.; Xu, H.; Peng, X., Colloidal CdSe quantum wires by oriented attachment. *Nano Letters* **2006,** *6* (4), 720-724.

116. Yong, K.-T.; Sahoo, Y.; Zeng, H.; Swihart, M. T.; Minter, J. R.; Prasad, P. N., Formation of ZnTe nanowires by oriented attachment. *Chemistry of Materials* **2007,** *19* (17), 4108-4110.

117. Zhang, H.; Banfield, J. F., Energy calculations predict nanoparticle attachment orientations and asymmetric crystal formation. *The Journal of Physical Chemistry Letters* **2012,** *3* (19), 2882-2886.

118. Zhang, J.; Rowland, C.; Liu, Y.; Xiong, H.; Kwon, S.; Shevchenko, E.; Schaller, R. D.; Prakapenka, V. B.; Tkachev, S.; Rajh, T., Evolution of self-assembled ZnTe magic-sized nanoclusters. *Journal of the American Chemical Society* **2015,** *137* (2), 742-749.

119. Panda, A. B.; Acharya, S.; Efrima, S.; Golan, Y., Synthesis, assembly, and optical properties of shape-and phase-controlled ZnSe nanostructures. *Langmuir* **2007,** *23* (2), 765-770.

120. Green, M., A new approach to the formal classification of covalent compounds of the elements. *Journal of Organometallic Chemistry* **1995,** *500* (1-2), 127-148.

121. Anderson, N. C.; Hendricks, M. P.; Choi, J. J.; Owen, J. S., Ligand

exchange and the stoichiometry of metal chalcogenide nanocrystals: spectroscopic observation of facile metal-carboxylate displacement and binding. *Journal of the American Chemical Society* **2013,** *135* (49), 18536-18548.

122. Houtepen, A. J.; Hens, Z.; Owen, J. S.; Infante, I., On the origin of surface traps in colloidal II–VI semiconductor nanocrystals. *Chemistry of Materials* **2017,** *29* (2), 752-761.

123. Zhou, J.; Zhu, M.; Meng, R.; Qin, H.; Peng, X., Ideal CdSe/CdS core/shell nanocrystals enabled by entropic ligands and their core size-, shell thickness-, and ligand-dependent photoluminescence properties. *Journal of the American Chemical Society* **2017,** *139* (46), 16556-16567.

124. Rossinelli, A. A.; Riedinger, A.; Marqués-Gallego, P.; Knüsel, P. N.; Antolinez, F. V.; Norris, D. J., High-temperature growth of thick-shell CdSe/CdS core/shell nanoplatelets. *Chemical Communications* **2017,** *53* (71), 9938-9941.

125. Chen, O.; Zhao, J.; Chauhan, V. P.; Cui, J.; Wong, C.; Harris, D. K.; Wei, H.; Han, H.-S.; Fukumura, D.; Jain, R. K., Compact high-quality CdSe–CdS core–shell nanocrystals with narrow emission linewidths and suppressed blinking. *Nature Materials* **2013,** *12* (5), 445.

126. Talapin, D. V.; Mekis, I.; Götzinger, S.; Kornowski, A.; Benson, O.; Weller, H., CdSe/CdS/ZnS and CdSe/ZnSe/ZnS core−shell−shell nanocrystals. *The Journal of Physical Chemistry B* **2004,** *108* (49), 18826-18831.

127. Peng, X.; Schlamp, M. C.; Kadavanich, A. V.; Alivisatos, A. P., Epitaxial growth of highly luminescent CdSe/CdS core/shell nanocrystals with photostability and electronic accessibility. *Journal of the American Chemical Society* **1997,** *119* (30), 7019-7029.

128. Reiss, P.; Protiere, M.; Li, L., Core/shell semiconductor nanocrystals. *Small* **2009,** *5* (2), 154-168.

129. Kim, S.; Fisher, B.; Eisler, H.-J.; Bawendi, M., Type-II quantum dots: CdTe/CdSe (core/shell) and CdSe/ZnTe (core/shell) heterostructures. *Journal of the American Chemical Society* **2003,** *125* (38), 11466-11467.

130. Pu, C.; Peng, X., To battle surface traps on CdSe/CdS core/shell nanocrystals: shell isolation versus surface treatment. *Journal of the American Chemical Society* **2016,** *138* (26), 8134-8142.

131. Vaxenburg, R.; Rodina, A.; Lifshitz, E.; Efros, A. L., Biexciton auger recombination in CdSe/CdS core/shell semiconductor nanocrystals. *Nano Letters* **2016,** *16* (4), 2503-2511.

132. Kai, S.; Xi, B.; Wang, Y.; Xiong, S., One-pot synthesis of size-controllable core–shell CdS and derived CdS@$Zn_xCd_{1-x}S$ structures for photocatalytic hydrogen production. *Chemistry–A European Journal* **2017,** *23* (65), 16653-16659.

133. Lohmann, S.-H.; Harder, P.; Bourier, F.; Strelow, C.; Mews, A.; Kipp, T., Influence of interface-driven strain on the spectral diffusion properties of core/shell CdSe/CdS dot/rod nanoparticles. *The Journal of Physical Chemistry C* **2019**.

134. Li, Z.-J.; Hofman, E.; Blaker, A.; Davis, A. H.; Dzikovski, B.; Ma, D.-K.; Zheng, W., Interface engineering of Mn-doped ZnSe-based core/shell nanowires for tunable host–dopant coupling. *ACS Nano* **2017,** *11* (12), 12591-12600.

135. Sowers, K. L.; Swartz, B.; Krauss, T. D., Chemical mechanisms of semiconductor nanocrystal synthesis. *Chemistry of Materials* **2013,** *25* (8), 1351-1362.

136. Maiti, S.; Debnath, T.; Maity, P.; Ghosh, H. N., Tuning the charge carrier dynamics via interfacial alloying in core/shell CdTe/ZnSe NCs. *The Journal of Physical Chemistry C* **2016,** *120* (3), 1918-1925.

137. Hofman, E.; Robinson, R. J.; Li, Z.-J.; Dzikovski, B.; Zheng, W., Controlled dopant migration in CdS/ZnS core/shell quantum dots. *Journal of the American Chemical Society* **2017,** *139* (26), 8878-8885.

138. Kudera, S.; Zanella, M.; Giannini, C.; Rizzo, A.; Li, Y.; Gigli, G.; Cingolani, R.; Ciccarella, G.; Spahl, W.; Parak, W. J.; Manna, L., Sequential growth of magic-size CdSe nanocrystals. *Advanced Materials* **2007,** *19* (4), 548-552.

139. Yang, Y.; Qin, H.; Jiang, M.; Lin, L.; Fu, T.; Dai, X.; Zhang, Z.; Niu, Y.; Cao, H.; Jin, Y.; Zhao, F.; Peng, X., Entropic ligands for nanocrystals: from unexpected solution properties to outstanding processability. *Nano Letters* **2016,** *16* (4), 2133-2138.

140. Yang, Y.; Qin, H.; Peng, X., Intramolecular entropy and size-dependent solution properties of nanocrystal–ligands complexes. *Nano Letters* **2016,** *16* (4), 2127-2132.

141. Pein, B. C.; Chang, W.; Hwang, H. Y.; Scherer, J.; Coropceanu, I.; Zhao, X.; Zhang, X.; Bulovic, V.; Bawendi, M.; Nelson, K. A., Terahertz-driven luminescence and colossal Stark effect in CdSe–CdS colloidal quantum dots. *Nano Letters* **2017,** *17* (9), 5375-5380.

142. Pinchetti, V.; Meinardi, F.; Camellini, A.; Sirigu, G.; Christodoulou, S.; Bae, W. K.; De Donato, F.; Manna, L.; Zavelani-Rossi, M.; Moreels, I., Effect of core/shell interface on carrier dynamics and optical gain properties of dual-color emitting CdSe/CdS nanocrystals. *ACS Nano* **2016,** *10* (7), 6877-6887.

143. Niu, Y.; Pu, C.; Lai, R.; Meng, R.; Lin, W.; Qin, H.; Peng, X., One-pot/three-step synthesis of zinc-blende CdSe/CdS core/shell nanocrystals with thick shells. *Nano Research* **2017,** *10* (4), 1149-1162.

144. Shen, W.; Tang, H.; Yang, X.; Cao, Z.; Cheng, T.; Wang, X.; Tan, Z.; You, J.; Deng, Z., Synthesis of highly fluorescent InP/ZnS small-core/thick-shell tetrahedral-shaped quantum dots for blue light-emitting diodes. *Journal of Materials Chemistry C* **2017,** *5* (32), 8243-8249.

145. Yang, S. J.; Oh, J. H.; Kim, S.; Yang, H.; Do, Y. R., Realization of InP/ZnS quantum dots for green, amber and red down-converted LEDs and their color-tunable, four-package white LEDs. *Journal of Materials Chemistry C* **2015,** *3* (15), 3582-3591.

146. Li, Y.; Hou, X.; Dai, X.; Yao, Z.; Lv, L.; Jin, Y.; Peng, X., Stoichiometry-controlled InP-based quantum dots: synthesis, photoluminescence, and electroluminescence. *Journal of the American Chemical Society* **2019,** *141* (16), 6448-6452.

147. Mastria, R.; Rizzo, A., Mastering heterostructured colloidal nanocrystal properties for light-emitting diodes and solar cells. *Journal of Materials Chemistry C* **2016,** *4* (27), 6430-6446.

148. Brus, L. E., Electron–electron and electron-hole interactions in small semiconductor crystallites: the size dependence of the lowest excited electronic state. *The Journal of Chemical Physics* **1984,** *80* (9), 4403-4409.

149. El-Sayed, M. A., Small is different: shape-, size-, and composition-dependent properties of some colloidal semiconductor nanocrystals. *Accounts of Chemical Research* **2004,** *37* (5), 326-333.

150. Liu, Y.-H.; Wayman, V. L.; Gibbons, P. C.; Loomis, R. A.; Buhro, W. E., Origin of high photoluminescence efficiencies in CdSe quantum belts. *Nano*

Letters **2009,** *10* (1), 352-357.

151. Thibert, A.; Frame, F. A.; Busby, E.; Larsen, D. S., Primary photodynamics of water-solubilized two-dimensional CdSe nanoribbons. *The Journal of Physical Chemistry C* **2011,** *115* (40), 19647-19658.

152. Yang, J.; Son, J. S.; Yu, J. H.; Joo, J.; Hyeon, T., Advances in the colloidal synthesis of two-dimensional semiconductor nanoribbons. *Chemistry of Materials* **2013,** *25* (8), 1190-1198.

153. Olutas, M.; Guzelturk, B.; Kelestemur, Y.; Yeltik, A.; Delikanli, S.; Demir, H. V., Lateral size-dependent spontaneous and stimulated emission properties in colloidal CdSe nanoplatelets. *ACS Nano* **2015,** *9* (5), 5041-5050.

154. Jana, S.; Phan, T. N.; Bouet, C.; Tessier, M. D.; Davidson, P.; Dubertret, B.; Abécassis, B., Stacking and colloidal stability of CdSe nanoplatelets. *Langmuir* **2015,** *31* (38), 10532-10539.

155. Guzelturk, B.; Kelestemur, Y.; Olutas, M.; Delikanli, S.; Demir, H. V., Amplified spontaneous emission and lasing in colloidal nanoplatelets. *ACS Nano* **2014,** *8* (7), 6599-6605.

156. Jana, S.; Davidson, P.; Abécassis, B., CdSe nanoplatelets: living polymers. *Angewandte Chemie* **2016,** *128* (32), 9517-9520.

157. Delikanli, S.; Guzelturk, B.; Hernández-Martínez, P. L.; Erdem, T.; Kelestemur, Y.; Olutas, M.; Akgul, M. Z.; Demir, H. V., Continuously tunable emission in inverted type-I CdS/CdSe core/crown semiconductor nanoplatelets. *Advanced Functional Materials* **2015,** *25* (27), 4282-4289.

158. Li, Z.; Peng, X., Size/shape-controlled synthesis of colloidal CdSe quantum disks: ligand and temperature effects. *Journal of the American Chemical Society* **2011,** *133* (17), 6578-6586.

159. Li, Z.; Qin, H.; Guzun, D.; Benamara, M.; Salamo, G.; Peng, X., Uniform thickness and colloidal-stable CdS quantum disks with tunable thickness: Synthesis and properties. *Nano Research* **2012,** *5* (5), 337-351.

160. Wang, Y.; Liu, Y.-H.; Zhang, Y.; Wang, F.; Kowalski, P. J.; Rohrs, H. W.; Loomis, R. A.; Gross, M. L.; Buhro, W. E., Isolation of the magic-size CdSe nanoclusters $(CdSe)_{13}$(n-octylamine)$_{13}$ and $(CdSe)_{13}$(oleylamine)$_{13}$. *Angewandte Chemie International Edition* **2012,** *51* (25), 6154-6157.

161. Park, H.; Chung, H.; Kim, W., Synthesis of ultrathin wurtzite ZnSe nanosheets. *Materials Letters* **2013,** *99*, 172-175.

162. Ithurria, S.; Dubertret, B., Quasi 2D colloidal CdSe platelets with thicknesses controlled at the atomic level. *Journal of the American Chemical Society* **2008,** *130* (49), 16504-5.

163. Riedinger, A.; Ott, F. D.; Mule, A.; Mazzotti, S.; Knüsel, P. N.; Kress, S. J.; Prins, F.; Erwin, S. C.; Norris, D. J., An intrinsic growth instability in isotropic materials leads to quasi-two-dimensional nanoplatelets. *Nature Materials* **2017,** *16* (7), 743.

Chapter 2 Material characterization techniques and analysis methods

Chapter two introduces the material characterization techniques and analysis methods, including UV-vis spectroscopy, nuclear magnetic resonance (NMR) spectroscopy, Fourier-transform infrared (FTIR) spectroscopy, transmission electron microscopy (TEM), X-ray photoelectron spectroscopy (XPS), powder X-ray diffraction (XRD) and density function theory (DFT) calculation.

2.1 UV-vis spectroscopy

UV-vis absorption spectroscopy is the principal research technique employed to record the absorbance spectra of a compound in solution. Herein, we used a Cary 4000 UV−vis spectrophotometer. The spectrometer is equipped with a mercury light source and measurements were made with 1 nm resolution and step of 0.1 nm between 200 and 800 nm. Diluted samples were loaded into polished quartz cuvettes for analysis. Purified samples were taken directly from a glovebox using airtight quartz cuvettes. The schematic illustration of the experimental setup is shown in Figure 2.1. The beam from the mercury light source is split through a monochromators and passes through a series of mirrors and the reference and sample. Then the photodetector measures the difference in energy of the transmitted beam from the reference and the sample.

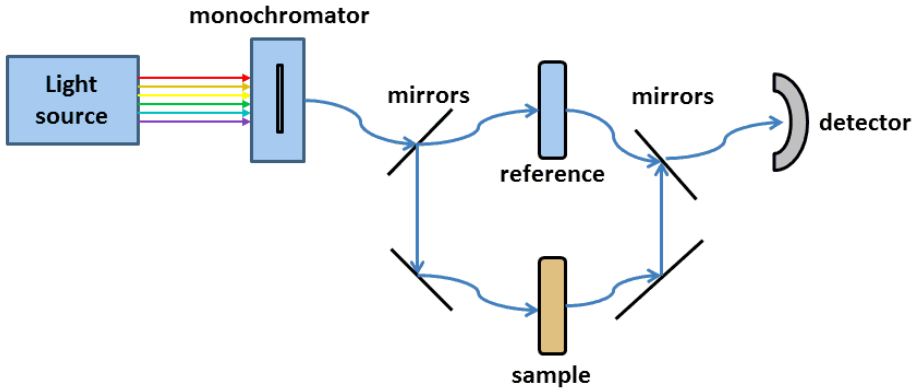

Figure 2.1 The schematic illustration of an UV-vis spectrometer.

2.2 Photoluminescence spectroscopy

PL spectra were measured using a Hitachi F-7000 fluorimeter. Diluted samples were loaded into polished quartz cuvettes for analysis. Purified samples were taken directly from a glovebox using airtight quartz cuvettes. Figure 2.2 presents the schematic illustration of a photoluminescence (PL) spectrometer.

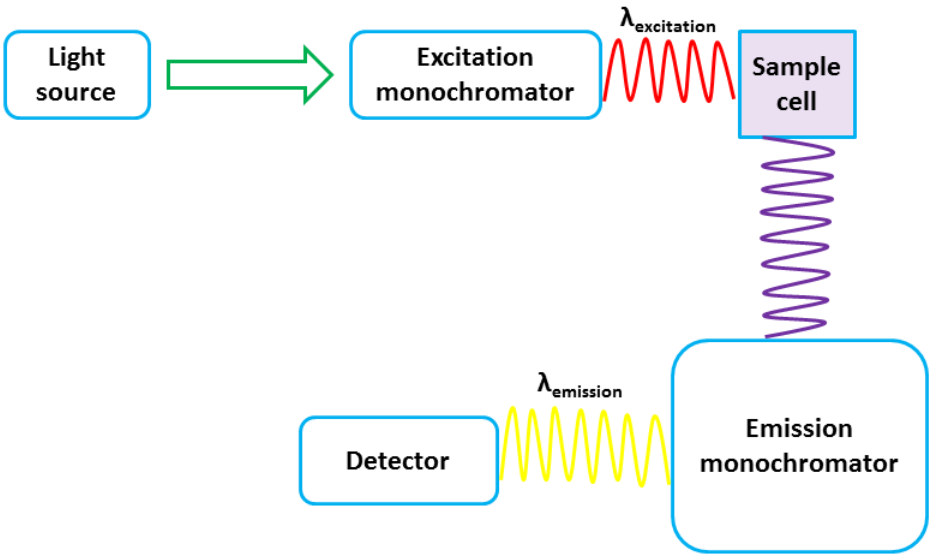

Figure 2.2 The schematic illustration of photoluminescence spectrometer.

2.3 Nuclear magnetic resonance (NMR) spectroscopy

The principle of NMR spectroscopy is shown in Figure 2.3. NMR spectroscopy is commonly used to determine the molecular structure of organic compounds. The theory behind NMR is that the nuclei of atoms can line up with or against external magnetic field by spinning clockwise or counter clockwise as shown in Figure 2.4. Solution ^{1}H and ^{31}P NMR spectroscopy was conducted on a Bruker Avance III 500 MHz spectrometers. NMR samples were prepared in $CDCl_3$. Chemical shift values are given in ppm. ^{1}H NMR spectra were measured with sufficient relaxation delay to enable complete relaxation between pulses.

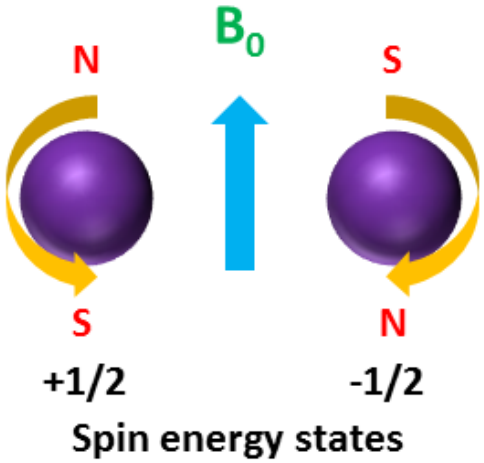

Figure 2.3 The principle of NMR spectroscopy.

2.4 TEM, HRTEM, SAED, HAADF-STEM, and STEM-EDX analysis

Low-resolution transmission electron microscopy (TEM) was conducted with a JEOL 2100 Model TEM as shown in Figure 2.4 with an accelerating voltage of 120 kV. High-resolution TEM (HRTEM), high angle annular dark field-scanning transmission electron microscopy (HAADF-STEM), selected area electron diffraction (SAED) and STEM-energy-dispersive X-ray spectroscopy (STEM-EDX) were conducted on a FEI Titan G2 80-200 Model TEM (Figure 2.5) operating at 200 kV. Fast Fourier transform (FFT) technique was employed on HRTEM images to analyze their crystalline orientation regarding their shape.

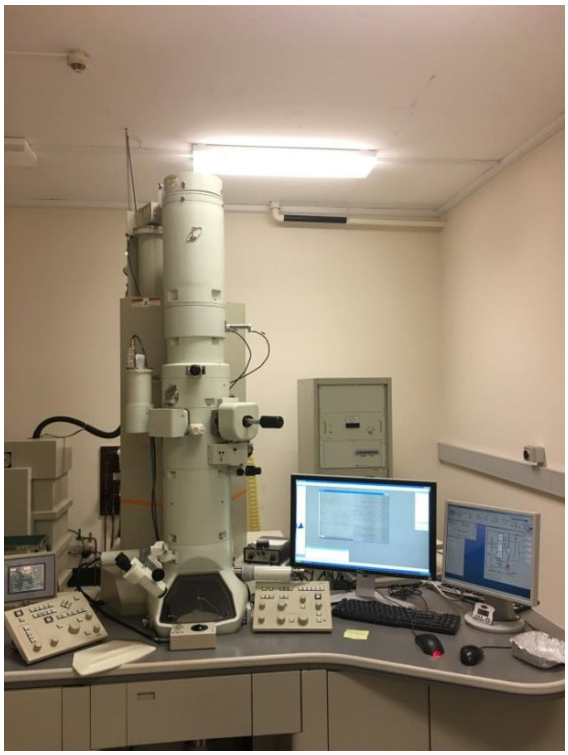

Figure 2.4 The digital photograph of JEOL 2100 Model TEM.

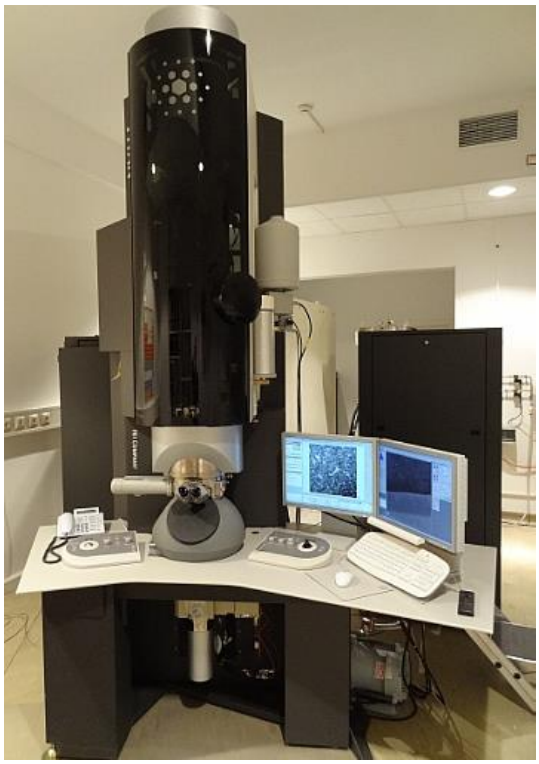

Figure 2.5 The digital photograph of FEI Titan G2 80-200 Model TEM

2.5 X-ray diffraction (XRD) principle and analysis

Figure 2.6 shows the principle of XRD based on the famous Bragg's Law. The interference pattern of the X-rays scattered by the crystals is explained by the formula $n\lambda = 2d_{hkl}\sin\theta$. λ is the wavelength of the incident X-ray; n is positive integer; d_{hkl} is the interplanar spacing of the crystal.

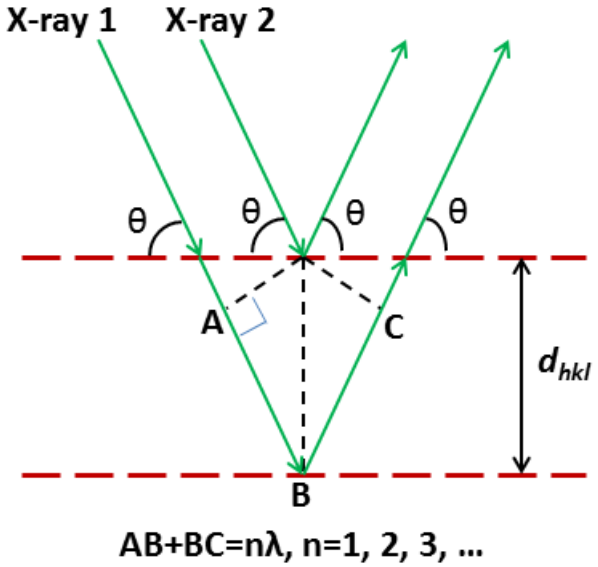

Figure 2.6 The illustration of the Bragg's Law.

After purification, samples of CSNCs were concentrated in toluene or chloroform and then were drop-casted on a <100> Si wafer. The solvent was allowed to evaporate to obtain powder sample. This was repeated for several repetitions until visible surface coverage was achieved. Powder X-ray diffraction (p-XRD) patterns were obtained with an X'per PRO (PANalytical) X-ray diffractometer equipped with a rotating anode and a Cu Kα (λ=1.5406 Å) operated at 40 kV and 40 mA. The size of CSNCs can be determined by the Scherrer equation[1-2]

$$\tau = K\lambda/\beta\cos\vartheta$$

where τ is the mean size of the ordered or crystalline domains, which is smaller or equal to the grain size; λ is the X-ray wavelength; *K* is known as the dimensionless shape factor or Scherrer constant with a value close to 0.9; β is the line broadening at full wavelength at the half the maximum (FWHM) intensity after deducting the instrumental line broadening with unit in radians; ϑ is the Bragg

angle. In terms of CSNCs with size less than 20 nm, diffraction peak broadening is considerably ordered due to the reduced crystalline size. Nevertheless the selected area electron diffraction (SAED) technique is more accurate for estimating the crystal structure of particularly tiny CSNCs due to its ability to isolate the diffraction pattern of a single crystal.

2.6 Fourier-transform infrared spectroscopy (FTIR)

Fourier-transform infrared spectroscopy (FTIR) is a spectroscopic analysis technique to record the infrared absorption spectrum of substance.

The infrared vibrational modes in a molecule are described by the anharmonic oscillator model. The frequencies *v* of basic bending and stretching modes are deduced from the following formula:

$$v = 1303\sqrt{\frac{F}{\mu}}, \quad \mu = \frac{1}{\mu_1} + \frac{1}{\mu_2}$$

where *F* is force constant; μ_1 and μ_1 are masses of involved atoms.

The infrared spectrum are divided into five major regions of interest (ROI), i.e. below 1000 cm^{-1} (out of plane modes, such as C-X: X=Cl, Br, I and heavier atoms), 1000-1500 cm^{-1} (E-X single bonds: E=B, C, N, O, deformation, rocking modes), 1500-2000 cm^{-1} (E-X double bonds: E=X=C, N, O), 2000-2700 cm^{-1} (E-X triple bonds: E=X=C, N, O), 2700-4000 cm^{-1} (E-H stretching, E=B, C, N, O). The molecule must have a net change in dipole moment when it absorbing infrared radiation, which results in vibrational or rotational motion. These vibrations are subdivided into two categories according to whether the bond length and bond angle are changing, i.e. bending (scissoring, rocking, wagging and twisting) and stretching (symmetric and asymmetric).

2.7 X-ray photoelectron spectroscopy (XPS)

X-ray photoelectron spectroscopy is a surface-sensitive quantitative spectroscopic analysis technique to investigate elemental composition at the chemical states and electronic states of the elements. XPS spectrum is recorded by illuminating samples with a beam of X-rays and measuring the number and kinetic energy of electrons that escape from the surface of samples. XPS can be used to analyse the elemental composition of the sample surface from top 0 to 10 nm.

2.8 Density functional theory (DFT)

The first-principles pseudo potential method and the first-principles method

based on the density function theory (DFT) are employed to investigate the surface energy of ZnTe NPLs. The DFT calculations were performed by the Vienna *Ab Initio* Simulation Package code with the projector-augmented wave method using the Perdew-Burke-Ernzerhof exchange-correlation functional.

The Projector-augmented wave (PAW) method is a technique employed for *Ab Initio* electronic structure calculations. This is a generalization of the pseudopotential and linear augmented-plane-wave methods, which enables DFT calculation with greater computational efficiency.[3]

Local-density approximations (LDA) are approximations to the exchage-correlation (XC) energy functional for DFT calculation which only depends on the value of the electronic density at each point in space. A local-density approximation for the exchange-correlation energy in a spin-unpolarized system is

$$E_{\mathrm{xc}}^{\mathrm{LDA}}|\rho| = \int \rho(\boldsymbol{r})\epsilon_{\mathrm{xc}}\big(\rho(\boldsymbol{r})\big)\mathrm{d}\boldsymbol{r}\,,$$

where ϵ_{xc} and ρ are the exchange-correlation energy per particle of a homogeneneous electron gas of charge density and the electronic density, respectively. The exchange-correlation energy can be further decomposed into correlation and exchange terms expressed as

$$E_{\mathrm{xc}} = E_{\mathrm{x}} + E_{\mathrm{c}}\,,$$

where the separate expressions for E_{x} and E_{c} can be sought. LDA are important to construct approximations to the exchange-correlation energy such as hybrid functionals and generalized gradient approximations (GGA). The local spin density approximation (LSDA) is an extension to the LDA methodology which resembles Unrestricted Hartree–Fock (UHF) calculations.

Hybrid functionals are approximations to the exchange-correlation energy functional in DFT which includes a portion of exact exchange from Hartree-Fock (HF) theory with the rest of the exchange-correlation energy from empirical *and ab initio* sources.

One of the most widely used version is B3LYP (Becke, 3-parameter, Lee–Yang–Parr). The hybrid density functional B3LYP is a popular exchange-correlation functional developed in late 1980s and expressed as[4]

$$E_{\mathrm{xc}}^{\mathrm{B3LYP}} = (1-a_0)E_{\mathrm{x}}^{\mathrm{LSDA}} + a_0E_{\mathrm{x}}^{\mathrm{HF}} + a_{\mathrm{x}}\Delta E_{\mathrm{x}}^{\mathrm{B88}} + E_{\mathrm{c}}^{\mathrm{LSDA}} + a_{\mathrm{c}}\Delta E_{\mathrm{c}}^{\mathrm{PW91}},$$

where the 3-paramter are a_0=0.20, a_{x}=0.72, and a_{c}=0.81;[5] $\Delta E_{\mathrm{c}}^{\mathrm{PW91}}$ is the Perdew-Wang gradient correction to the correlation functional;[6] $\Delta E_{\mathrm{x}}^{\mathrm{B88}}$ is Becke's gradient correction to the exchange functional; $E_{\mathrm{x}}^{\mathrm{LSDA}}$ is LSDA to the standard

local exchange functional;[7] $E_{\mathrm{c}}^{\mathrm{LSDA}}$ is LSDA to the correlation functional;[8] $E_{\mathrm{x}}^{\mathrm{HF}}$ is a linear combination of the Hartree-Fock exchange functional expressed as

$$E_{\mathrm{x}}^{\mathrm{HF}} = -\frac{1}{2}\sum_{i,j}\iint \varphi_i^*(\mathbf{r}_1)\varphi_j^*(\mathbf{r}_2)\frac{1}{\mathrm{r}_{12}}\varphi_j(\mathbf{r}_1)\varphi_i(\mathbf{r}_2)\mathrm{d}\mathbf{r}_1\mathrm{d}\mathbf{r}_2 .$$

A basis set in theoretical or computational chemistry is a set of functions employed to symbolize the electronic wave function in the DFT or HF method to enable the partial differential equations of the model into algebraic equations for efficient computation performance. The def2-Split valence polarization (def2-SVP) basis set is chosen in this work because it has the polarization functions on all atoms.

2.9 References

1. Patterson, A., The Scherrer formula for X-ray particle size determination. *Physical Review* **1939,** *56* (10), 978.
2. Holzwarth, U.; Gibson, N., The Scherrer equation versus the 'Debye-Scherrer equation'. *Nature Nanotechnology* **2011,** *6* (9), 534.
3. Blöchl, P. E., Projector augmented-wave method. *Physical Review B* **1994,** *50* (24), 17953.
4. Stephens, P.; Devlin, F.; Chabalowski, C.; Frisch, M. J., Ab initio calculation of vibrational absorption and circular dichroism spectra using density functional force fields. *The Journal of Physical Chemistry* **1994,** *98* (45), 11623-11627.
5. Becke, A. D., Density-functional thermochemistry. III. The role of exact exchange. *The Journal of Chemical Physics* **1993,** *98* (7), 5648-5652.
6. Perdew, J., In Electronic Structure of Solids. Akademie Verlag: Berlin: 1991.
7. Andzelm, J.; Wimmer, E.; Salahub, D. In *The challenge of d and f electrons: theory and computation*, by DR Salahub and MC Zerner, ACS Symposium Series, 1989; p 228.
8. Vosko, S. H.; Wilk, L.; Nusair, M., Accurate spin-dependent electron liquid correlation energies for local spin density calculations: a critical analysis. *Canadian Journal of Physics* **1980,** *58* (8), 1200-1211.

copyright material. I would be pleased to hear from any copyright owner who has been omitted or incorrectly acknowledged.

Chapter 3 Oriented attachment growth of wurtzite ZnTe nanoplatelets from metastable magic-sized nanoclusters

3.1 Introduction

Over the last decade, colloidal semiconductor nanoplatelets (NPLs) with a few layers of atomic thickness[1-18] have been of great interest due to their exceptional photophysical properties such as short PL lifetime,[19-23] extremely narrow PL linewidth,[24-28] ultralow optical gain thresholds,[29-35] large linear and nonlinear absorption cross-sections,[36-38] and giant oscillator strength.[39-41] Thanks to these advantageous optical and electronic properties, NPLs hold great potential in numerous applications including lasers, phototransistors,[42-44] photodectectors,[45-46] and light-emitting diodes (LEDs) with ultrahigh colour purity.[47-54] Unlike the synthesis of zinc-blende II-VI nanoplatelets in 1-octadecene (ODE), which combines fatty acid salts with fatty acids as the cation precursor solution at elevated temperatures, the colloidal synthesis of wurtzite II-VI nanoplatelets was proposed to be evolved from stoichiometric (1:1) magic-sized nanoclusters (MSNCs) as intermediate synthons within soft colloidal alkylamine bilayer templates under mild reaction temperature.[3-4, 55-58] Currently, the majority of II-VI colloidal nanoplatelets with wurtzite or zinc-blende structure are based on cadmium chalcogenides. The toxicity of materials and governing regulations, however, hinder the widespread use of heavy metals, especially semiconductor nanocrystals containing cadmium. Potential alternatives are heavy-metal-free zinc chalcogenide semiconductor nanocrystals because they are environment-benign and earth-abundant materials.

Among ZnX (X=S, Se, Te) semiconductors, ZnTe with a direct bandgap of 2.26 eV in bulk and excellent physical properties such as ultrafast charge separation and transfer dynamics, has important applications such as photodetector,[59] solar cells,[60] terahertz imaging.[61] Compared with the broad full width at half maximum (FWHM) of emission peaks of ZnTe spherical dots or nanorods, the narrow PL linewidth of ZnTe NPLs makes them more advantageous to fabricate optoelectronic devices such as lasers, phototransistors, and LEDs with ultrahigh

colour purity.

Although bulk ZnTe materials are stable under ambient conditions, their counterparts such as ZnTe nanocrystals are extremely vulnerable to air and moisture and are tend to undergo decomposition as they have a large portion of surface atoms. This makes the study on ZnTe nanocrystals challenging because of the instability of ZnTe nanocrystals as well as the rigid oxygen- and moisture-free conditions required in the post-synthesis handling. Furthermore, the chemistry of tellurium precursors is not well-developed and therefore substantial effort in this field is highly demanded.

Zhang *et al.* developed a synthetic approach for producing wurtzite ZnTe nanorods with controllable aspect ratio by tuning the reaction temperature.[62] In addition, they reported the self-assembly of two families of ZnTe MSNCs that evolved into one-dimensional (1D) wurtzite ZnTe ultrathin nanowires via alignment and fusion along the [002] crystal direction at a prolonged reaction time,[63] which is different from the growth behavior of CdSe MSNCs as nucleant for the growth of wurtzite CdSe nanoplatelets.[58, 64] Hyeon *et al.* suggested that the growth of wurtzite CdSe nanoplatelets preferred a mild reaction temperature because it can differentiate the subtle surface energy difference between the (100) and (110) facets of wurtzite structure and also stabilize the MSNCs and the soft colloidal alkylamine templates.[58] However, because of the metallic characteristics of both zinc and tellurium, a reaction for the synthesis of ZnTe nanocrystals conducted at a mild temperature may not be able to overcome the reaction activation energy barrier; therefore, tellurium precursors with appropriate reactivity are required. This suggests that care should be taken to keep the balance between the reactivity of tellurium precursors and the reaction temperature in the preparation of ZnTe nanocrystals with one-dimensional or two-dimensional shapes. Tellurium precursors such as bis(*tert*-butyldimethylsilyl) telluride,[64] trioctylphosphine telluride (TOP-Te),[62] polytellurides reduced from TOP-Te by superhydride,[65] tributylphosphine telluride (TBP-Te)[66] and tris(dimethylamino)phosphine telluride[67] were used to synthesize CdTe or ZnTe nanocrystals. For the synthesis conducted at a mild reaction temperature, high-quality ZnTe or CdTe nanocrystals can only be prepared by using polytellurides reduced from TOP-Te by superhydride or tris(dimethylamino)phosphine telluride as precursor, suggesting these tellurium precursors with higher reactivity.

As analyzed above, we speculate that the reaction temperature and the reactivity of tellurium precursor are two determinants of the evolution from ZnTe MSNCs to 1D nanowires or 2D nanoplatelets because of the subtle surface energy difference between the (100) and (110) facets of wurtzite structure and the higher reaction activiation energy required at a mild reaction temperature. To this end, we took both critical factors into account by the combination of the tellurium precursor with proper reactivity and a mild reaction temperature to prepare wurtzite ZnTe NPLs.

In this work, we have successfully synthesized free-standing single-layered wurtzite ZnTe NPLs with a thickness of 1.5 nm by using superhydride ($LiEt_3BH$) reduced tributylphosphine-Te (TBP-Te) as the tellurium precursor. From both experimental and theoretical perspective, we reveal that the growth process of ZnTe NPLs involved a stepwise evolution from metastable self-assembled ZnTe F323 magic-sized nanoclusters (MSNCs) to self-assembled ZnTe F398 MSNCs, then oriented attachment of ZnTe F398 MSNCs along [100] and [002] directions to form wurtzite ZnTe NPLs.

3.2 Experimental section

3.2.1 Materials

Zinc chloride (99.999%, trace metals basis), oleylamine (technical grade, 70%), dodecylamine (99%), tributylphosphine (mixture of isomers, 97%), super-hydride® solution (1.0 M lithium triethylborohydride in THF), anhydrous hexane (95%), anhydrous toluene (99.8%), and anhydrous methanol (99.8%) were purchased from Sigma-Aldrich. Tellurium powder (~325 mesh, 99.99% metals basis) was obtained from Alfa Aesar. $CDCl_3$ (deuterium, 99.8%) was purchased from Cambridge Isotope Laboratories, Inc. All materials were used as received without further purification.

3.2.2 Preparation of 0.5 M tributylphosphine tellurides (TBP-Te) stock solution

Transparent and yellow TBP-Te stock solution (0.5 M) were prepared by heating 30 ml tributylphosphine (TBP) and 1.914 g (15 mmol) tellurium powder at 240 ^{o}C for 3 hours under nitrogen atmosphere using the standard Schlenk line techniques. The color of the solution change from opaque black gradually to opaque dark green, light yellow, translucent orange, finally to transparent brick

red during the reaction period.

3.2.3 Synthesis of self-assembled ZnTe MSNCs and ZnTe NPLs using polytelluride species as tellurium precursor.

In a 50 ml flask, 272 mg $ZnCl_2$ (2 mmol), 3.224 g dodecylamine and 16 ml oleylamine were mixed and degassed at room temperature for three times, then the mixture was heated at 200 ^oC for an hour before cooling down to 60 ^oC under nitrogen for hot-injection of the tellurium precursor that was freshly prepared in a glove box by using 4 ml oleylamine, 2 ml TBP-Te stock solution (0.5 M) and 1.2 ml of superhydride solution. After hot-injection, the reaction temperature was increased from 60 ^oC to 120 ^oC in 6 minutes. As the reaction mixture was kept for 2 hours at 120 ^oC, the first aliquot was taken, which was the reaction product of self-assembled ZnTe F323 MSNCs. Then the reaction temperature was further increased to 200 ^oC in 5 minutes. As the reaction proceeded at 200 ^oC for 2 minutes, the second aliquot was taken, which was the reaction product of self-assembled ZnTe F398 MSNCs. After another 30 minutes, the reaction was stopped by removing the heating mantle and cooled it down to room temperature.

3.2.4 Measurement and characterization

UV–vis absorption spectra were recorded on a Cary 4000 UV–vis spectrophotometer with 1 nm resolution in a quartz cell with 1 cm path length. Low-resolution transmission electron microscopy (TEM) and selected-area electron diffraction (SAED) were conducted using a JEOL 2100 transmission electron microscope with an accelerating voltage of 120 kV. The SAED pattern was fitted using PASAD tools for Digital Micrograph. High-resolution TEM (HRTEM), high angle annular dark field-scanning transmission electron microscopy (HAADF-STEM) and STEM-energy- dispersive X-ray spectroscopy (STEM-EDX) were performed on a FEI Titan G2 80-200 transmission electron microscope operating at 200 kV. All the reaction products were purified in a glove box using anhydrous hexane or anhydrous toluene as solvent, and anhydrous methanol as antisolvent. The reaction products were centrifuged at 6000 rpm/3 minutes for ZnTe F323 MSNCs and at 5000 rpm/3 minutes for ZnTe F398 MSNCs and ZnTe NPLs. The purification was repeated again and then purified ZnTe MSNCs and NPLs were redispersed into anhydrous toluene, then a drop of the solution was added onto a ultra-thin carbon-coated copper grid and the grid with the nanocrystals was dried

in a glove box. Nuclear magnetic resonance (NMR) samples of TBP-Te were prepared in $CDCl_3$. ^{1}H and ^{31}P NMR spectra were recorded on a Bruker Avance Bruker Avance III 500 MHz spectrometer.

3.2.5 DFT calculations of surface energy

We employed the first-principles method based on the density function theory (DFT) and the first-principles pseudo-potential method to investigate the surface energy of ZnTe NPLs. The DFT calculations were carried out by the Vienna *Ab Initio* Simulation Package (VASP) code with the projector-augmented wave (PAW) method using the Perdew-Burke-Ernzerhof (PBE) exchange-correlation functional.[68-70] The plane wave cutoff was set as 500 eV, with the total energy convergence at 10^{-6} eV for the self-consistent iterations. The Gaussian smearing method with σ=0.05 eV was considered for Brillouin-zone integration and the geometry optimizations were stopped until the forces on the atoms were < 0.01 eV/Å. We used the finite-sized slab technique to investigate the surface energy of ZnTe NPLs. The slab models were built from the wurtzite ZnTe crystal structure determined by Kart *et al*.[71] The lattice parameters of bulk ZnTe, optimised with a 12×12×6 k-point grid, were a = b = 3.996Å, c = 6.626 Å, which are in good agreement with experimental values. According to the exposed surfaces of ZnTe NPLs, four different surfaces were studied: two non-polar surfaces of (110) and (100), and two polar surfaces (Zn-terminated (002) and Te-terminated $(00\bar{2})$ (Figure 3.1).

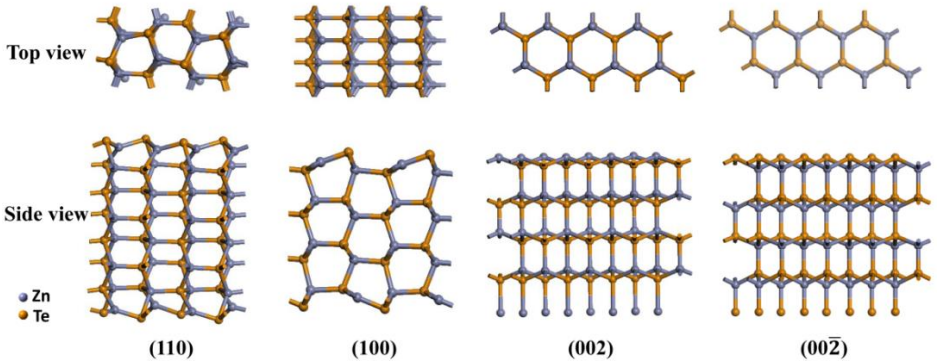

Figure 3.1 The slab model structures of (110), (100), Zn-terminated (002) and Te-terminated $(00\bar{2})$ surfaces of wurtzite ZnTe NPLs.

All these slab models in periodical super cell were separated by a vacuum region of 20 Å thick. Each slab of nonpolar surface models contains four zinc and four tellurium atoms within each Zn-Te layer in a repeated slab configuration,

whereas for the polar surface models each one contains eight zinc or eight tellurium atoms within each Zn-Te layer in a repeated slab configuration. The surface free energy of the particular slab with a repeated geometry is given by the equation:

$$\sigma = \left(E_{slab} - \sum_i n_i \mu_i\right)/2A$$

where E_{slab} is the total energy of the particular slab; n_i and μ_i are the number of atoms and the chemical potential of the i^{th} constituent of the slab, respectively; A is the surface area. The factor of 2 accounts for two equivalent surfaces in the particular slab. The surface energies of non-polar surface were found to converge with slab thickness and were converged to smaller than 0.001 eV/Å^2 with respect to eight-layer slab thickness. We therefore used the eight-layer thick ZnTe slabs for studying the surface energy of (110) facet and of (100) facet with 3×6×1 and 6×3×1 Monkhorst-Pack *k*-point grid, respectively. Special care should be taken with the computational treatment of the polar surface, in particular to avoid the build-up of an overall artificial dipole field. Here, we adopted symmetric structures of the nine-layer slab model for the Zn-terminated (002) and Te-terminated ($00\bar{2}$) surfaces, as shown in Figure 3.1. The surface free energy equation is a thermodynamic function of the chemical potential of the constituent in the slab. Therefore, the surface energy is governed by the chemical potentials of the constituents of the slab, i.e. μ_{Zn} and μ_{Te}. Invoking equilibrium of ZnTe bulk, μ_{Zn}+ μ_{Te} = E_{bulk}^{ZnTe}, the dependence of the surface free energy on the chemical potential can be further simplified by eliminating μ_{Te}, leading to a dependence on μ_{Zn}only. We restricted the values of $\mu_{Zn}$to μ_{bulk}^{Zn} + $\Delta H_f(ZnTe) \leq \mu_{Zn} \leq \mu_{bulk}^{Zn}$, i.e. $\Delta H_f(ZnTe) \leq \Delta\mu_{Zn} = \mu_{Zn} - \mu_{bulk}^{Zn} \leq 0$, according to thermodynamically allowed ranges. These ranges were determined by the assumed constraints, $\mu_{Zn} \leq \mu_{bulk}^{Zn}$ and $\mu_{Te} \leq \mu_{bulk}^{Te}$, which means that Zn and Te do not crystalline on the surface. In addition, the formation enthalpy of bulk ZnTe was given by $\Delta H_f(ZnTe) = E_{bulk}^{ZnTe} - \mu_{Zn} - \mu_{Te}$. We have calculated the surface energies as linear function of μ_{Zn}, -2.360 eV$\leq \Delta\mu_{Zn} \leq 0$. The chemical potential $\Delta\mu_{Zn} = 0$, i.e. $\mu_{Zn} = \mu_{bulk}^{Zn}$, represents the Zn-rich condition while $\Delta\mu_{Zn} = -2.360$eV represents the Te-rich condition.

3.2.6 DFT calculations for simulating UV-vis absorption spectra of $(ZnTe)_{34}$ isomers and the growth of wurtzite ZnTe NPLs

We used DFT as implemented in the Gaussian 09 to simulate the growth of ZnTe NPLs.[7] We have chosen the hybrid density functional B3LYP with def2-svp basis set. UV-vis absorption spectra of model systems were calculated at the time-dependent density functional theory (TDDFT) level. The convergence thresholds for total energy and the forces were set to 10^{-8} eV and 10^{-3} eV/Å respectively. Solvent effects were simulated using the polarized continuum model (PCM) with the appropriate dielectric constant-propylame, as incorporated the Gaussian-09 software package.

3.3 Results and discussion

Figure 3.2 and 3.3 show the ^{1}H and ^{31}P NMR spectra of TBP and TBP-Te, respectively. The chemical shifts from the H atoms in TBP and TBP-Te were labled as shown in Figure 3.2. The main resonance appearing at -30.8 ppm (upper curve in Figure 3.3) was from TBP in the absence of Te. The broad resonance at -24.7 ppm (bottom curve in Figure 3.3) was from the mixture of TBP-Te and TBP, which results from the fast exchange of Te between TBP-Te and TBP.

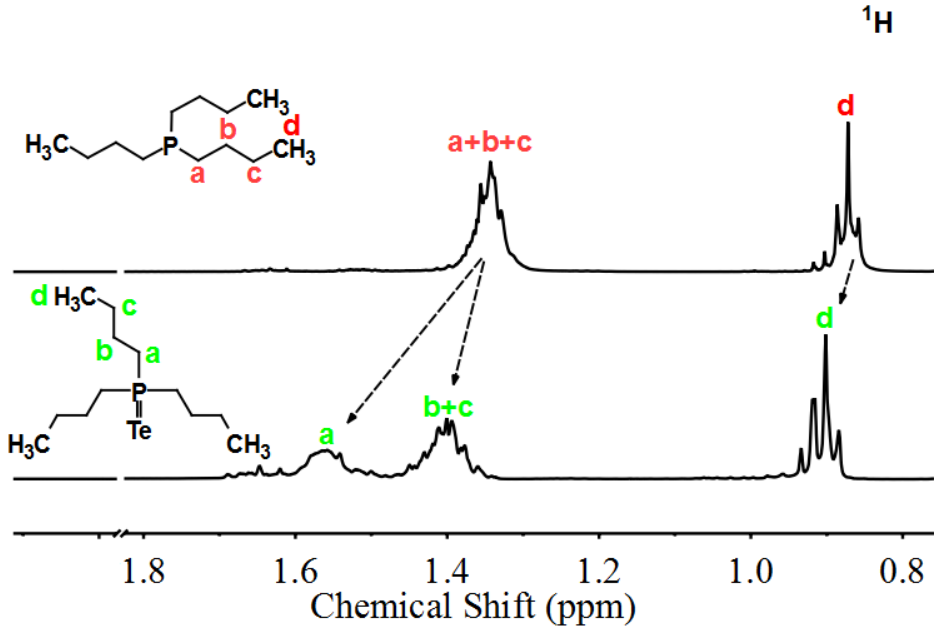

Figure 3.2 ^{1}H NMR spectra of TBP and TBP-Te.

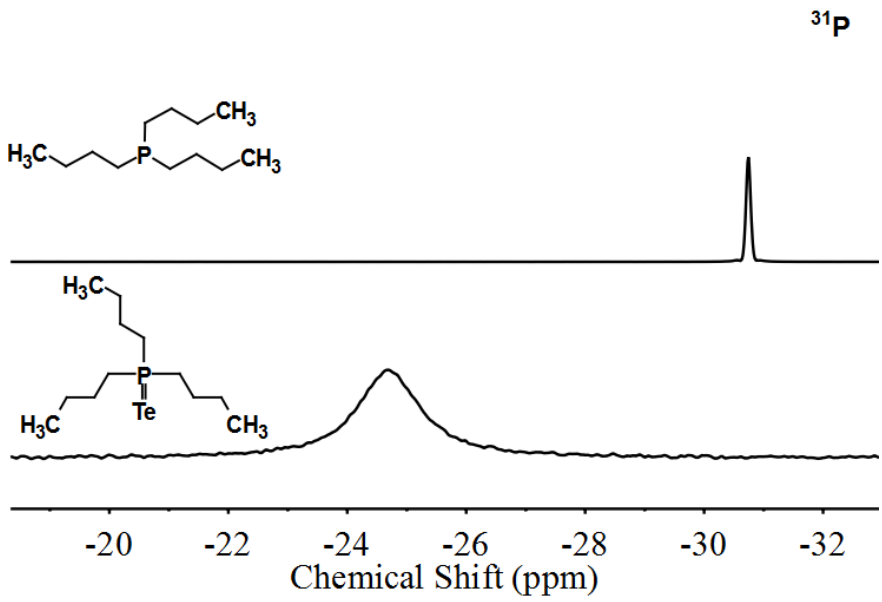

Figure 3.3 ^{31}P NMR spectra of TBP and TBP-Te.

Figure 3.4 presents the absorption spectra of aliquots taken at various reaction stages, which clearly shows the sharp absorption peaks of ZnTe MSNCs and NPLs. After hot-injection of tellurium precursor at 60 °C, the reaction mixture was increased to 120 °C in 6 minutes. The mild hot-injection temperature is necessary to stabilize the MSNCs because we found that ZnTe MSNCs were not produced if the injection temperature is higher than 60 °C. The first aliquot was taken from the turbid white solution when the reaction proceeded for 2 hours at 120 °C. The corresponding absorption spectrum (red curve in Figure 3.4) presents a sharp peak at 323 nm along with a shoulder at 297 nm, which matches well with the characteristic absorption peak locations of ZnTe F323 MSNCs.[63] Within 5 minutes, the reaction temperature further increased to 200 °C and the reaction mixture turned turbid light-yellow gradually. As the reaction proceeded for 2 minutes at 200 °C, the second aliquot was taken and its absorption spectrum (green curve in Figure 3.4) exhibits two peaks at 362 and 398 nm, matching the unique absorption peak locations of ZnTe F398 MSNCs.[63] As the reaction proceeded for 30 minutes at 200 °C, ZnTe NPLs were obtained and the exciton absorption peaks of ZnTe NPLs (blue curve in Figure 3.4) appear at 360 and 396 nm. In addition, the first exciton absorption peak of ZnTe NPLs is much sharper than that of ZnTe F398 MSNCs. Here, the “double absorption peaks” feature is usually observed for both zinc blende and wurtzite II-VI semiconductor nanoplatelets due to the electron-light hole (e-lh) and electron-heavy hole (e-hh) transitions.[4, 56, 64]

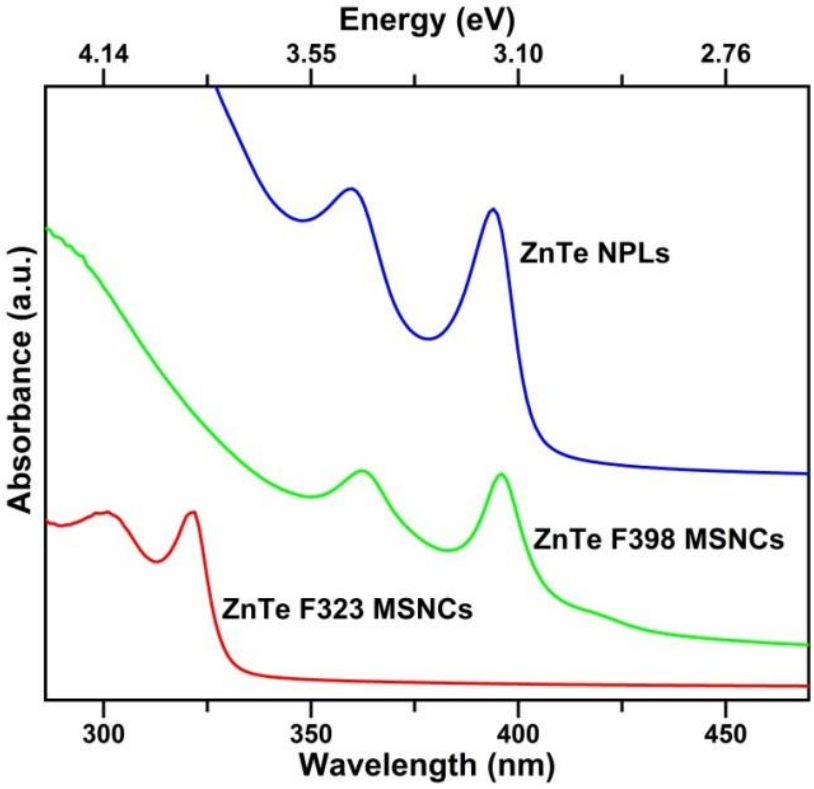

Figure 3.4 UV-vis absorption spectra (red curve) of ZnTe F323 MSNCs, ZnTe F398 MSNCs (green curve) and ZnTe NPLs (blue curve).

To analyse the detailed transition from metastable ZnTe MSNCs to ZnTe NPLs, more aliquots were taken to investigate this process. The temporal evolution of UV-vis absorption spectra of aliquots was compared in Figure 3.5 as the reaction temperature increased from 120 ^{o}C to 200 ^{o}C. As the temperature increased from 60 ^{o}C to 120 ^{o}C, the absorption spectrum of the aliquot shows a broad peak at 325 nm (curve 1, Figure 3.5). As the reaction evolved from 10 to 120 min at this temperature, this broad peak becomes sharper (curve 1-4, Figure 3.5) and two absorption peaks emerged at 302 nm and 323 nm. The absorption spectrum (curve 4, Figure 3.5) of ZnTe F323 MSNCs displays two distinctive exciton peaks at 302 nm and 323 nm, which are the characteristic absorption features of ZnTe F323 MSNCs. As the reaction temperature increased from 120 ^{o}C to 200 ^{o}C, the absorption peaks of ZnTe F323 MSNCs fade along with the appearance of the characteristic absorption peaks of ZnTe F398 MSNCs (curve 5-6, Figure 3.5). The coincidence of the characteristic absorption features of both ZnTe F323 MSNCs and F398 MSNCs confirms the stepwise transition from metastable ZnTe F323

MSNCs to ZnTe F398 MSNCs, which is similar to that observed in CdSe MSNCs reported elsewhere.[72] Interestingly, the exciton absorption peak of ZnTe NPLs (curve 8, Figure 3.5) shows a slight blue shift of 2 nm with respect to that of ZnTe F398 MSNCs (curve 7, Figure 3.5). This might indicate that ZnTe NPLs form an atomically flat basal plan therefore the excitons are confined only in the thickness direction of ZnTe NPLs. Both ZnTe MSNCs and NPLs do not have detectable PL, which may result from surface traps and the dynamic nature of alkylamine ligands.[73]

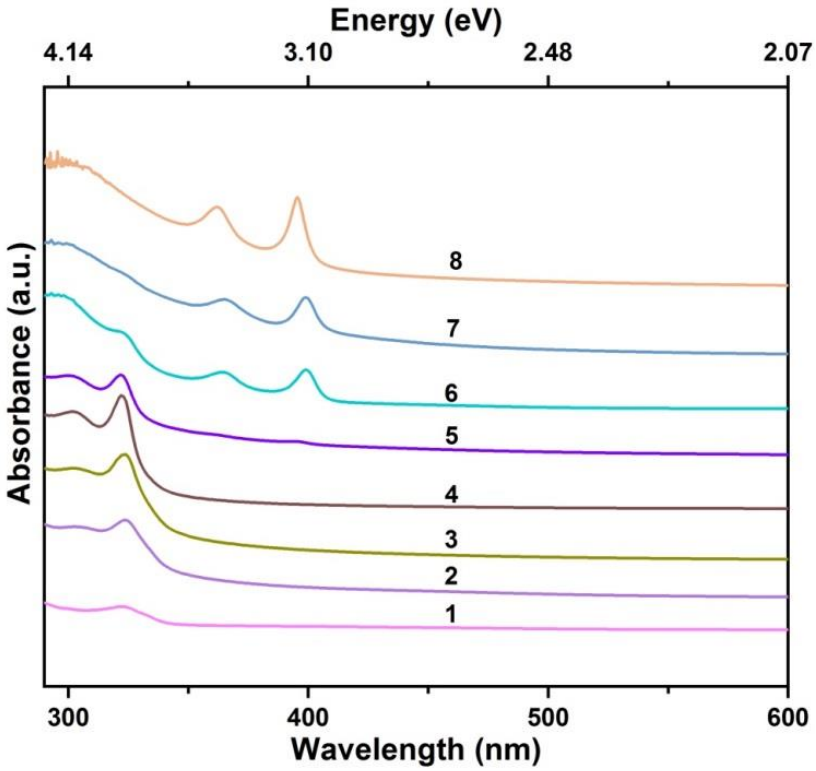

Figure 3.5 Temporal evolutions of UV-vis absorption spectra of ZnTe MSNCs and NPLs. Aliquots taken at (1) 120 °C/0 min, (2) 120 °C/10 min, (3) 120 °C/60 min, (4) 120 °C/120 min, (5) 140 °C/0 min, (6) 160 °C/0 min, (7) 200 °C/2 min, (8) 200 °C/30 min.

The TEM image of ZnTe F323 MSNCs (Figure 3.6a) obtained at 120 °C for 120 minutes shows that the MSNCs self-assembled in coin-like plates with a lateral size of ~20 nm. Interestingly, those self-assembled MSNCs (Figure 3.7) can stack with each other due to weak interactions between the bilayer mesophase template.[64] As the reaction temperature increased from 120 °C to 200 °C and proceeded for 2

minutes at this temperature, the first exciton absorption peak has a profound red-shift from 323 nm to 398 nm (red and green curve in Figure 3.4), which corresponds to the transition from metastable ZnTe F323 MSNCs to ZnTe F398 MSNCs. This suggests that the increase of the reaction temperature broke the structural stability of metastable self-assembled ZnTe F323 MSNCs and resulted in the formation of ZnTe F398 MSNCs from the transition of self-assembled ZnTe F323 MSNCs.

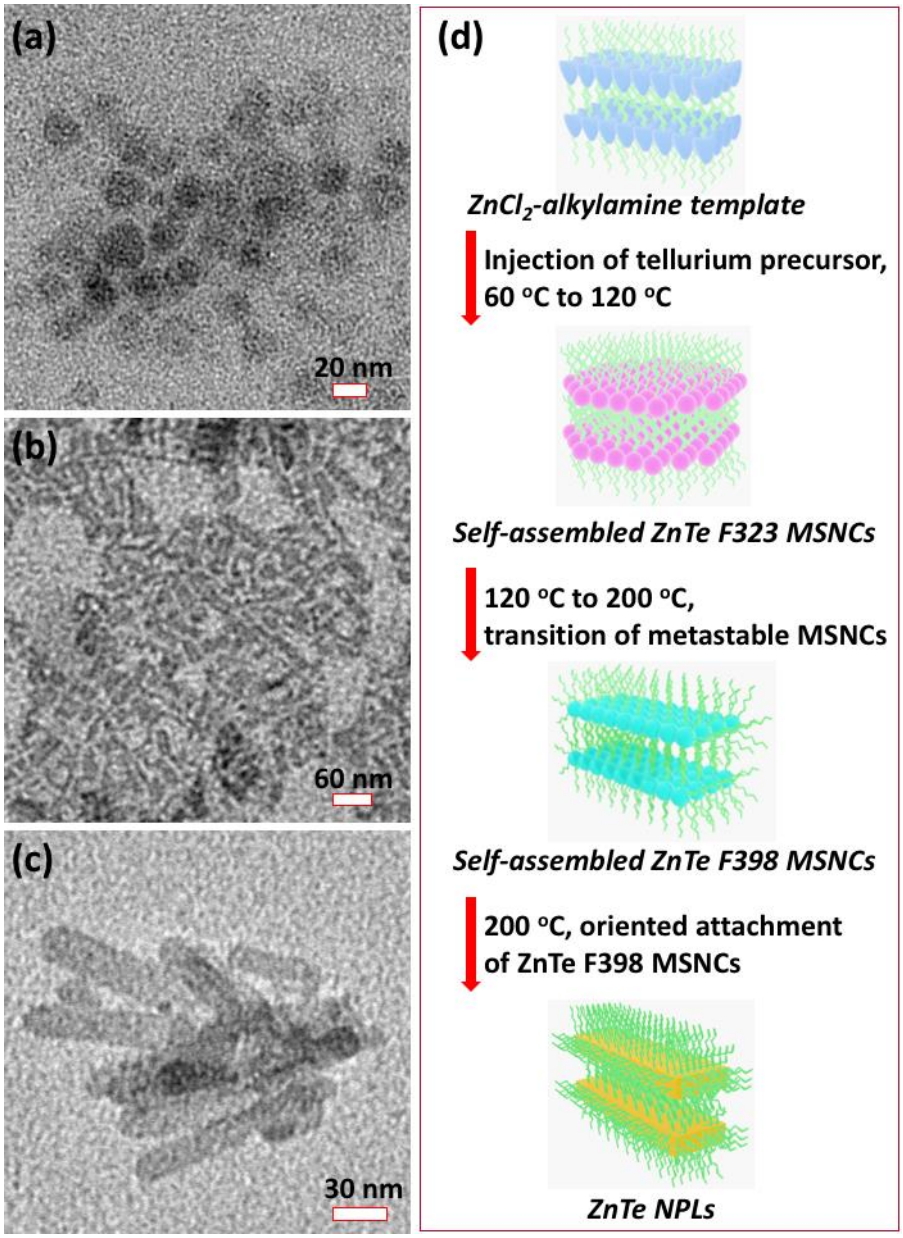

Figure 3.6 Formation of ZnTe NPLs. TEM image of (a) self-assembled ZnTe F323 MSNCs, (b) F398 MSNCs, and (c) ZnTe NPLs. (d) Schematic illustration of the synthesis of ZnTe NPLs converted from the stepwise transition of metastable self-

assembled ZnTe F323 and F398 MSNCs.

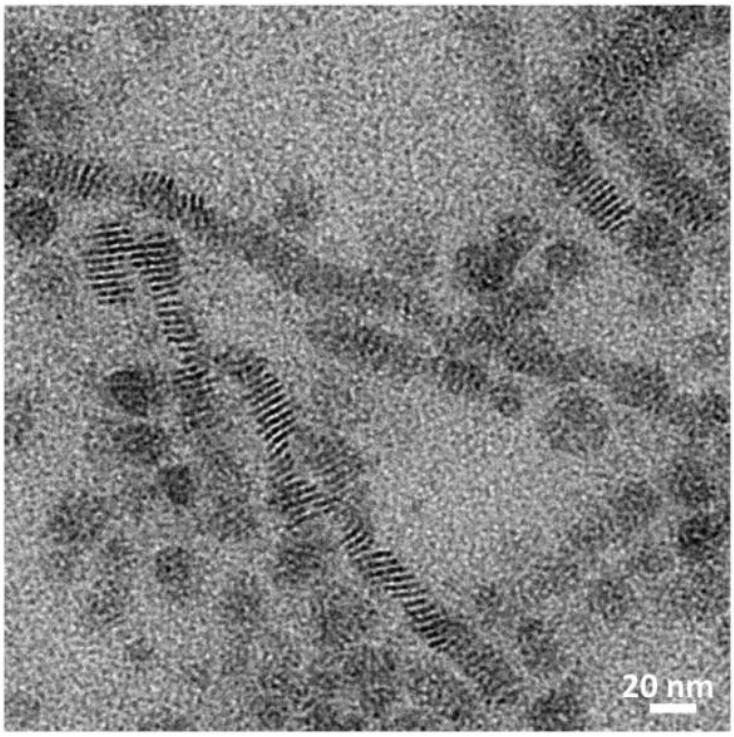

Figure 3.7 TEM image of stacking self-assembled ZnTe F323 MSNCs.

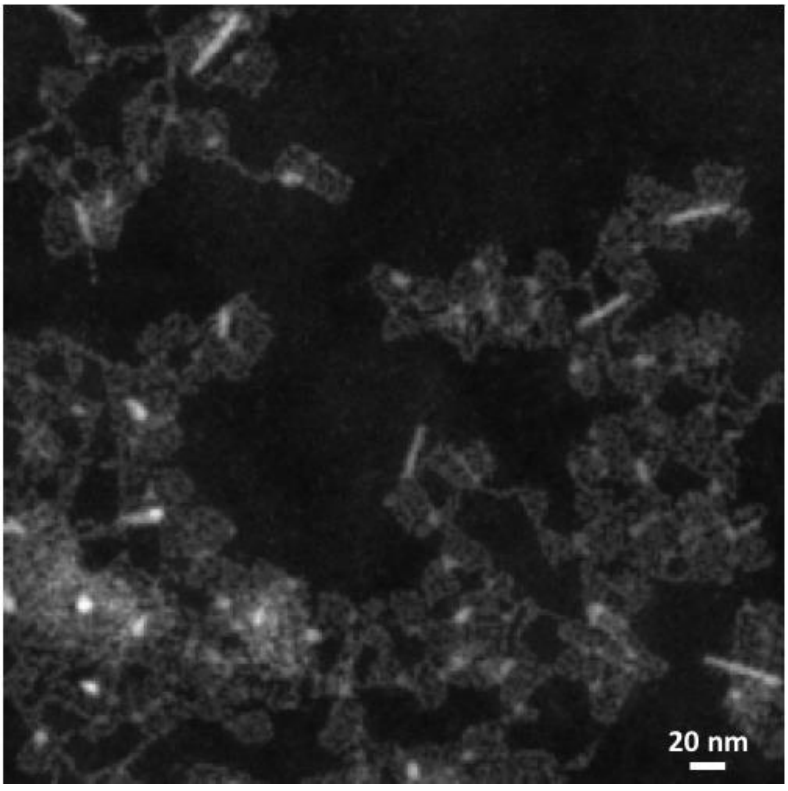

Figure 3.8 HAADF-STEM image of self-assembled ZnTe F398 MSNCs.

Figure 3.6b presents the TEM of self-assembled ZnTe F398 MSNCs with irregular plate-like shape. In addition, the high-angle annular dark-field scanning transmission electron microscopy (HAADF-STEM) image (Figure 3.8) reveals that these self-assembled ZnTe F398 MSNCs were composed of individual small particles, being similar to those reported by Zhang *et al.*[63] After the reaction proceeded for 30 minutes at 200 °C, well-defined rectangle-shaped ZnTe NPLs (Figure 3.6c) with lateral dimensions of ~20 nm×~60 nm. Figure 3.6d presents a schematic illustration to summarise the synthesis of ZnTe NPLs converted from the stepwise transition of metastable self-assembled ZnTe F323 and F398 MSNCs.

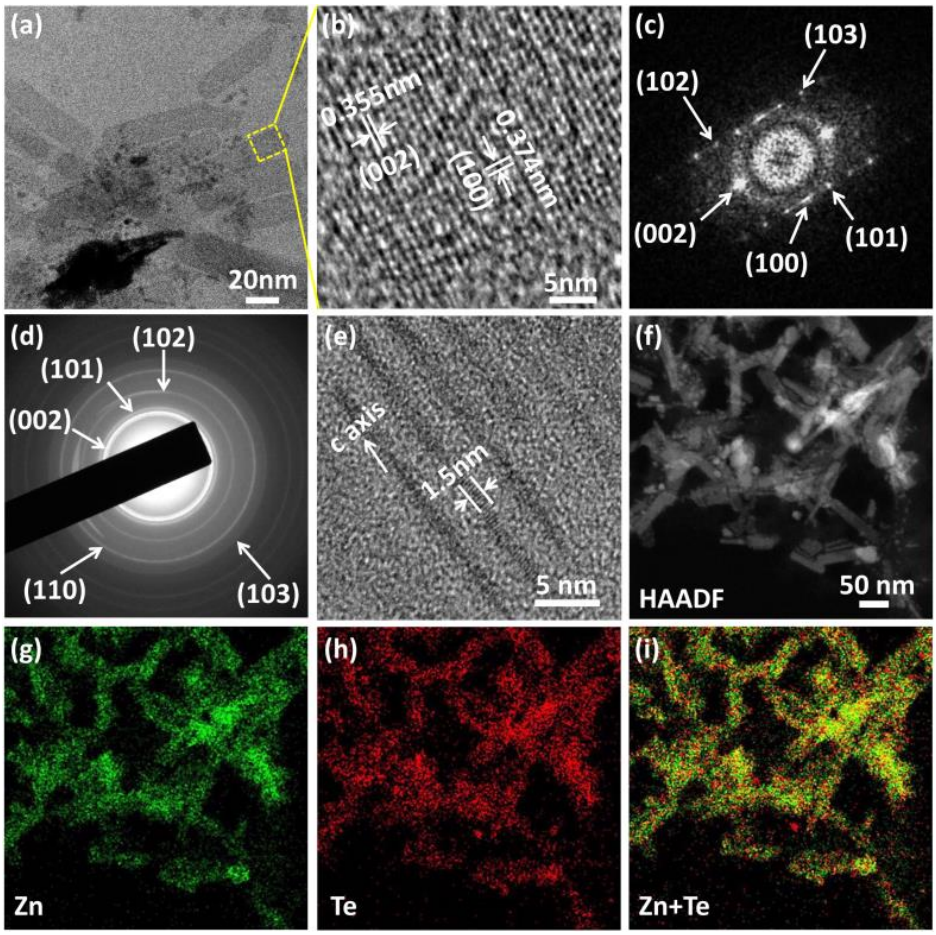

Figure 3.9 Structural characterizations of ZnTe NPLs. (a) TEM image of single-layered ZnTe NPLs. (b) HRTEM image of an individual ZnTe NPL. (c) FFT of the HRTEM image. (d) SAED pattern of ZnTe NPLs. (e) TEM image of ZnTe NPLs standing on their edges. (f-i) HAADF-STEM image and STEM-EDX elemental maps

of ZnTe NPLs.

Figure 3.9a shows the TEM image of single-layered ZnTe NPLs. ZnTe NPLs with a two dimensional rectangle shape are observed alongside with black dots. These black dots are Te metal dots due to the oxidizaiton of ZnTe NPLs. The high-resolution TEM (HRTEM) image (Figure 3.9b), the fast Fourier transform (FFT) of the HRTEM (Figure 3.9c) and selected-area electron diffraction (SAED) pattern (Figure 3.9d) of ZnTe NPLs reveal that ZnTe NPLs are single-crystalline with a hexagonal wurtzite structure. Lattice spacing values extracted from the FFT of the HRTEM are 0.355 nm and 0.374 nm for (002) and (100) crystal facets, respectively, confirming that the long lateral direction of ZnTe NPLs corresponds to the *c*-axis of wurtzite structure. To further analyze the crystal structure of the as-prepared ZnTe NPLs, the SAED pattern of ZnTe NPLs was resolved by using PASAD tools (Figure 3.10). The corresponding Miller indices were annotated to the diffraction peaks (Figure 3.11) according to the resolved lattice spacing values as listed in Table 3.1, which confirms the as-prepared ZnTe NPLs with a wurtzite structure. The fitted lattice spacing values of ZnTe NPLs were a little bit smaller than the standard values for wurtzite bulk CdTe (JCPDS No. 19-1482), which results from the lattice contraction phenemenon that was also observed in CdSe nanosheets[64] and CdTe quantum belts.[74] Figure 3.9e shows that each ZnTe NPL stands on its edge. The thickness of a single ZnTe NPL is estimated to be ~1.5 nm, which is close to ~1.4nm thickness of ZnSe and CdSe nanosheet.[64, 75] Figures 3.9f-i presents the HAADF-STEM image and the corresponding STEM-EDX elemental maps of ZnTe NPLs. The element maps show that the obtained NPLs contain both Zn and Te elements, with both elements being evenly distributed throughout the ZnTe NPLs. The element maps shown in Figure 3.9i also confirms the formation of the Te metal dots, which is attributed to the oxidizaiton of ZnTe NPLs during the preparation or purification or characterizations of the TEM samples.

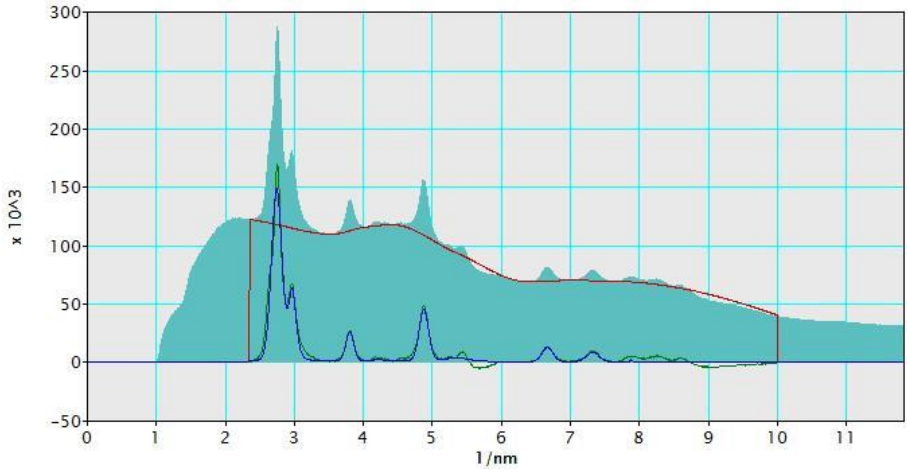

Figure 3.10 The SAED profile fitted by PASAD tools. Red curve (reduced background), green curve (residual plot), blue curve (final fitted profile).

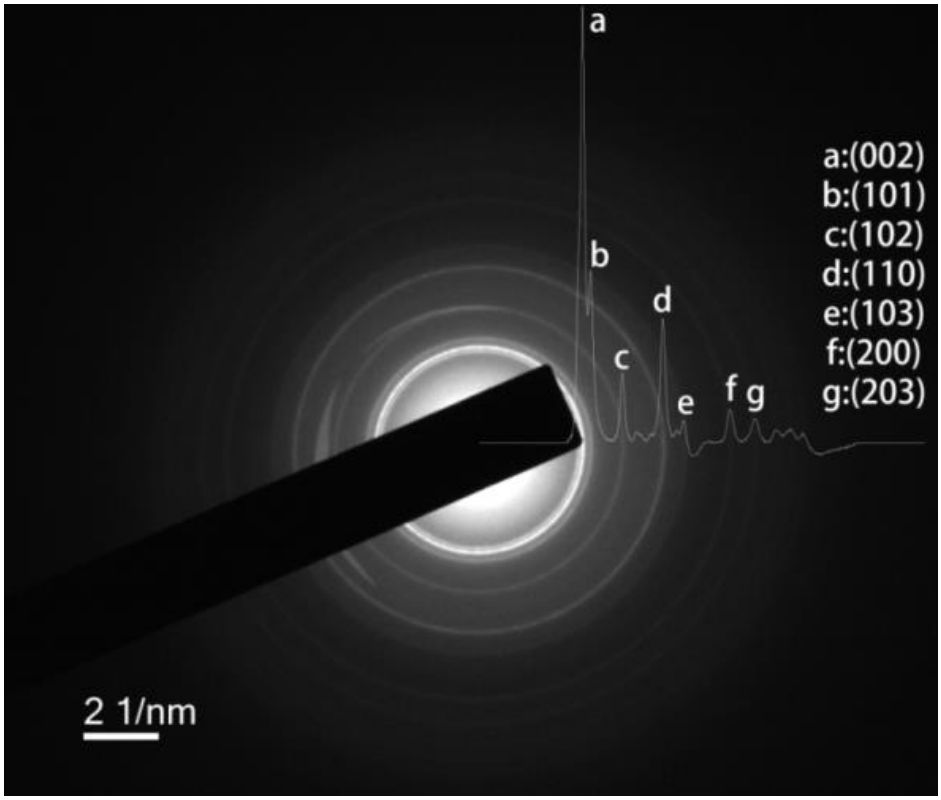

Figure 3.11 The fitted SAED profile by using PASAD tools annotated to the original SAED pattern with labeled Miller indices.

Table 3.1 Lattice spacings of ZnTe NPLs fitted by using PASAD tools.

k (nm^{-1})	Fitted lattice spacings d (Å)	Miller indices (hkl)	Standard lattice spacings d (Å) (JCPDS No. 19-1482)	Lattice contraction (%)
2.72	3.47	(002)	3.55	2.2
2.95	3.24	(101)	3.31	2.1
3.78	2.50	(102)	2.57	3.1
4.19	2.11	(110)	2.16	2.3
4.86	1.96	(103)	2.00	2.0
5.34	1.79	(200)	1.86	3.7
6.65	1.44	(203)	1.46	1.4

To elucidate the growth mechanism of wurtzite ZnTe NPLs, density functional theory (DFT) calculations were performed. We studied the surface energies of (110), (100) and (002)/(00$\bar{2}$) facets, which are relevant to the growth of wurtzite ZnTe NPLs. The (110), (100) and (002)/(00$\bar{2}$) terminated facets of wurtzite ZnTe NPLs are shown in Figure 3.1. The surface energy calculations show that the polar (002)/(00$\bar{2}$) facets have significantly higher surface energy than any of the non-polar (110) and (100) facets over almost the entire thermodynamically allowed range (Figure 3.12), being similar to other system with a hexagonal wurtzite crystal structure.[76] In this sense, fast growth or oriented-attachment of ZnTe nanocrystal or MSNCs along polar [002]/[00$\bar{2}$] directions is thermodynamically favoured, dominating the growth of wurtzite ZnTe NPLs. Since the surface energies of (110) and (100) facets are almost equal, which cannot explain the size difference between (110) and (100) facets of as-synthesized wurtzite ZnTe NPLs.

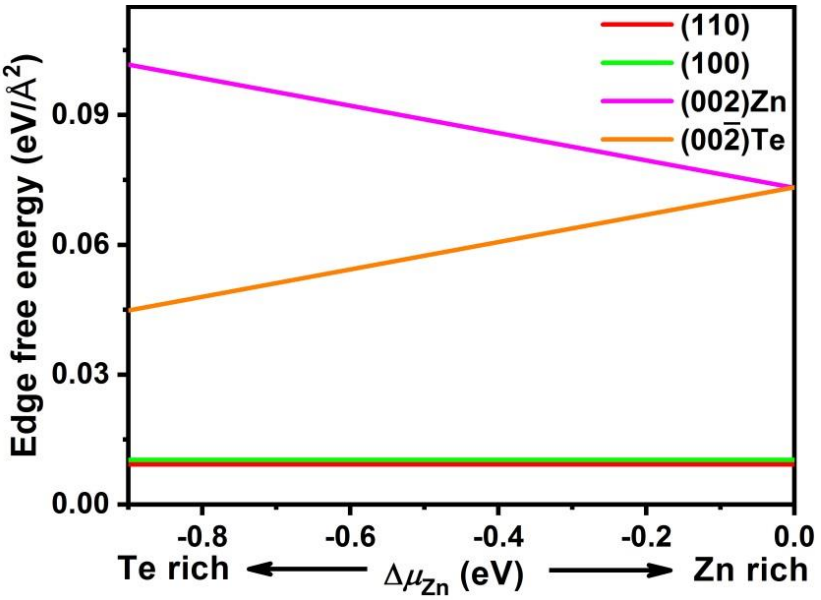

Figure 3.12 Surface energy as a function of the chemical potential $\Delta\mu_{Zn}$ of wurtzite ZnTe slab surface.

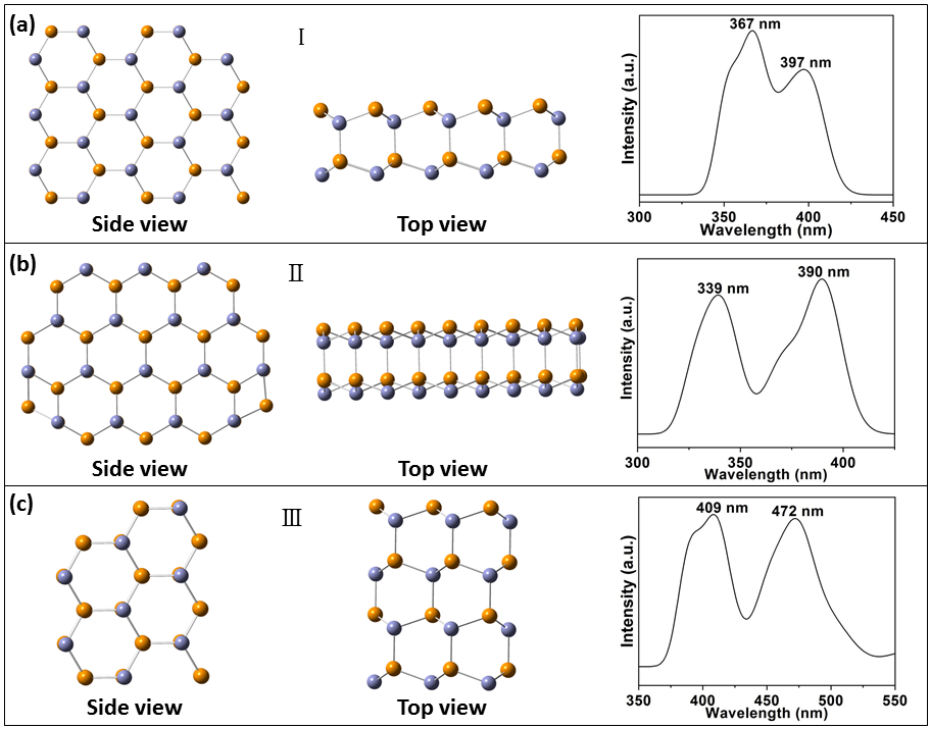

Figure 3.13 The simulated cluster structure I (a), II (b) and III (c) and their simulated UV-vis absorption spectrum of $(ZnTe)_{34}$ MSNCs. Zn and Te atom is labeled with blue and yellow color, respectively.

To further investigate the growth behaviour along [110] and [100] directions,

we chose a wurtzite $(ZnTe)_{34}$ MSNC as a nucleate because the magic number 34 has been experimentally determined for other II-IV MSNCs.[74, 77] Three isomers of $(ZnTe)_{34}$ MSNCs with a stackable morphology are shown in Figure 3.13. Structure I in Figure 3.13a presents a bilayer wurtzite stack which contains ten hexagons rings and one complementary atom connecting two hexagonal edges on each layer with the calculated energies of -69611.6675 au; structure II in Figure 3.13b also corresponds to the bilayer wurtzite stack with ten hexagons on each layer and a complementary atom connecting two hexagonal edges on each layer with the calculated energies of -69611.6302 au; structure III in Figure 3.13c corresponds to a four-layer wurtzite stack with four hexagons on each layer and a complementary atom connecting two hexagonal edges on each layer with the calculated energies of -69611.4918 au. Among these three isomers of $(ZnTe)_{34}$, structure I is the most stable structure. Furthermore, we have used the time-dependent DFT method to calculate the UV-vis absorption spectra of these $(ZnTe)_{34}$ isomers (Figure 3.13). Among all the simulated structures, the calculated adsorption spectrum of structure I has two strongest peaks located at 367 nm and 397 nm, respectively, agreeing well with the two distinct absorption peaks of as-prepared ZnTe F398 MSNCs located at 362 nm and 398 nm. However, the absorption peak locations of the calculated adsorption spectrum of structure II and III do not match with the expermental results. Therefore, structure I was chosen as the structure model of $(ZnTe)_{34}$ MSNCs.

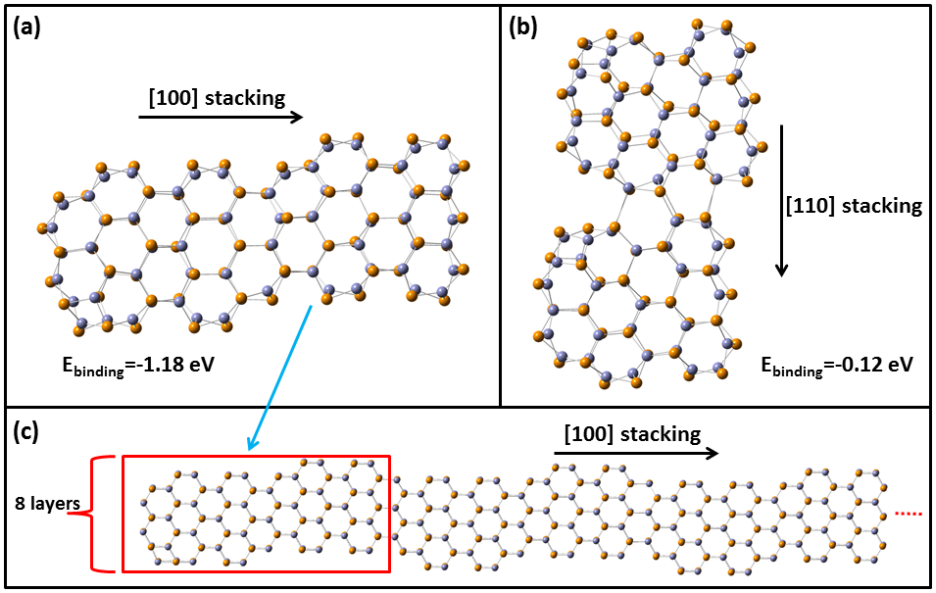

Figure 3.14 (a) Two $(ZnTe)_{34}$ MSNCs stacking along [100] direction. (b) Two $(ZnTe)_{34}$ MSNCs stacking along [110] direction. (c) Schematic illustration of the formation of zigzag ZnTe lateral size by more [100] stacking of $(ZnTe)_{68}$ nanoclusters. Zn and Te atom is labeled with blue and yellow color, respectively.

Then we stacked two structure models of $(ZnTe)_{34}$ MSNCs along [110] and [100] directions to simulate the growth of wurtzite ZnTe NPLs and calculated the formation energy of the resulted $(ZnTe)_{68}$ MSNCs (Figure 3.14a and 3.14b). The binding energy was calculated as $E_{binding} = E_{68} - 2E_{34}$, where E_{68} and E_{34} are the total binding energy of $(ZnTe)_{68}$ nanocluster and the energy of $(ZnTe)_{34}$ nanocluster, respectively. The binding energy of [110] stacking and [100] stacking are -0.12 eV and -1.18 eV, respectively. For [100] stacking, the rhombic ring of one $(ZnTe)_{34}$ nanocluster is opened and bonded to another $(ZnTe)_{34}$ cluster, which leads to two new hexagons ring and enhance the stability of $(ZnTe)_{68}$ clusters. The calculation results show that [100] stacking is a thermodynamically spontaneous process and more energy preferable than that of [110] stacking. Thus, we can speculate that $(ZnTe)_{68}$ nanoclusters will continue to attach orientally along [100] direction, which leads to the formation of zigzag lateral structure (Figure 3.14c) with larger size along [100] direction and the flat dominant (110) facet. In addition, the thickness of the zigzag lateral structure is determined to ~1.4 nm from the eight layers of $(ZnTe)_{68}$ cluster, which is close to the experimental measurement of 1.5 nm. In summary, experimental results and DFT calculations reveal that oriented

attachment growth of ZnTe F398 MSNCs along [100] and [002] directions form (110) facet dominant wurtzite ZnTe NPLs.

3.4 Conclusion

In conclusion, we have synthesized free-standing wurtzite ZnTe NPLs with an atomically uniform thickness of ~1.5 nm by using polytelluride species reduced by superhydride from TBP-Te as tellurium precursor. This growth process involved a stepwise evolution from metastable self-assembled ZnTe MSNCs and oriented attachment of ZnTe F398 MSNCs along [100] and [002] directions. The availability of ZnTe NPLs opens the gate for extending their properties of multiple-quantum well structures with a variety of potential applications in optoelectronics, sensors and detectors.

3.5 References

1. Diroll, B. T.; Schaller, R. D., Shape-selective optical transformations of CdSe nanoplatelets driven by halide ion ligand exchange. *Chemistry of Materials* **2019**.

2. Christodoulou, S.; Climente, J. I.; Planelles, J.; Brescia, R.; Prato, M.; Martin-Garcia, B.; Khan, A. H.; Moreels, I., Chloride-induced thickness control in CdSe nanoplatelets. *Nano Letters* **2018,** *18* (10), 6248-6254.

3. Bouet, C.; Tessier, M. D.; Ithurria, S.; Mahler, B.; Nadal, B.; Dubertret, B., Flat colloidal semiconductor nanoplatelets. *Chemistry of Materials* **2013,** *25* (8), 1262-1271.

4. Bouet, C.; Mahler, B.; Nadal, B.; Abecassis, B.; Tessier, M. D.; Ithurria, S.; Xu, X. Z.; Dubertret, B., Two-dimensional growth of CdSe nanocrystals, from nanoplatelets to nanosheets. *Chemistry of Materials* **2013,** *25* (4), 639-645.

5. Ithurria, S.; Tessier, M. D.; Mahler, B.; Lobo, R. P.; Dubertret, B.; Efros, A. L., Colloidal nanoplatelets with two-dimensional electronic structure. *Nature Materials* **2011,** *10* (12), 936-41.

6. Lim, S. J.; Kim, W.; Shin, S. K., Surface-dependent, ligand-mediated photochemical etching of CdSe nanoplatelets. *Journal of the American Chemical Society* **2012,** *134* (18), 7576-7579.

7. Khan, A. H.; Brescia, R.; Polovitsyn, A.; Angeloni, I.; Martín-García, B.; Moreels, I., Near-infrared emitting colloidal PbS nanoplatelets: lateral size control and optical spectroscopy. *Chemistry of Materials* **2017,** *29* (7), 2883-

2889.

8. Jana, S.; Phan, T. N.; Bouet, C.; Tessier, M. D.; Davidson, P.; Dubertret, B.; Abécassis, B., Stacking and colloidal stability of CdSe nanoplatelets. *Langmuir* **2015,** *31* (38), 10532-10539.

9. Jana, S.; Davidson, P.; Abécassis, B., CdSe nanoplatelets: living polymers. *Angewandte Chemie* **2016,** *128* (32), 9517-9520.

10. Dufour, M.; Qu, J.; Greboval, C.; Méthivier, C.; Lhuillier, E.; Ithurria, S., Halide ligands to release strain in cadmium chalcogenide nanoplatelets and achieve high brightness. *ACS Nano* **2019,** *13* (5), 5326-5334.

11. Galle, T.; Samadi Khoshkhoo, M.; Martin-Garcia, B.; Meerbach, C.; Sayevich, V.; Koitzsch, A.; Lesnyak, V.; Eychmüller, A., Colloidal PbSe nanoplatelets of varied thickness with tunable optical properties. *Chemistry of Materials* **2019,** *31* (10), 3803-3811.

12. Liu, Y.; Rowell, N.; Willis, M.; Zhang, M.; Wang, S.; Fan, H.; Huang, W.; Chen, X.; Yu, K., Photoluminescent colloidal nanohelices self-assembled from CdSe magic-size clusters via nanoplatelets. *The Journal of Physical Chemistry Letters* **2019**, 2794-2801.

13. Pandya, R.; Chen, R. Y. S.; Cheminal, A.; Dufour, M.; Richter, J. M.; Thomas, T. H.; Ahmed, S.; Sadhanala, A.; Booker, E. P.; Divitini, G.; Deschler, F.; Greenham, N. C.; Ithurria, S.; Rao, A., Exciton–phonon interactions govern charge-transfer-state dynamics in CdSe/CdTe two-dimensional colloidal heterostructures. *Journal of the American Chemical Society* **2018,** *140* (43), 14097-14111.

14. Winkler, J. M.; Rabouw, F. T.; Rossinelli, A. A.; Jayanti, S. V.; McPeak, K. M.; Kim, D. K.; le Feber, B.; Prins, F.; Norris, D. J., Room-temperature strong coupling of CdSe nanoplatelets and plasmonic hole arrays. *Nano Letters* **2019,** *19* (1), 108-115.

15. Tessier, M. D.; Spinicelli, P.; Dupont, D.; Patriarche, G.; Ithurria, S.; Dubertret, B., Efficient exciton concentrators built from colloidal core/crown CdSe/CdS semiconductor nanoplatelets. *Nano Letters* **2014,** *14* (1), 207-213.

16. Kunneman, L. T.; Tessier, M. D.; Heuclin, H.; Dubertret, B.; Aulin, Y. V.; Grozema, F. C.; Schins, J. M.; Siebbeles, L. D. A., Bimolecular Auger recombination of electron–hole pairs in two-dimensional CdSe and CdSe/CdZnS core/shell nanoplatelets. *The Journal of Physical Chemistry*

Letters **2013,** *4* (21), 3574-3578.

17. Wu, K.; Li, Q.; Jia, Y.; McBride, J. R.; Xie, Z.-x.; Lian, T., Efficient and ultrafast formation of long-lived charge-transfer exciton state in atomically thin cadmium selenide/cadmium telluride type-II heteronanosheets. *ACS Nano* **2015,** *9* (1), 961-968.

18. Benchamekh, R.; Gippius, N. A.; Even, J.; Nestoklon, M. O.; Jancu, J. M.; Ithurria, S.; Dubertret, B.; Efros, A. L.; Voisin, P., Tight-binding calculations of image-charge effects in colloidal nanoscale platelets of CdSe. *Physical Review B* **2014,** *89* (3), 035307.

19. Meerbach, C.; Tietze, R.; Voigt, S.; Sayevich, V.; Dzhagan, V. M.; Erwin, S. C.; Dang, Z.; Selyshchev, O.; Schneider, K.; Zahn, D. R., Brightly luminescent core/shell nanoplatelets with continuously tunable optical properties. *Advanced Optical Materials* **2019**, 1801478.

20. Achtstein, A. W.; Scott, R.; Kickhöfel, S.; Jagsch, S. T.; Christodoulou, S.; Bertrand, G. H.; Prudnikau, A. V.; Antanovich, A.; Artemyev, M.; Moreels, I., p-state luminescence in CdSe nanoplatelets: role of lateral confinement and a longitudinal optical phonon bottleneck. *Physical Review Letters* **2016,** *116* (11), 116802.

21. Planelles, J.; Achtstein, A. W.; Scott, R.; Owschimikow, N.; Woggon, U.; Climente, J. I., Tuning intraband and interband transition rates via excitonic correlation in low-dimensional semiconductors. *ACS Photonics* **2018,** *5* (9), 3680-3688.

22. Delikanli, S.; Guzelturk, B.; Hernández-Martínez, P. L.; Erdem, T.; Kelestemur, Y.; Olutas, M.; Akgul, M. Z.; Demir, H. V., Continuously tunable emission in inverted type-I CdS/CdSe core/crown semiconductor nanoplatelets. *Advanced Functional Materials* **2015,** *25* (27), 4282-4289.

23. Li, M.; Zhi, M.; Zhu, H.; Wu, W.-Y.; Xu, Q.-H.; Jhon, M. H.; Chan, Y., Ultralow-threshold multiphoton-pumped lasing from colloidal nanoplatelets in solution. *Nature Communications* **2015,** *6*, 8513.

24. Guzelturk, B.; Kelestemur, Y.; Olutas, M.; Delikanli, S.; Demir, H. V., Amplified spontaneous emission and lasing in colloidal nanoplatelets. *ACS Nano* **2014,** *8* (7), 6599-6605.

25. Olutas, M.; Guzelturk, B.; Kelestemur, Y.; Yeltik, A.; Delikanli, S.; Demir, H. V., Lateral size-dependent spontaneous and stimulated emission properties in

colloidal CdSe nanoplatelets. *ACS Nano* **2015,** *9* (5), 5041-5050.

26. Biadala, L.; Liu, F.; Tessier, M. D.; Yakovlev, D. R.; Dubertret, B.; Bayer, M., Recombination dynamics of band edge excitons in quasi-two-dimensional CdSe nanoplatelets. *Nano Letters* **2014,** *14* (3), 1134-1139.

27. Mahler, B.; Nadal, B.; Bouet, C.; Patriarche, G.; Dubertret, B., Core/shell colloidal semiconductor nanoplatelets. *Journal of the American Chemical Society* **2012,** *134* (45), 18591-18598.

28. Pelton, M.; Ithurria, S.; Schaller, R. D.; Dolzhnikov, D. S.; Talapin, D. V., Carrier cooling in colloidal quantum wells. *Nano Letters* **2012,** *12* (12), 6158-6163.

29. Tomar, R.; Kulkarni, A.; Chen, K.; Singh, S.; van Thourhout, D.; Hodgkiss, J. M.; Siebbeles, L. D. A.; Hens, Z.; Geiregat, P., Charge carrier cooling bottleneck opens up nonexcitonic gain mechanisms in colloidal CdSe quantum wells. *The Journal of Physical Chemistry C* **2019,** *123* (14), 9640-9650.

30. Gao, Y.; Li, M.; Delikanli, S.; Zheng, H.; Liu, B.; Dang, C.; Sum, T. C.; Demir, H. V., Low-threshold lasing from colloidal CdSe/CdSeTe core/alloyed-crown type-II heteronanoplatelets. *Nanoscale* **2018,** *10* (20), 9466-9475.

31. Antanovich, A. V.; Prudnikau, A. V.; Melnikau, D.; Rakovich, Y. P.; Chuvilin, A.; Woggon, U.; Achtstein, A. W.; Artemyev, M. V., Colloidal synthesis and optical properties of type-II CdSe–CdTe and inverted CdTe–CdSe core–wing heteronanoplatelets. *Nanoscale* **2015,** *7* (17), 8084-8092.

32. Li, Q.; Lian, T., A model for optical gain in colloidal nanoplatelets. *Chemical Science* **2018,** *9* (3), 728-734.

33. She, C.; Fedin, I.; Dolzhnikov, D. S.; Demortière, A.; Schaller, R. D.; Pelton, M.; Talapin, D. V., Low-threshold stimulated emission using colloidal quantum wells. *Nano Letters* **2014,** *14* (5), 2772-2777.

34. Grim, J. Q.; Christodoulou, S.; Di Stasio, F.; Krahne, R.; Cingolani, R.; Manna, L.; Moreels, I., Continuous-wave biexciton lasing at room temperature using solution-processed quantum wells. *Nature Nanotechnology* **2014,** *9*, 891.

35. Dede, D.; Taghipour, N.; Quliyeva, U.; Sak, M.; Kelestemur, Y.; Gungor, K.; Demir, H. V., Highly stable multicrown heterostructures of type-II nanoplatelets for ultralow threshold optical gain. *Chemistry of Materials* **2019,** *31* (5), 1818-1826.

36. Yeltik, A.; Delikanli, S.; Olutas, M.; Kelestemur, Y.; Guzelturk, B.; Demir, H. V., Experimental determination of the absorption cross-section and molar extinction coefficient of colloidal CdSe nanoplatelets. *The Journal of Physical Chemistry C* **2015,** *119* (47), 26768-26775.

37. Achtstein, A. W.; Antanovich, A.; Prudnikau, A.; Scott, R.; Woggon, U.; Artemyev, M., Linear absorption in CdSe nanoplates: thickness and lateral size dependency of the intrinsic absorption. *The Journal of Physical Chemistry C* **2015,** *119* (34), 20156-20161.

38. Scott, R.; Achtstein, A. W.; Prudnikau, A.; Antanovich, A.; Christodoulou, S.; Moreels, I.; Artemyev, M.; Woggon, U., Two photon absorption in II–VI semiconductors: the influence of dimensionality and size. *Nano Letters* **2015,** *15* (8), 4985-4992.

39. Li, Q.; Liu, Q.; Schaller, R. D.; Lian, T., Reducing the optical gain threshold in two-dimensional CdSe nanoplatelets by the giant oscillator strength transition effect. *The Journal of Physical Chemistry Letters* **2019,** *10* (7), 1624-1632.

40. Achtstein, A. W.; Schliwa, A.; Prudnikau, A.; Hardzei, M.; Artemyev, M. V.; Thomsen, C.; Woggon, U., Electronic structure and exciton–phonon interaction in two-dimensional colloidal CdSe nanosheets. *Nano Letters* **2012,** *12* (6), 3151-3157.

41. Naeem, A.; Masia, F.; Christodoulou, S.; Moreels, I.; Borri, P.; Langbein, W., Giant exciton oscillator strength and radiatively limited dephasing in two-dimensional platelets. *Physical Review B* **2015,** *91* (12), 121302.

42. Lhuillier, E.; Robin, A.; Ithurria, S.; Aubin, H.; Dubertret, B., Electrolyte-gated colloidal nanoplatelets-based phototransistor and its use for bicolor detection. *Nano Letters* **2014,** *14* (5), 2715-2719.

43. Lhuillier, E.; Ithurria, S.; Descamps-Mandine, A.; Douillard, T.; Castaing, R.; Xu, X. Z.; Taberna, P.-L.; Simon, P.; Aubin, H.; Dubertret, B., Investigating the n- and p-type electrolytic charging of colloidal nanoplatelets. *The Journal of Physical Chemistry C* **2015,** *119* (38), 21795-21799.

44. Lhuillier, E.; Pedetti, S.; Ithurria, S.; Heuclin, H.; Nadal, B.; Robin, A.; Patriarche, G.; Lequeux, N.; Dubertret, B., Electrolyte-gated field effect transistor to probe the surface defects and morphology in films of thick CdSe colloidal nanoplatelets. *ACS Nano* **2014,** *8* (4), 3813-3820.

45. Lhuillier, E.; Dayen, J.-F.; Thomas, D. O.; Robin, A.; Doudin, B.; Dubertret, B., Nanoplatelets bridging a nanotrench: a new architecture for photodetectors with increased sensitivity. *Nano Letters* **2015,** *15* (3), 1736-1742.

46. Bi, W.; Zhou, M.; Ma, Z.; Zhang, H.; Yu, J.; Xie, Y., $CuInSe_2$ ultrathin nanoplatelets: novel self-sacrificial template-directed synthesis and application for flexible photodetectors. *Chemical Communications* **2012,** *48* (73), 9162-9164.

47. Vitukhnovsky, A.; Lebedev, V.; Selyukov, A.; Vashchenko, A.; Vasiliev, R.; Sokolikova, M., Electroluminescence from colloidal semiconductor CdSe nanoplatelets in hybrid organic–inorganic light emitting diode. *Chemical Physics Letters* **2015,** *619*, 185-188.

48. Zhang, F.; Wang, S.; Wang, L.; Lin, Q.; Shen, H.; Cao, W.; Yang, C.; Wang, H.; Yu, L.; Du, Z., Super color purity green quantum dot light-emitting diodes fabricated by using CdSe/CdS nanoplatelets. *Nanoscale* **2016,** *8* (24), 12182-12188.

49. Liu, B.; Delikanli, S.; Gao, Y.; Dede, D.; Gungor, K.; Demir, H. V., Nanocrystal light-emitting diodes based on type II nanoplatelets. *Nano Energy* **2018,** *47*, 115-122.

50. Giovanella, U.; Pasini, M.; Lorenzon, M.; Galeotti, F.; Lucchi, C.; Meinardi, F.; Luzzati, S.; Dubertret, B.; Brovelli, S., Efficient solution-processed nanoplatelet-based light-emitting diodes with high operational stability in air. *Nano Letters* **2018,** *18* (6), 3441-3448.

51. Zhang, F.; Wang, S.; Wang, L.; Lin, Q.; Shen, H.; Cao, W.; Yang, C.; Wang, H.; Yu, L.; Du, Z.; Xue, J.; Li, L. S., Super color purity green quantum dot light-emitting diodes fabricated by using CdSe/CdS nanoplatelets. *Nanoscale* **2016,** *8* (24), 12182-12188.

52. Chen, Z.; Nadal, B.; Mahler, B.; Aubin, H.; Dubertret, B., Quasi-2D colloidal semiconductor nanoplatelets for narrow electroluminescence. *Advanced Functional Materials* **2014,** *24* (3), 295-302.

53. Fan, F.; Kanjanaboos, P.; Saravanapavanantham, M.; Beauregard, E.; Ingram, G.; Yassitepe, E.; Adachi, M. M.; Voznyy, O.; Johnston, A. K.; Walters, G.; Kim, G.-H.; Lu, Z.-H.; Sargent, E. H., Colloidal $CdSe_{1-x}S_x$ nanoplatelets with narrow and continuously-tunable electroluminescence. *Nano Letters* **2015,**

15 (7), 4611-4615.

54. Vitukhnovsky, A. G.; Lebedev, V. S.; Selyukov, A. S.; Vashchenko, A. A.; Vasiliev, R. B.; Sokolikova, M. S., Electroluminescence from colloidal semiconductor CdSe nanoplatelets in hybrid organic–inorganic light emitting diode. *Chemical Physics Letters* **2015,** *619*, 185-188.

55. Pedetti, S.; Nadal, B.; Lhuillier, E.; Mahler, B.; Bouet, C. c.; Abécassis, B.; Xu, X.; Dubertret, B., Optimized synthesis of CdTe nanoplatelets and photoresponse of CdTe nanoplatelets films. *Chemistry of Materials* **2013,** *25* (12), 2455-2462.

56. Li, Z.; Peng, X., Size/shape-controlled synthesis of colloidal CdSe quantum disks: ligand and temperature effects. *Journal of the American Chemical Society* **2011,** *133* (17), 6578-6586.

57. Li, Z.; Qin, H. Y.; Guzun, D.; Benamara, M.; Salamo, G.; Peng, X. G., Uniform thickness and colloidal-stable CdS quantum disks with tunable thickness: synthesis and properties. *Nano Research* **2012,** *5* (5), 337-351.

58. Liu, Y.-H.; Wang, F.; Wang, Y.; Gibbons, P. C.; Buhro, W. E., Lamellar assembly of cadmium selenide nanoclusters into quantum belts. *Journal of the American Chemical Society* **2011,** *133* (42), 17005-17013.

59. Cao, Y. L.; Liu, Z. T.; Chen, L. M.; Tang, Y. B.; Luo, L. B.; Jie, J. S.; Zhang, W. J.; Lee, S. T.; Lee, C. S., Single-crystalline ZnTe nanowires for application as high-performance green/ultraviolet photodetector. *Optics Express* **2011,** *19* (7), 6100-6108.

60. Lee, K. S.; Oh, G.; Kim, E. K., High performance intermediate-band solar cells based on ZnTe:Cr with ZnO:Al electron transport layer. *Solar Energy* **2018,** *164*, 262-266.

61. Loffler, T.; Hahn, T.; Thomson, M.; Jacob, F.; Roskos, H., Large-area electro-optic ZnTe terahertz emitters. *Optics Express* **2005,** *13* (14), 5353-5362.

62. Zhang, J.; Jin, S.; Fry, H. C.; Peng, S.; Shevchenko, E.; Wiederrecht, G. P.; Rajh, T., Synthesis and characterization of wurtzite ZnTe nanorods with controllable aspect ratios. *Journal of the American Chemical Society* **2011,** *133* (39), 15324-7.

63. Zhang, J.; Rowland, C.; Liu, Y.; Xiong, H.; Kwon, S.; Shevchenko, E.; Schaller, R. D.; Prakapenka, V. B.; Tkachev, S.; Rajh, T., Evolution of self-

assembled ZnTe magic-sized nanoclusters. *Journal of the American Chemical Society* **2015,** *137* (2), 742-749.

64. Son, J. S.; Wen, X. D.; Joo, J.; Chae, J.; Baek, S. I.; Park, K.; Kim, J. H.; An, K.; Yu, J. H.; Kwon, S. G.; Choi, S. H.; Wang, Z.; Kim, Y. W.; Kuk, Y.; Hoffmann, R.; Hyeon, T., Large-scale soft colloidal template synthesis of 1.4 nm thick CdSe nanosheets. *Angewandte Chemie International Edition* **2009,** *48* (37), 6861-6864.

65. Hu, D.; Zhang, P.; Gong, P.; Lian, S.; Lu, Y.; Gao, D.; Cai, L., A fast synthesis of near-infrared emitting CdTe/CdSe quantum dots with small hydrodynamic diameter for in vivo imaging probes. *Nanoscale* **2011,** *3* (11), 4724-32.

66. Smith, D. K.; Luther, J. M.; Semonin, O. E.; Nozik, A. J.; Beard, M. C., Tuning the synthesis of ternary lead chalcogenide quantum dots by balancing precursor reactivity. *ACS Nano* **2010,** *5* (1), 183-190.

67. Sun, H.; Wang, F.; Buhro, W. E., Tellurium precursor for nanocrystal synthesis: tris(dimethylamino)phosphine telluride. *ACS Nano* **2018,** *12* (12), 12393-12400.

68. Blöchl, P. E., Projector augmented-wave method. *Physical Review B* **1994,** *50* (24), 17953.

69. Kresse, G.; Furthmuller, J., Efficient iterative schemes for ab initio total-energy calculations using a plane-wave basis set. *Physical Review B* **1996,** *54* (16), 11169-11186.

70. Perdew, J. P.; Burke, K.; Ernzerhof, M., Generalized gradient approximation made simple. *Physical Review Letters* **1996,** *77* (18), 3865-3868.

71. Soykan, C.; Kart, S. Ö., Structural, mechanical and electronic properties of ZnTe polymorphs under pressure. *Journal of Alloys and Compounds* **2012,** *529*, 148-157.

72. Liu, Y.; Willis, M.; Rowell, N.; Luo, W.; Fan, H.; Han, S.; Yu, K., Effect of small molecule additives in the prenucleation stage of semiconductor CdSe quantum dots. *The Journal of Physical Chemistry Letters* **2018,** *9* (21), 6356-6363.

73. Ji, X.; Copenhaver, D.; Sichmeller, C.; Peng, X., Ligand bonding and dynamics on colloidal nanocrystals at room temperature: the case of alkylamines on CdSe nanocrystals. *Journal of the American Chemical Society*

2008, *130* (17), 5726-5735.

74. Wang, Y.; Zhou, Y.; Zhang, Y.; Buhro, W. E., Magic-size II-VI nanoclusters as synthons for flat colloidal nanocrystals. *Inorganic Chemistry* **2015,** *54* (3), 1165-1177.

75. Park, H.; Chung, H.; Kim, W., Synthesis of ultrathin wurtzite ZnSe nanosheets. *Materials Letters* **2013,** *99*, 172-175.

76. Gutsev, L. G.; Ramachandran, B. R.; Gutsev, G. L., Pathways of growth of CdSe nanocrystals from nucleant $(CdSe)_{34}$ clusters. *Journal of Physical Chemistry C* **2018,** *122* (5), 3168-3175.

77. Zhou, Y.; Jiang, R.; Wang, Y.; Rohrs, H. W.; Rath, N. P.; Buhro, W. E., Isolation of amine derivatives of $(ZnSe)_{34}$ and $(CdTe)_{34}$. Spectroscopic comparisons of the $(II–VI)_{13}$ and $(II–VI)_{34}$ magic-size nanoclusters. *Inorganic Chemistry* **2019,** *58* (3), 1815-1825.

Chapter 4 Shape-controllable synthesis of wurtzite CdTe nanoplatelets by tuning Te precursor reactivity

4.1 Introduction

In the past decade, colloidal semiconductor nanoplatelets (NPLs),[1-6] quantum disk,[7-9] nanosheets,[10-16] nanoribbons,[17-21] quantum belts,[22-25] quantum platelets[26-27] with excitons only confined in the thickness dimension have been of great interest due to their attractive photophysical properties such as extremely narrow photoluminescence linewidth,[28-30] giant oscillator strengths,[31-32] and large nonlinear absorption cross-section.[33-38] Unlike the synthesis of zinc-blende II-VI nanoplatelets in 1-octadecene (ODE) as solvent and fatty acid salts as cation precursor at elevated temperatures,[3, 39-41] wurtzite II-VI NPLs prone to form from magic-sized nanoclusters (MSNCs) at a relatively low temperature.[26, 42-43] Buhro *et al.* have systematically investigated the synthesis, the conversion and optical spectroscopic properties of II-VI magic-sized nanoclusters.

Among the II-VI semiconductors, CdTe with a direct bandgap of 1.47 eV in bulk at room temperature[44] and a bulk exciton Bhor radius of ~7.3nm[45] has important applications in photovoltatics[46-51] and photodetectors[52-55] due to its high optical absorption coefficient in the visible-infrared region and excellent photo responsivity. Although there are many reports on colloidal synthesis of CdTe quantum dots,[56-59] nanorods[60-62] and nanowires,[63-64] synthesizing CdTe NPLs still remains challenging. This is so because there are limited choices of tellurium precursor for the synthesis of CdTe nanocrystals. Currently, tellurium precursors such as trioctylphosphine telluride (TOP-Te),[65-67] tributylphosphine telluride (TBP-Te),[68-69] polytellurides reduced from TOP-Te by superhydride,[70-71] bis(tert-butyldimethylsilyl) telluride,[42] and tris(dimethylamino)phosphine telluride[72] have been used as the tellurium precursors for synthesizing ZnTe or CdTe nanocrystals. For the synthesis of high quality CdTe nanocrystals, tellurium precursors with appropriate reactivities are required.

In 2013, Dubertret *et al.* reported the colloidal synthesis of zinc-blende CdTe nanoplatelets with photoluminescence emission at 428, 500 and 556 nm due to their different thicknesses.[73] In that work, cadmium propionate ($Cd(prop)_2$) or

cadmium oleate ($Cd(OA)_2$) was used as the cadmium precursor and TOP-Te was used as the tellurium precursor. 1-octadecene (ODE) and oleic acid (OA) were used as the non-coordinating solvents and ligands, respectively. The hot-injection of tellurium precursor into the cadmium precursor was performed at 180, 210 and 215 ^oC, which produced CdTe NPLs with their first excitonic emission peak at 428, 500, 556 nm, respectively. As shown in Figure 4.1, there is a nearly zero shift between the first exciton absorption peak and PL emission peak of these CdTe NPLs, which is a characteristic of colloidal semiconductor NPLs. Interestingly, these synthesized CdTe NPLs have different lateral size and shape. By changing the hot-injection temperature or the molar ratio of oleic acid to the cadmium precursor with short-chain carboxylate groups, the lateral size and shape can be further controlled as illustrated in Figure 4.2.

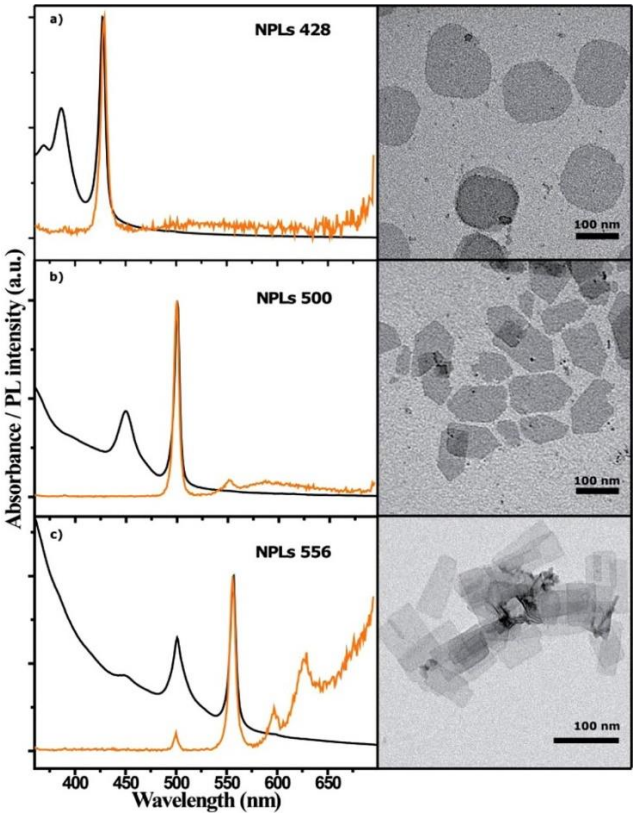

Figure 4.1 CdTe NPLs with three different thicknesses. Left, absorption (black) and photoluminescence (orange) spectra of NPLs with different thicknesses. Right, TEM images of the corresponding samples. (a) NPLs with the first excitonic peak at 428 nm, (b) NPLs with the first excitonic peak at 500 nm, (c) NPLs with the first excitonic peak at 556 nm. Reprinted with permission from ref. 73. Copyright 2013 American Chemical Society.[73]

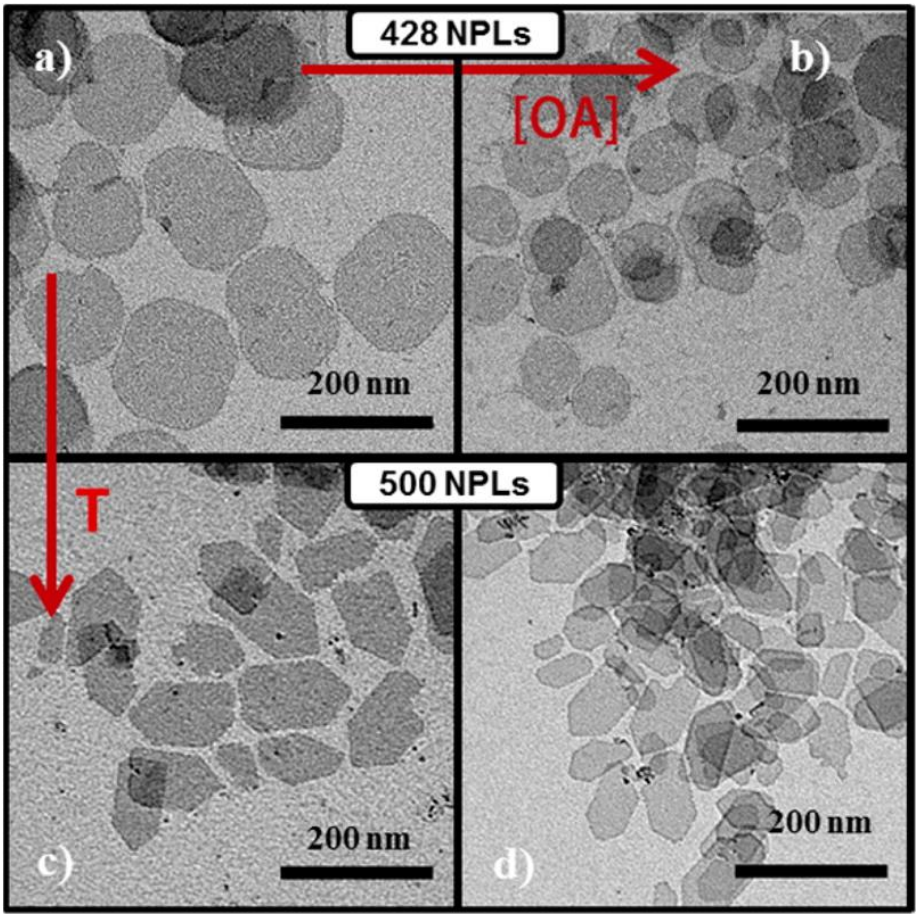

Figure 4.2 Control of the NPLs lateral sizes. TEM images of NPLs synthesized in presence of 0.5 mmol of $Cd(prop)_2$ in 10 mL of ODE. The concentration of OA acid is 25 mM in a and c and 50 mM in b and c. 0.1 mmol of TOP-Te 1 M is injected at 180 °C in a and b giving 428 NPLs, while at 210 °C in c and d giving as final product 500 NPLs. Reprinted with permission from ref. 73. Copyright 2013 American Chemical Society.[73]

Two growth mechanisms of zinc-blende CdTe NPLs were proposed to explain the formation of NPLs with different thicknesses as presented in Scheme 4.1. The mechanism A illustrates that the thinnest CdTe NPLs dissolve completely to form crystal seeds which react rapidly with precursors to produce thicker NPLs with better stability. The mechanism B presents that the thinnest CdTe NPLs dissovle partially to assist the growth of another layer on existing NPLs for reacting with precursors in ripening.

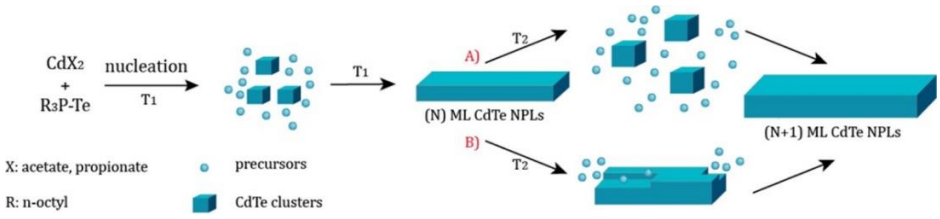

Scheme 4.1 Possible mechanistic schemes to explain the thickness evolution CdTe NPLs during the synthesis. Reprinted with permission from ref. 73. Copyright 2013 American Chemical Society.[73]

In 2018, Buhro *et al*. prepared tris(dimethylamino)phosphine telluride ($(Me_2N)_3PTe$) by dissolving tellurium granules in tris(dimethylamino)phosphine ($(Me_2N)_3P$) at 100 °C for 3h as a new telluride precursor to synthesize CdTe nanocrystals.[72] The molecular structures of transaminated phosphine tellurides are shown in Scheme 4.2. This new tellurium compound is sufficiently reactive for synthesizing CdTe nanocrystals at 100 °C.

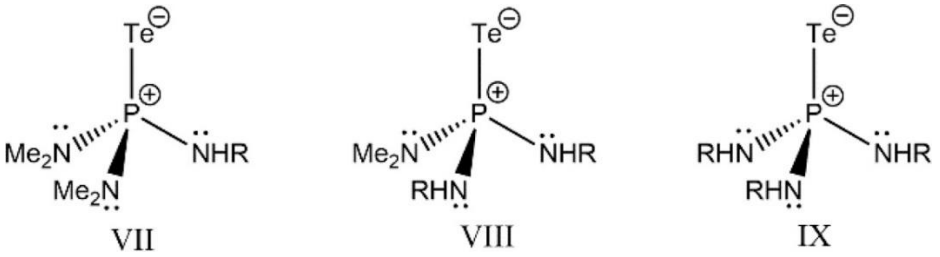

Scheme 4.2 Transaminated phosphine tellurides. R=*n*-octyl. Reprinted with permission from ref. 72. Copyright 2018 American Chemical Society.[72]

As a benchmark approach of the bottom-up method, shape-controllable synthesis of colloidal semiconductor nanocrystals is of great importance due to the shape-dependent optical properties of semiconductor nanocrystals. In addition, it provides chemical insights into the nucleation and growth kinetics and growth mechanisms of nanocrystals. Generally, the shape control of semiconductor nanocrystals can be achieved with different reaction conditions such as by changing the reaction temperature and duration, and tuning the precursor reactivity and concentration.

In this work, we report a shape-controllable synthesis of 2D wurtzite CdTe nanoplatelets by simply tailoring Te precursor reactivity. Ribbon-, shield- and bullet-like NPLs were prepared by a stepwise conversion from CdTe MSNCs by

using Te_3^{2-}, Te_2^{2-} and Te^{2-} polytellurides as tellurium precursor, respectively. In addition, the surface chemical environment and composition of as-prepared CdTe NPLs were investigated by X-ray photoelectron spectroscopy (XPS) and Fourier-transform infrared (FTIR) spectroscopy.

4.2 Experimental section

4.2.1 Materials

Anhydrous cadmium chloride ($CdCl_2$, trace metals basis, 99.99%), oleylamine (70%, technical grade), octylamine (99%), tributylphosphine (97%, mixture of isomers), super-hydride® solution (1.0 M lithium triethylborohydride in tetrahydrofuran), anhydrous toluene (99.8%), and anhydrous methanol (99.8%) were obtained from Sigma-Aldrich Pty Ltd, Australia. Tellurium (Te) powder (~325 mesh, 99.99% metals basis) was purchased from Alfa Aesar, Thermo Fisher Scientific Australia Pty Ltd. All chemicals were used as received without further purification.

4.2.2 Preparation of TBP-Te stock solution (1.0 M)

In a 25 ml round-bottom flask, a mixture of 15 ml TBP and 1.914 g (15 mmol) tellurium powder were heating at 240 °C for 3 hours under nitrogen atmosphere using the standard Schlenk line techniques. The color of the solution changed from opaque black gradually to opaque dark green, light yellow, translucent orange, finally to transparent brick red during the reaction period. After the reaction solution was cooled to room temperature, clear yellow TBP-Te stock solution was prepared and stored in a glove box for use.

4.2.3 Preparation of Te_3^{2-}, Te_2^{2-} and Te^{2-} species as tellurium precursor

First, 2 ml oleylamine and 0.6 ml TBP-Te stock solution (1.0M) were well mixed in a 12 ml glass vial using syringe in a glove box. Into this mixture, 0.4ml (2/3 equivalent of TBP-Te) was injected and further mixed using syringe. After the injection of superhydride solution, many bubbles were observed and the color of the mixture turned from yellow into red. For preparation of Te_2^{2-} and Te^{2-}, 0.6 (1 molar equivalent of TBP-Te) and 1.2 ml (2 equivalent of TBP-Te) superhydride solution was injected, respectively. Also, many bubbles were observed, and the color of the mixture turned into purple from yellow for preparation of Te_2^{2-} and into pale rustic from yellow for preparation of Te^{2-} as tellurium precursor, respectively.

4.2.4 Synthesis of free-standing CdTe NPLs using Te_3^{2-}, Te_2^{2-} and Te^{2-} as tellurium precursor

In a typical synthesis, 1 mmol $CdCl_2$, 7 ml oleylamine and 3 ml octylamine were mixed and degassed three times at room temperature. Then, this mixture was heated to 110 ^oC and kept at 110 ^oC for an hour, followed by cooling it down to 60 ^oC under nitrogen for injecting the freshly prepared Te_3^{2-} or Te_2^{2-} or Te^{2-} as tellurium precursor in a glove box. After the hot injection, the reaction temperature was increased from 60 ^oC to 120 °C and was kept at 120 °C for the growth of CdTe NPLs. Aliquots were taken out at different time intervals to monitor the formation of CdTe NPLs.

4.2.5 Synthesis of stacking CdTe NPLs using Te^{2-} as tellurium precursor

First, 1 mmol $CdCl_2$ and 10 ml oleylamine were mixed and degassed three times at room temperature. Then, this mixture was heated to 110 ^oC and kept at 110 ^oC for an hour, followed by cooling it down to 60 ^oC under nitrogen for injecting the freshly prepared Te^{2-} as tellurium precursor in a glove box. After the hot injection, the reaction temperature was increased from 60 ^oC to 120 °C and was kept at 120 °C for the growth of stacking CdTe NPLs.

4.2.6 Measurement and characterization

UV−vis spectra were measured using a Cary 4000 UV−Vis spectrophotometer with 1 nm resolution in a quartz cell with 1 cm path length. Low-resolution transmission electron microscopy (TEM) and selected-area electron diffraction (SAED) were recorded using a JEOL 2100 transmission electron microscope with an accelerating voltage of 120 kV. The SAED pattern was fitted with PASAD tools for Digital Micrograph.[74] High-resolution transmission electron microscopy (HRTEM) images were performed on a FEI Titan G2 80-200 transmission electron microscope operating at 200 kV. All the reaction mixtures were purified using anhydrous toluene as the solvent and anhydrous methanol as the antisolvent. After the second purification, purified CdTe nanocrystals were redispersed into anhydrous toluene and a drop of the solution was added onto a ultra-thin carbon-coated copper grid. X-ray photoelectron spectroscopy (XPS) measurements were performed on a Kratos Axis Ultra DLD spectrometer equipped with a monochromatic AlKα (1486.6 eV) irradiation source operating at an X-ray gun power of 150 W. The vacuum pressure of the analysis chamber within the

spectrometer was maintained at 8 x 10^{-9} Torr or lower. The binding energy scale was calibrated by setting the main line of the C 1s spectrum to 284.8 eV. XPS spectrum was recorded with a pass energy of 160 eV for the survey spectrum and 40 eV for the high-resolution spectra. Shirley background corrections were applied to the survey and high-resolution spectra. Each high-resolution spectrum was fitted with a Gaussian-Lorentzian (70%-30%) line shape with the full-width half maximum (FWHM) constrained to values considered reasonably for each element. Shirley background corrections were applied to the survey and high-resolution spectra. Each high-resolution spectrum was fitted with a Gaussian-Lorentzian (70%-30%) line shape with the full-width half maximum (FWHM) constrained to values considered reasonably for each element. Fourier-transform infrared (FTIR) spectrum was measured by using a Nicolet iS50 FT-IR spectrometer. Powder X-ray diffraction (XRD) patterns was recorded using Cu Kα (λ=1.5406 Å) photons from an X'per PRO (PANalytical) X-ray diffractometer operated at 40 kV and 40 mA.

4.3 Results and discussion

In this work, the shape control of 2D wurtzite CdTe nanoplatelets was achieved by simply tuning the reaction activity of a Te precursor. The Te precursor with a different reactivity was obtained by adding different equivalent (equiv.) superhydride to reduce tributylphosphine-telluride (TBP-Te). To investigate the effect of the Te precursor reactivity on the shape control of CdTe nanoplatelets, detailed studies on the Te precursor with or without the addition of superhydride were performed.

4.3.1 Polytelluride precursors

According to previous investigations, the reactivity of chalcogenide precursor has a significant effect on the synthesis and shape control of colloidal semiconductor nanocrystals.[65, 75-77] Figure 4.3(a) shows a digital photograph of the TBP-Te stock solution without and with adding of different equivalent superhydride solution. After the addition of superhydride, the colour of the TBP-Te stock solution gradually turned from yellow to red (3#, superhydride:TBP-Te=2/3:1), violet (4#, superhydride:TBP-Te=1:1), and pale rustic (5#, superhydride:TBP-Te=2:1) by mixing using syringe. The obvious colour change in the TBP-Te stock solution is related to the formation of different polytelluride species. The polytelluride with distinctive red, violet and pale rustic colour is Te_3^{2-},

Te_2^{2-} and Te^{2-} species, respectively, which was also investigated by Schultz *et al.* although they reduced the tellurium using alkali metal as the reducing agent in liquid ammonia soution.[78] Figure 4.3(b) presents the proposed reaction pathways for preparing soluble polytellurides by reducing TBP-Te with different molar equivalent of superhydride solution. In addition to the production of three kinds of polytellurides, hydrogen and triethylboron (Et_3B) as byproducts were also produced. The production of hydrogen was further proved by occurrence of many bubbles after adding superhydride solution to Te-TBP stock solution and mixing the solution. In addition, superhydride can gradually reduce TBP-Te to Te_3^{2-}, Te_2^{2-} and Te^{2-} with an increase molar equivalent, which presents different colours as shown in Figure 4.3(a) due to the different valence states of polytellurides.

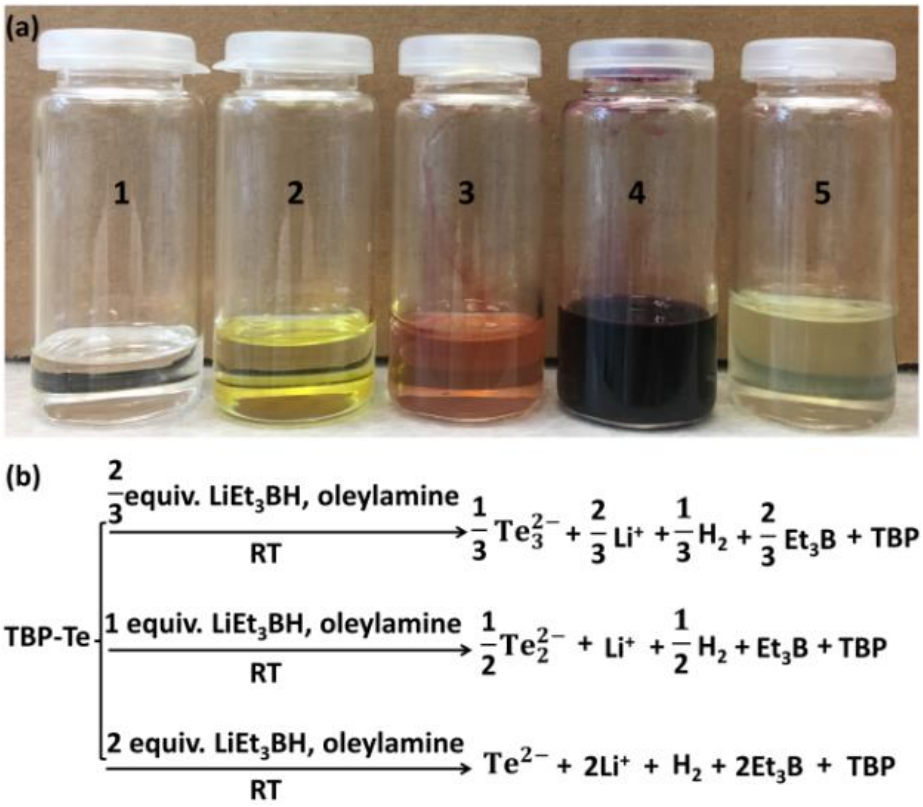

Figure 4.3 (a) A digital photograph of 2ml oleylamine (1#), 0.6ml TBP-Te stock solution (1.0M) in 2ml oleylamine (2#), and with adding different molar equivalent superhydride solution of Te-TBP: 2/3(3#), 1(4#), 2(5#). (b) Proposed reaction pathways for preparing soluble polytellurides by reducing TBP-Te with different molar equivalent of superhydride solution.

Among the three polytelluride species, the reactivity of Te^{2-}could be highest because it is ready to form ZnTe monomer as shown in the following reaction:

$$Zn^{2+} + Te^{2-} \rightarrow ZnTe$$

whereas the other two polytellurides Te_3^{2-} and Te_2^{2-} need to be further reduced to Te^{2-}. In addition, the *Ab initio* calculations of the Gibbs free-reaction energies for the formation of ZnSe, $ZnSe_2$ and $ZnSe_3$ from Zn^{2+} and Se^{2-}, Se_2^{2-} and Se_3^{2-} shows that the exergonicity of these reactions increases in the order: $Se_3^{2-} < Se_2^{2-} \ll Se^{2-}$, and the reactivity of polytellurides is expected to follow this trend as: $Te_3^{2-} < Te_2^{2-} \ll Te^{2-}$ because Se and Te are at the same VI main group in the periodic table with similar chemical properties.

4.3.2 Morphological and structural characterizations

Figure 4.4(a) shows the absorption spectra of as-prepared CdTe MSNCs and NPLs using Te^{2-} as tellurium precursor. The absorption spectrum (red curve in Figure 4.4(a)) exhibits a sharp peak at 366 nm along with a shoulder at 347 nm, matching well with the characteristic absorption peaks of $(CdTe)_{13}$ MSNCs.[43] Then, the absorption peaks of $(CdTe)_{13}$ MSNCs (green curve in Figure 4.4(a)) faded away and another two absorption peaks present at 433 and 476 nm, which are the unique absorption peaks of $(CdTe)_{34}$ MSNCs.[79] The coexistence of the featured absorption peaks of $(CdTe)_{13}$ and $(CdTe)_{34}$ MSNCs proves the stepwise evolution from $(CdTe)_{13}$ MSNCs to $(CdTe)_{34}$ MSNCs. The blue curve in Figure 4.4(a) presents the absorption spectrum of CdTe NPLs, wherein a sharp absorption peak appears at 489 nm and a shoulder at 444 nm. These absorption peak positions of CdTe NPLs match well with the spectral features in wurtzite CdTe quantum belts reported previously with only a shift of 2nm due to different ligand effect.[43] However, these absorption peak positions of as-synthesized wurtzite CdTe NPLs are not in accordance with those of zinc-blende CdTe NPLs because of different size in thickness. This “double absorption peaks” feature is usually observed for both zinc blende and wurtzite II-VI semiconductor nanoplatelets due to the electron-light hole (e-lh) and electron-heavy hole (e-hh) transitions.[1, 3, 35, 39-40, 80] Figure 4.4(b) shows the temporal evolution of UV-vis absorption spectra of CdTe MSNCs and NPLs, which gives a clearer picture of the evolution process. When the reaction was allowed to proceeded for 30 mins at 120 ˚C, $(CdTe)_{34}$ MSNCs completely transformed themselves into CdTe NPLs (curve 3 in Figure 4.4(b)). Gradual sharpening of the first exciton absorption peak of CdTe NPLs was observed for a longer annealing at 120 ^{o}C for 180 mins (curve 3 to curve 5 in Figure 4.4(b)), which indicates that CdTe NPLs gradually form an atomically flat

basal plane therefore the excitons are better confined only in the thickness dimension of CdTe NPLs.

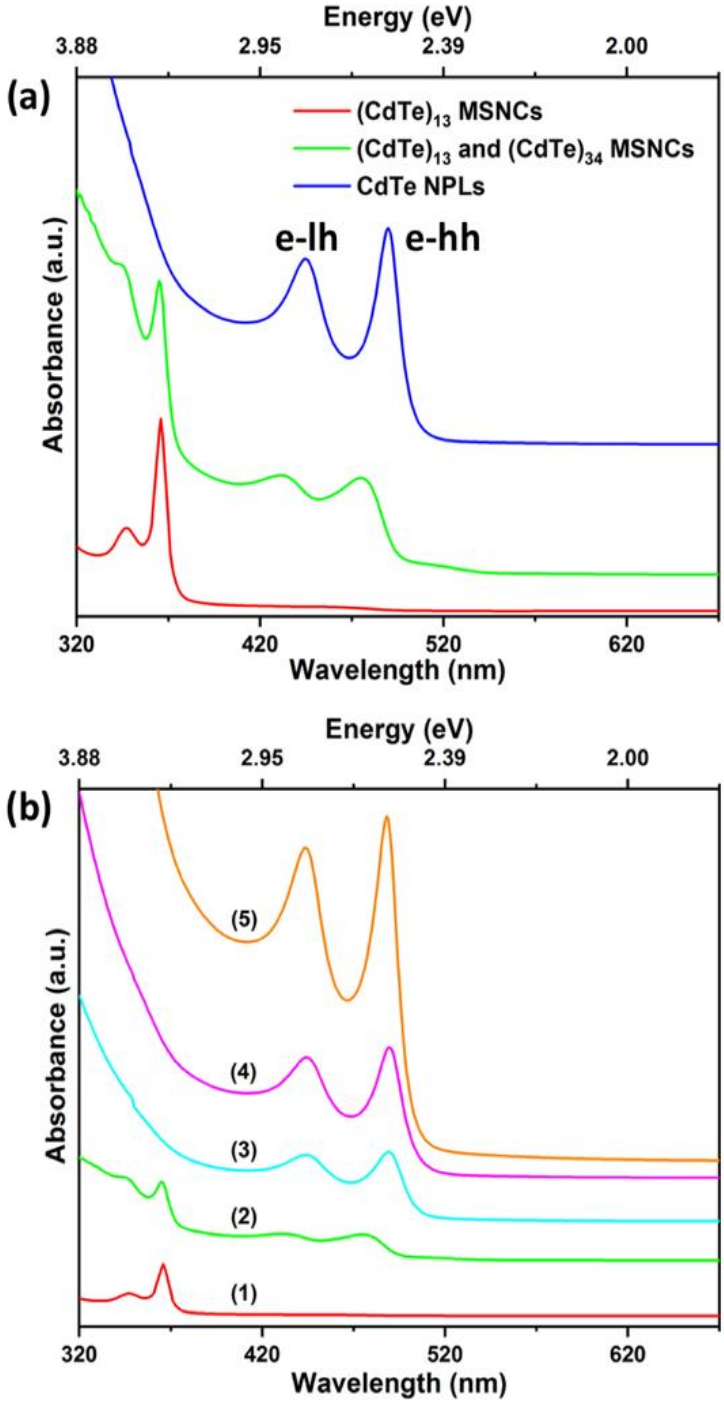

Figure 4.4 (a) UV-vis absorption spectra of as-prepared CdTe MSNCs and NPLs using Te^{2-} as tellurium precursor; (b) Temporal evolution of UV-vis spectra of CdTe MSNCs and NPLs. Aliquots taken at (1) 120 °C/1 min ($(CdTe)_{13}$ MSNCs), (2) 120 °C/2 min ($(CdTe)_{34}$ MSNCs), (3) 120 °C/30 min (CdTe NPLs), (4) 120 °C/90 min

(CdTe NPLs), (5) 120 °C/180 min (CdTe NPLs).

In addition, Figure 4.5 and 4.6 respectively present the UV-vis absorption spectra of as-prepared CdTe MSNCs and NPLs using Te_3^{2-} and Te_2^{2-} as tellurium precursor, wherein the absorption peak positons also match well with these of CdTe MSNCs and NPLs. However, it is notable that the absorption peaks of as-prepared CdTe NPLs using Te_3^{2-} as tellurium precursor are slightly broaden. This could result from the imperfect planes in the thick dimension, which will be further discussed later.

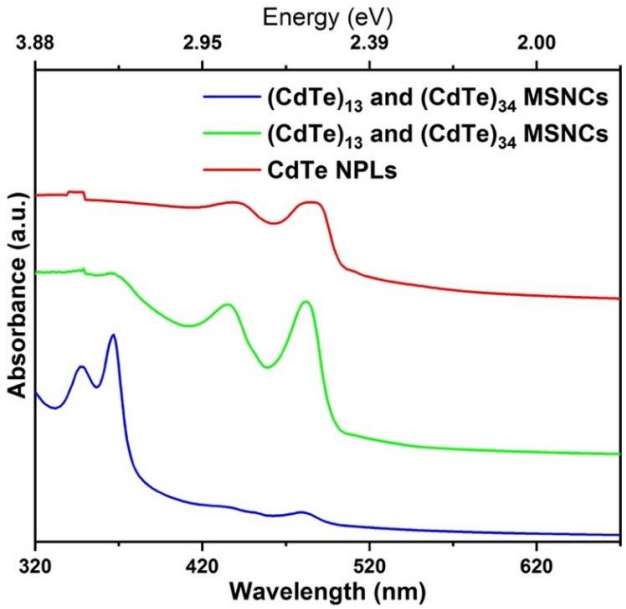

Figure 4.5 UV-vis absorption spectra of as-prepared CdTe MSNCs and ribbon-like NPLs using Te_3^{2-} as tellurium precursor.

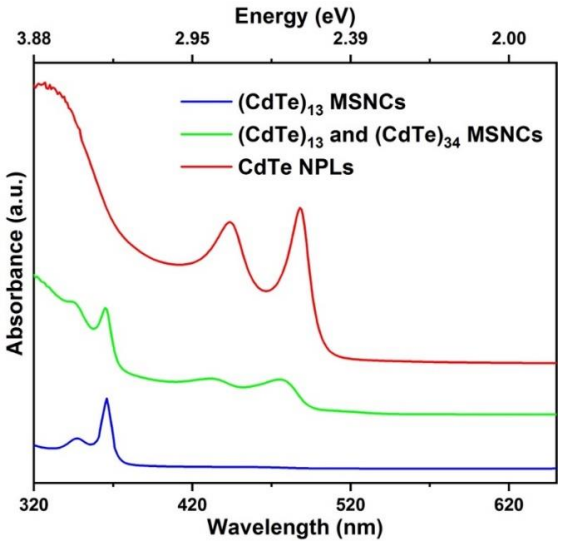

Figure 4.6 UV-vis absorption spectra of as-prepared CdTe MSNCs and sheild-like

NPLs using Te_2^{2-} as tellurium precursor.

Figure 4.7(a) presents the TEM image of CdTe NPLs prepared using Te_3^{2-} as tellurium precursor. From these NPLs standing on their edges (labeled by red dotted line) and non-standing NPLs, we can see that these ribbon-like NPLs have a large aspect ratio reaching up to 9. In addition, these NPLs are not perfectly grown due to the co-existence of nanodots, which broadens the absorption peaks of the products as shown in Figure 4.5. However, the as-prepared CdTe NPLs have a shield-like shape with a much smaller aspect ratio when Te_2^{2-} was used as tellurium precursor. Interestingly, bullet-like CdTe NPLs were prepared when Te^{2-} was used as tellurium precursor. The absorption peaks of shield- and bullet-like CdTe NPLs are featured sharply without broadening, which suggests that these NPLs have uniform thickness dimension. This demonstrates that the shape-controllable synthesis of CdTe NPLs can be achieved simply by tailoring the reactivity of Te precursor. Generally, two-dimensional II-IV colloidal semiconductor nanocrystals have regular sheet- or plate-like shapes.[10-11, 81] Nevertheless, it is also possible to tune the shape of CdSe nanosheets from hexangon to quadragon to triangle by altering the nucleation and growth process via simply increasing the concentration of bromoalkanes that act as complexing agents and ligands.[13] In this work, the reactivity of polytelluride tellurium precursor plays a key role in the nucleation and growth of CdTe nanoplatelets. Here, we may suggest that the polytelluride tellurium precursor with different reactivity might have different impact on the oriented attachment of CdTe MSNCs along the lateral direction, which results in the formation of these different shape-like CdTe NPLs. As reported by Hyeon *et al.* that sole alkylamine as ligand favors the synthesis of stacked CdSe nanosheets,[42] the stacked CdTe NPLs were also prepared by using Te^{2-} as tellurium precursor and oleylamine as sole ligand. Figure 4.8 presents the TEM image of these stacked CdTe NPLs. The thickness of those CdTe NPLs was estimated to be around 1.6 nm from the NPLs standing on their edges (the inset of Figure 4.8).

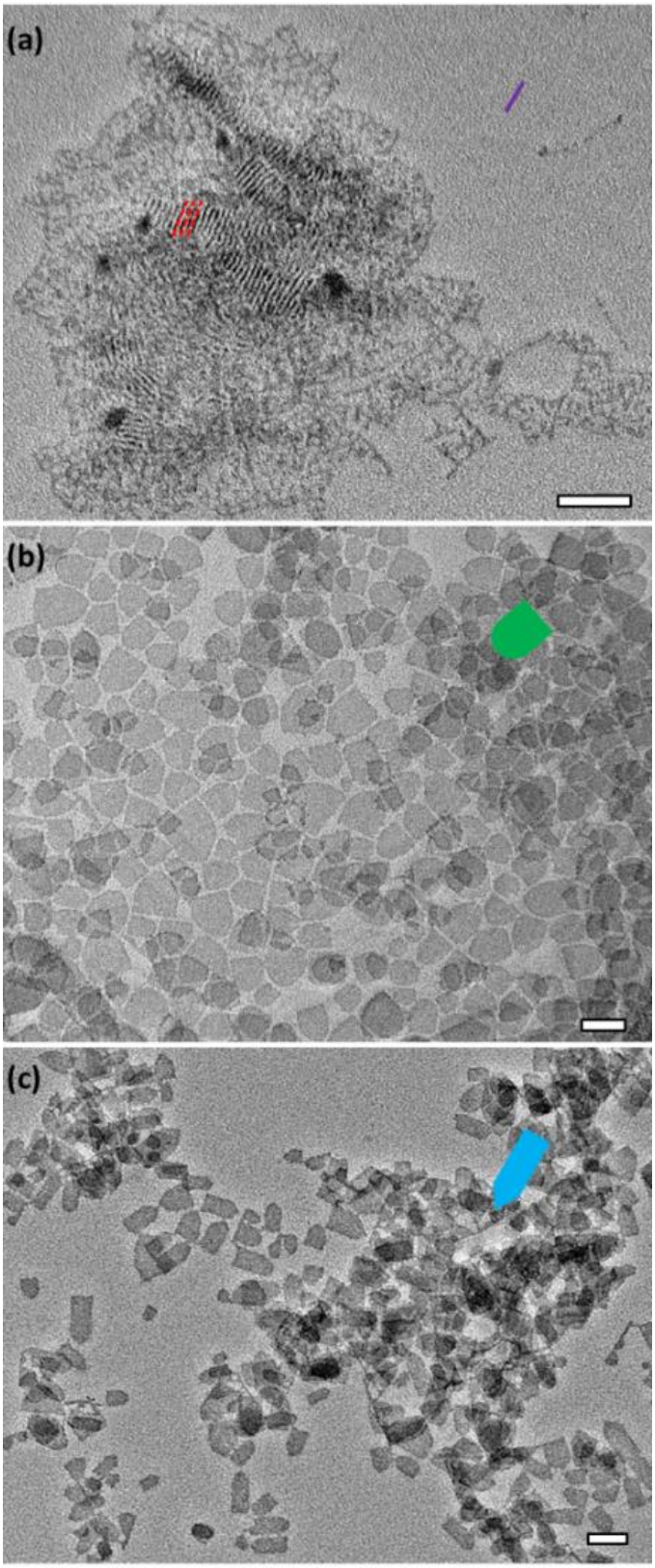

Figure 4.7 TEM images of ribbon-, sheild-, bullet-like CdTe NPLs prepared using (a) Te_3^{2-}, (b) Te_2^{2-}, (c) Te^{2-} as tellurium precursor, respectively. All scale bars: 50 nm.

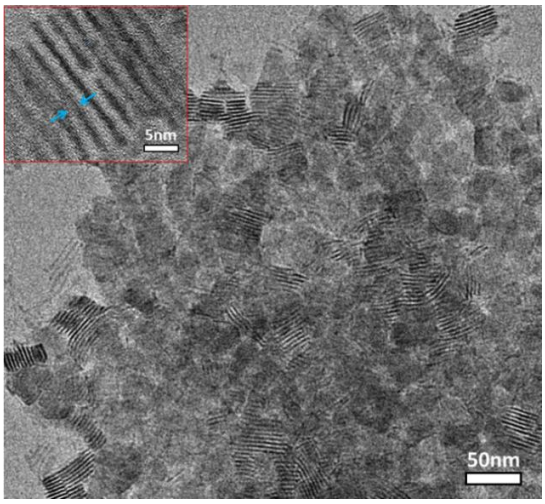

Figure 4.8 TEM image of stacked CdTe NPLs prepared by using Te^{2-} as tellurium precursor and oleylamine as sole ligand.

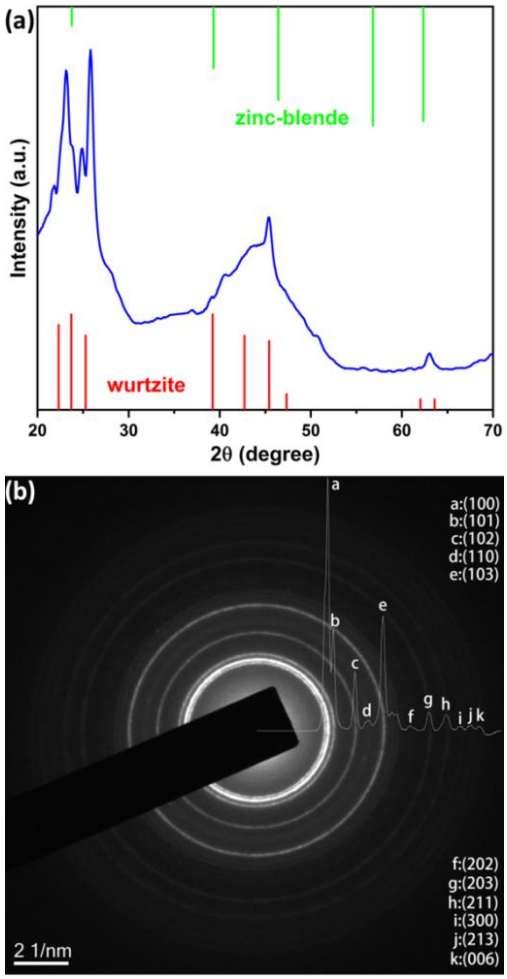

Figure 4.9 (a) XRD pattern (blue curve) of CdTe NPLs and standard XRD pattern of bulk CdTe with zinc-blende (green lines) and wurtzite (red lines) structure; (b) SAED pattern of CdTe NPLs resolved by using PASAD tools.

Table 4.1 Lattice spacings vaules of CdTe NPLs fitted by using PASAD tools.

k (nm^{-1})	Fitted lattice spacings d (Å)	Miller indices (hkl)	Standard lattice spacingsd (Å) [a]	Lattice contraction (%)
2.56	3.85	(100)	3.98	3.2
2.79	3.43	(101)	3.52	2.6
3.58	2.66	(102)	2.74	2.9
4.05	2.23	(110)	2.30	3.0
4.60	2.06	(103)	2.12	2.8
5.62	1.71	(202)	1.76	2.8
6.28	1.51	(203)	1.55	2.6
6.90	1.42	(211)	1.46	2.7
7.42	1.29	(300)	1.32	2.3
7.77	1.26	(213)	1.29	2.3
8.06	1.22	(006)	1.25	2.4

[a] standard lattice spacings of wurtzite bulk CdTe referenced from JCPDS No. 19-0193.

Figure 4.9(a) presents the XRD pattern of CdTe NPLs and standard XRD pattern of bulk CdTe with zinc-blende and wurtzite structure. The crystal structure of CdTe NPLs is indexed to wurtzite due to good agreement with the standard PDF card (JCPDS No. 19-0193) of wurtzite bulk CdTe. The significantly small shift of XRD diffraction peaks to higher angles can be attributed to the lattice contraction which was also observed in CdSe[42] and ZnSe[82] NPLs. The intense diffraction peaks with shoulders ranging from 20^o to 30^o are assigned to the diffraction peaks of (100), (002), and (101) crystal facets, respectively. To further analyze the crystal structure of the as-prepared CdTe NPLs, the SAED pattern of CdTe NPLs shown in Figure 4.9(b) was resolved by using PASAD tools. The corresponding Miller indices were annotated to the diffraction peaks according to the resolved lattice spacing values as listed in Table 4.1, which further confirms the as-prepared CdTe NPLs with a wurtzite structure. The fitted lattice spacing values of CdTe NPLs were smaller than the standard values for wurtzite bulk CdTe, which results from the lattice contraction of 1.6 nm thick CdTe nanosheets and was also oberseved in

CdTe quantum belts.[43] Compared with the standard lattice spacing values of wurtzite bulk CdTe, these smaller lattice spacing values are also in consistance with the slight shift of XRD diffraction peaks to higher angles according to the Bragg law 2dsinθ=nλ.

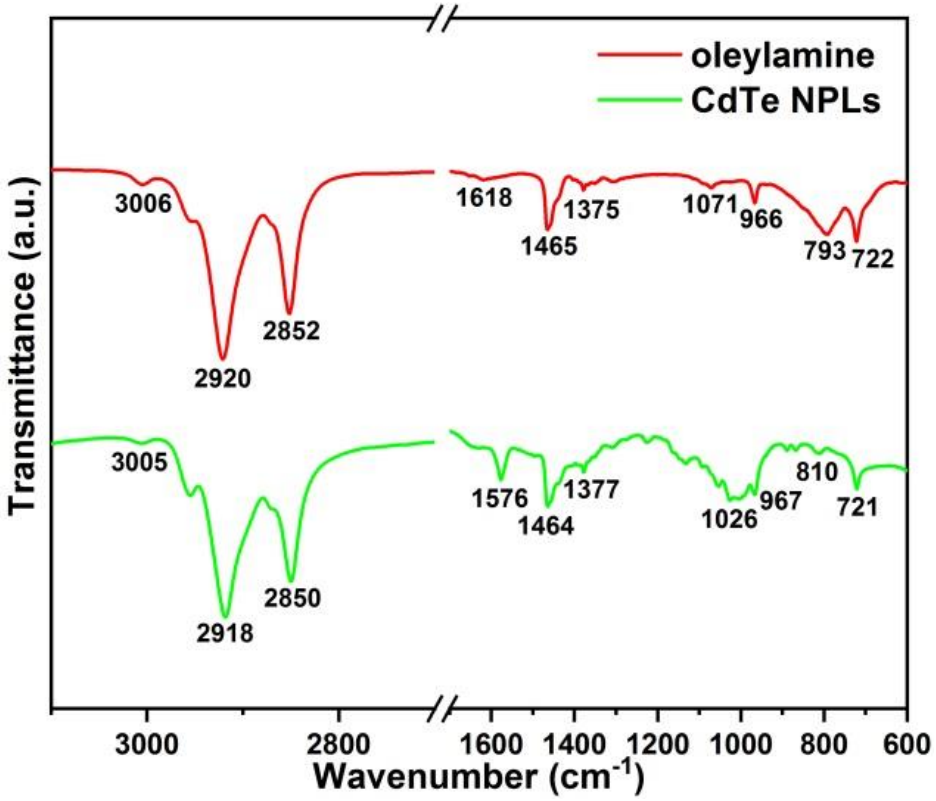

Figure 4.10 The FTIR spectra of oleylamine and purified CdTe NPLs.

To characterize the surface chemistry of the as-prepared CdTe NPLs and investigate the interaction between alkylamine ligands and CdTe NPLs, FTIR spectra of oleylamine and purified CdTe NPLs were measured and shown in Figure 4.10. The absorption bands were assigned to corresponding vibrational modes, as depicted in Table 4.2. The FTIR spectrum of CdTe NPLs is similar to the standard FTIR spectrum of oleylamine, suggesting that the CdTe NPLs are passivated with oleylamine which acts as surface ligands. Due to the coordination between the -NH_2 group from oleylamine and the cadmium atom from CdTe nanocrystals, significant absorption peak shifts from N-H_2 bending (1618 cm^{-1}), C-N stretching (alkyl) (1071 cm^{-1}), N-H bending (out of plane, 793 cm^{-1}) are observed in nitrogen-related functional groups. In addition, marginal absorption peak shifts are observed from non-nitrogen related function groups such as the =CH

stretching (3006 cm^{-1}), C-H_2 stretching (2920, 2852 cm^{-1}), CH_2 bending (1465 cm^{-1}), CH_3 bending (1375 cm^{-1}), C-H bending (966 cm^{-1}), and CH_2 bending (722 cm^{-1}).

Table 4.2 Infrared vibrational assignments.

Vibrational modes	Frequency (cm^{-1})
=CH stretching	3006
C-H_2 stretching	2920, 2852
N-H_2 bending	1618
CH_2 bending	1465
CH_3 bending	1375
C-N stretching (alkyl)	1071
C-H bending	966
N-H bending (out of plane)	793
CH_2 bending	722

XPS measurements were further used to characterize the composition of the as-prepared wurtzite CdTe NPLs. Figure 4.11(a) shows the survey XPS spectrum of the obtained wurtzite CdTe NPLs. The survey spectrum indicates the presence of Cd, O, Te and C element. The presence of C and O is likely from the capping ligands and oxidation of CdTe NPLs during the characterization process, respectively. The C 1s level at 284.8 eV was used for calibration of the binding energy scale. High-resolution XPS of the most intense peaks of the two main elements (Cd 3d and Te 3d levels) was furthered investigated as depicted in Figure 4.11(b-c). The peak of Cd 3d in Figure 4.11(b) is split into 411.1 (Cd-Te $3d_{3/2}$) and 404.3 eV (Cd-Te $3d_{5/2}$) with a split orbit of about 7 eV, which is in good accordance with the value of Cd (II).[83] The binding energy of 582.1 and 571.5 eV in Figure 4.11(c) corresponds to the Te-Cd $3d_{3/2}$ and $3d_{5/2}$ levels, respectively.[84] The XPS shoulders located at 584.1 and 574.5 eV corresponds to the Te-O $3d_{3/2}$ and $3d_{5/2}$ levels,[84] respestively, suggesting the partial oxidation state of Te from the as-prepared wurtzite CdTe NPLs.

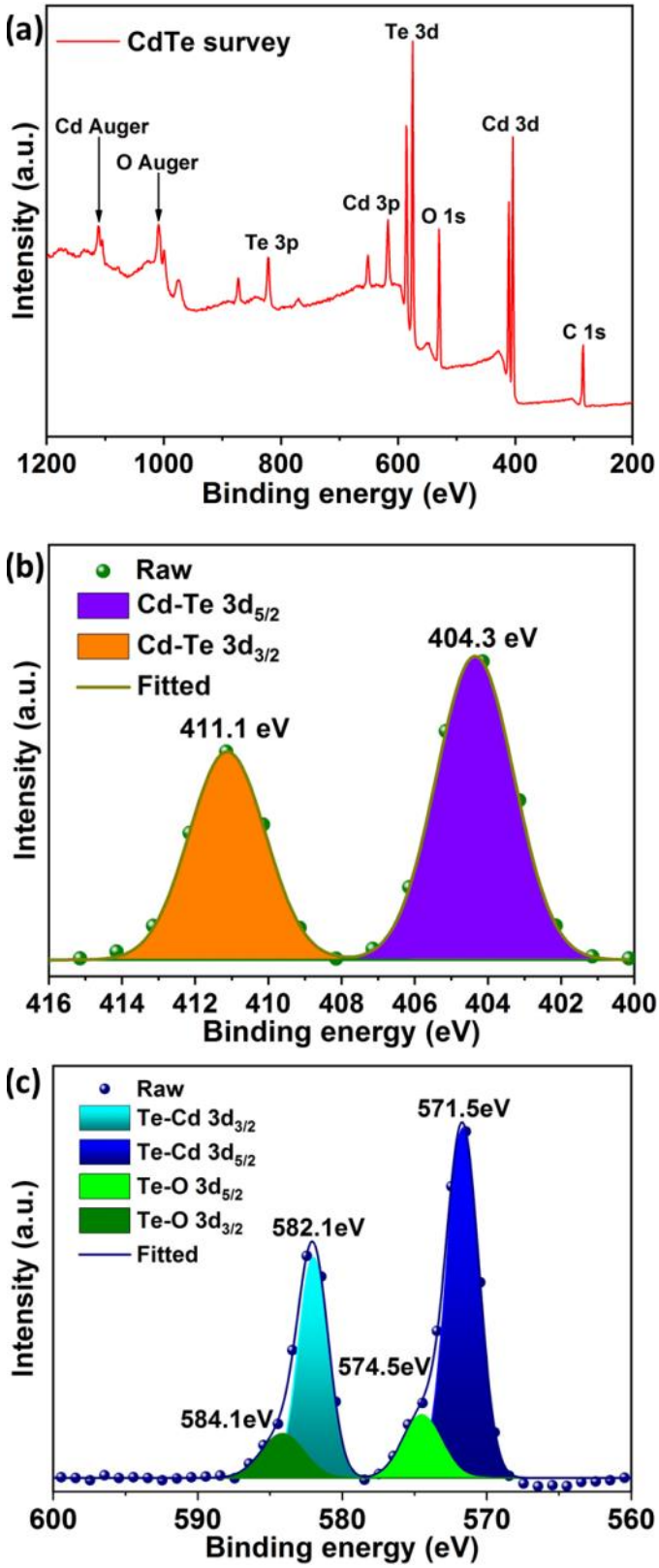

Figure 4.11 (a) The survey XPS spectrum of the obtained wurtzite CdTe NPLs. XPS spectra of CdTe NPLs: (b) Cd and (c) Te regions.

4.4 Conclusion

In conclusion, we report a shape-controllable synthesis of 2D wurtzite CdTe nanoplatelets by simply tailoring Te precursor reactivity. Ribbon-, shield- and bullet-like CdTe NPLs were synthesized from a stepwise conversion of CdTe MSNCs by using Te_3^{2-}, Te_2^{2-} and Te^{2-} species as tellurium precursor, respectively. X-ray photoelectron spectroscopy and Fourier-transform infrared spectroscopy were used to investigated the surface chemical environment and composition of as-prepared CdTe NPLs. The availability of wurtzite CdTe NPLs provides exciting opportunity to explore its photophysical properties for potential applications in optoelectronics, sensors and detectors.

4.5 References

1. Ithurria, S.; Tessier, M. D.; Mahler, B.; Lobo, R. P.; Dubertret, B.; Efros, A. L., Colloidal nanoplatelets with two-dimensional electronic structure. *Nature Materials* **2011,** *10* (12), 936-41.

2. Delikanli, S.; Guzelturk, B.; Hernández-Martínez, P. L.; Erdem, T.; Kelestemur, Y.; Olutas, M.; Akgul, M. Z.; Demir, H. V., Continuously tunable emission in inverted type-I CdS/CdSe core/crown semiconductor nanoplatelets. *Advanced Functional Materials* **2015,** *25* (27), 4282-4289.

3. Bouet, C.; Mahler, B.; Nadal, B.; Abecassis, B.; Tessier, M. D.; Ithurria, S.; Xu, X. Z.; Dubertret, B., Two-dimensional growth of CdSe nanocrystals, from nanoplatelets to nanosheets. *Chemistry of Materials* **2013,** *25* (4), 639-645.

4. Ithurria, S.; Dubertret, B., Quasi 2D colloidal CdSe platelets with thicknesses controlled at the atomic level. *Journal of the American Chemical Society* **2008,** *130* (49), 16504-5.

5. Mahler, B.; Nadal, B.; Bouet, C.; Patriarche, G.; Dubertret, B., Core/shell colloidal semiconductor nanoplatelets. *Journal of the American Chemical Society* **2012,** *134* (45), 18591-18598.

6. Galle, T.; Samadi Khoshkhoo, M.; Martin-Garcia, B.; Meerbach, C.; Sayevich, V.; Koitzsch, A.; Lesnyak, V.; Eychmüller, A., Colloidal PbSe nanoplatelets of varied thickness with tunable optical properties. *Chemistry of Materials* **2019,** *31* (10), 3803-3811.

7. Li, Z.; Qin, H. Y.; Guzun, D.; Benamara, M.; Salamo, G.; Peng, X. G., Uniform thickness and colloidal-stable CdS quantum disks with tunable thickness: synthesis and properties. *Nano Research* **2012,** *5* (5), 337-351.

8. Li, Z.; Peng, X., Size/shape-controlled synthesis of colloidal CdSe quantum disks: ligand and temperature effects. *Journal of the American Chemical Society* **2011,** *133* (17), 6578-6586.

9. Li, H.; Brescia, R.; Povia, M.; Prato, M.; Bertoni, G.; Manna, L.; Moreels, I., Synthesis of uniform disk-shaped copper telluride nanocrystals and cation exchange to cadmium telluride quantum disks with stable red emission. *Journal of the American Chemical Society* **2013,** *135* (33), 12270-12278.

10. Chhowalla, M.; Shin, H. S.; Eda, G.; Li, L.-J.; Loh, K. P.; Zhang, H., The chemistry of two-dimensional layered transition metal dichalcogenide nanosheets. *Nature Chemistry* **2013,** *5*, 263.

11. Huang, X.; Zeng, Z.; Zhang, H., Metal dichalcogenide nanosheets: preparation, properties and applications. *Chemical Society Reviews* **2013,** *42* (5), 1934-1946.

12. Wen, X. D.; Hoffmann, R.; Ashcroft, N., Two-dimensional CdSe nanosheets and their interaction with stabilizing ligands. *Advanced Materials* **2013,** *25* (2), 261-266.

13. Gerdes, F.; Navío, C.; Juárez, B. H.; Klinke, C., Size, shape, and phase control in ultrathin CdSe nanosheets. *Nano Letters* **2017,** *17* (7), 4165-4171.

14. Aerts, M.; Bielewicz, T.; Klinke, C.; Grozema, F. C.; Houtepen, A. J.; Schins, J. M.; Siebbeles, L. D., Highly efficient carrier multiplication in PbS nanosheets. *Nature Communications* **2014,** *5*, 3789.

15. Halder, O.; Pradhani, A.; Sahoo, P.; Satpati, B.; Rath, S., Highly luminescent two dimensional excitons in atomically thin CdSe nanosheets. *Applied Physics Letters* **2014,** *104* (18), 182109.

16. Khan, S.; Jiang, Z.; Premathilka, S. M.; Antu, A.; Hu, J.; Voevodin, A. A.; Roland, P. J.; Ellingson, R. J.; Sun, L., Few-atom-thick colloidal PbS/CdS core/shell nanosheets. *Chemistry of Materials* **2016,** *28* (15), 5342-5346.

17. Xie, X.; Kwok, S.-Y.; Lu, Z.; Liu, Y.; Cao, Y.; Luo, L.; Zapien, J. A.; Bello, I.; Lee, C.-S.; Lee, S.-T., Visible–NIR photodetectors based on CdTe nanoribbons. *Nanoscale* **2012,** *4* (9), 2914-2919.

18. Thibert, A.; Frame, F. A.; Busby, E.; Larsen, D. S., Primary photodynamics of water-solubilized two-dimensional CdSe nanoribbons. *The Journal of Physical Chemistry C* **2011,** *115* (40), 19647-19658.

19. Antu, A. D.; Jiang, Z.; Premathilka, S. M.; Tang, Y.; Hu, J.; Roy, A.; Sun, L.,

Bright colloidal PbS nanoribbons. *Chemistry of Materials* **2018,** *30* (11), 3697-3703.

20. Yang, J.; Son, J. S.; Yu, J. H.; Joo, J.; Hyeon, T., Advances in the colloidal synthesis of two-dimensional semiconductor nanoribbons. *Chemistry of Materials* **2013,** *25* (8), 1190-1198.

21. Fainblat, R.; Frohleiks, J.; Muckel, F.; Yu, J. H.; Yang, J.; Hyeon, T.; Bacher, G., Quantum confinement-controlled exchange coupling in manganese (II)-doped CdSe two-dimensional quantum well nanoribbons. *Nano Letters* **2012,** *12* (10), 5311-5317.

22. Liu, Y.-H.; Wayman, V. L.; Gibbons, P. C.; Loomis, R. A.; Buhro, W. E., Origin of high photoluminescence efficiencies in CdSe quantum belts. *Nano Letters* **2009,** *10* (1), 352-357.

23. Liu, Y.-H.; Wang, F.; Wang, Y.; Gibbons, P. C.; Buhro, W. E., Lamellar assembly of cadmium selenide nanoclusters into quantum belts. *Journal of the American Chemical Society* **2011,** *133* (42), 17005-17013.

24. Zhou, Y.; Buhro, W. E., Reversible exchange of L-type and bound-ion-pair X-type ligation on cadmium selenide quantum belts. *Journal of the American Chemical Society* **2017,** *139* (37), 12887-12890.

25. Yao, Y.; Zhou, Y.; Sanderson, W. M.; Loomis, R. A.; Buhro, W. E., Metal-halide-ligated cadmium selenide quantum belts by facile surface exchange. *Chemistry of Materials* **2018**.

26. Wang, Y.; Zhang, Y.; Wang, F.; Giblin, D. E.; Hoy, J.; Rohrs, H. W.; Loomis, R. A.; Buhro, W. E., The magic-size nanocluster $(CdSe)_{34}$ as a low-temperature nucleant for cadmium selenide nanocrystals; room-temperature growth of crystalline quantum platelets. *Chemistry of Materials* **2014,** *26* (7), 2233-2243.

27. Morrison, P. J.; Loomis, R. A.; Buhro, W. E., Synthesis and growth mechanism of lead sulfide quantum platelets in lamellar mesophase templates. *Chemistry of Materials* **2014,** *26* (17), 5012-5019.

28. Fan, F.; Kanjanaboos, P.; Saravanapavanantham, M.; Beauregard, E.; Ingram, G.; Yassitepe, E.; Adachi, M. M.; Voznyy, O.; Johnston, A. K.; Walters, G.; Kim, G.-H.; Lu, Z.-H.; Sargent, E. H., Colloidal $CdSe_{1-x}S_x$ nanoplatelets with narrow and continuously-tunable electroluminescence. *Nano Letters* **2015,** *15* (7), 4611-4615.

29. Li, Q.; Lian, T., Ultrafast charge separation in two-dimensional $CsPbBr_3$ perovskite nanoplatelets. *The Journal of Physical Chemistry Letters* **2019,** *10* (3), 566-573.

30. Wen, Z.; Fang, F.; Zhang, C.; Ding, S.; Sun, J.; Tang, H.; Xu, B.; Wang, K.; Teo, K. L.; Sun, X. W., Ultrawide color gamut LCD display with CdSe/CdS nanoplatelets. *Journal of the Society for Information Display* **2019**.

31. Zhao, F.; Li, J.; Gao, X.; Qiu, X.; Lin, X.; He, T.; Chen, R., Comparison studies of the linear and nonlinear optical properties of $CsPbBr_xI_{3-x}$ nanocrystals: the influence of dimensionality and composition. *The Journal of Physical Chemistry C* **2019,** *123* (14), 9538-9543.

32. Akkerman, Q. A.; Motti, S. G.; Srimath Kandada, A. R.; Mosconi, E.; D'Innocenzo, V.; Bertoni, G.; Marras, S.; Kamino, B. A.; Miranda, L.; De Angelis, F.; Petrozza, A.; Prato, M.; Manna, L., Solution synthesis approach to colloidal cesium lead halide perovskite nanoplatelets with monolayer-level thickness control. *Journal of the American Chemical Society* **2016,** *138* (3), 1010-1016.

33. Yeltik, A.; Delikanli, S.; Olutas, M.; Kelestemur, Y.; Guzelturk, B.; Demir, H. V., Experimental determination of the absorption cross-section and molar extinction coefficient of colloidal CdSe nanoplatelets. *The Journal of Physical Chemistry C* **2015,** *119* (47), 26768-26775.

34. Olutas, M.; Guzelturk, B.; Kelestemur, Y.; Yeltik, A.; Delikanli, S.; Demir, H. V., Lateral size-dependent spontaneous and stimulated emission properties in colloidal CdSe nanoplatelets. *ACS Nano* **2015,** *9* (5), 5041-5050.

35. Tessier, M. D.; Javaux, C.; Maksimovic, I.; Loriette, V.; Dubertret, B., Spectroscopy of single CdSe nanoplatelets. *ACS Nano* **2012,** *6* (8), 6751-6758.

36. Li, M.; Zhi, M.; Zhu, H.; Wu, W.-Y.; Xu, Q.-H.; Jhon, M. H.; Chan, Y., Ultralow-threshold multiphoton-pumped lasing from colloidal nanoplatelets in solution. *Nature Communications* **2015,** *6*, 8513.

37. Li, Q.; Xu, Z.; McBride, J. R.; Lian, T., Low threshold multiexciton optical gain in colloidal CdSe/CdTe core/crown type-II nanoplatelet heterostructures. *ACS Nano* **2017,** *11* (3), 2545-2553.

38. Li, Q.; Lian, T., A model for optical gain in colloidal nanoplatelets. *Chemical Science* **2018,** *9* (3), 728-734.

39. Bouet, C.; Tessier, M. D.; Ithurria, S.; Mahler, B.; Nadal, B.; Dubertret, B.,

Flat colloidal semiconductor nanoplatelets. *Chemistry of Materials* **2013,** *25* (8), 1262-1271.

40. Christodoulou, S.; Climente, J. I.; Planelles, J.; Brescia, R.; Prato, M.; Martin-Garcia, B.; Khan, A. H.; Moreels, I., Chloride-induced thickness control in CdSe nanoplatelets. *Nano Letters* **2018,** *18* (10), 6248-6254.

41. Chen, Y.; Chen, D.; Li, Z.; Peng, X., Symmetry-breaking for formation of rectangular CdSe two-dimensional nanocrystals in zinc-blende structure. *Journal of the American Chemical Society* **2017,** *139* (29), 10009-10019.

42. Son, J. S.; Wen, X. D.; Joo, J.; Chae, J.; Baek, S. I.; Park, K.; Kim, J. H.; An, K.; Yu, J. H.; Kwon, S. G.; Choi, S. H.; Wang, Z.; Kim, Y. W.; Kuk, Y.; Hoffmann, R.; Hyeon, T., Large-scale soft colloidal template synthesis of 1.4 nm thick CdSe nanosheets. *Angewandte Chemie International Edition* **2009,** *48* (37), 6861-6864.

43. Wang, Y.; Zhou, Y.; Zhang, Y.; Buhro, W. E., Magic-size II–VI nanoclusters as synthons for flat colloidal nanocrystals. *Inorganic Chemistry* **2015,** *54* (3), 1165-1177.

44. Ferekides, C. S.; Marinskiy, D.; Viswanathan, V.; Tetali, B.; Palekis, V.; Selvaraj, P.; Morel, D., High efficiency CSS CdTe solar cells. *Thin Solid Films* **2000,** *361*, 520-526.

45. Wu, F.; Lewis, J. W.; Kliger, D. S.; Zhang, J. Z., Unusual excitation intensity dependence of fluorescence of CdTe nanoparticles. *The Journal of Chemical Physics* **2003,** *118* (1), 12-16.

46. Britt, J.; Ferekides, C., Thin-film CdS/CdTe solar cell with 15.8% efficiency. *Applied Physics Letters* **1993,** *62* (22), 2851-2852.

47. Awni, R. A.; Li, D. B.; Grice, C. R.; Song, Z.; Razooqi, M. A.; Phillips, A. B.; Bista, S. S.; Roland, P. J.; Alfadhili, F. K.; Ellingson, R. J., The effects of hydrogen iodide back surface treatment on CdTe solar cells. *Solar RRL* **2019,** *3* (3), 1800304.

48. Milan, P.; Peralta, J.; Guerrero, M.; Wang, P. W., Barrier height measurement of cadmium telluride (CdTe) solar cells. *Bulletin of the American Physical Society* **2019**.

49. Patel, S.; Chander, S.; Kannan, M.; Dhaka, M., Impact of chloride treatment on the physical properties of polycrystalline thin CdTe films for solar cell applications. *Physics Letters A* **2019**.

50. Mendis, B. G.; Ramasse, Q. M.; Shalvey, T.; Major, J. D.; Durose, K., Optical properties and dielectric functions of grain boundaries and interfaces in CdTe thin-film solar cells. *ACS Applied Energy Materials* **2019,** *2* (2), 1419-1427.

51. McCandless, B.; Buchanan, W.; Sriramagiri, G.; Thompson, C.; Duenow, J.; Albin, D.; Jensen, S. A.; Moseley, J.; Al-Jassim, M.; Metzger, W. K., Enhanced p-type doping in polycrystalline CdTe films: deposition and activation. *IEEE Journal of Photovoltaics* **2019**.

52. Wang, X.; Dai, G.; Chen, Y.; Mo, X.; Li, X.; Huang, W.; Sun, J.; Yang, J., Piezo-phototronic enhanced photoresponsivity based on single CdTe nanowire photodetector. *Journal of Applied Physics* **2019,** *125* (9), 094505.

53. Shaygan, M.; Davami, K.; Kheirabi, N.; Baek, C. K.; Cuniberti, G.; Meyyappan, M.; Lee, J.-S., Single-crystalline CdTe nanowire field effect transistors as nanowire-based photodetector. *Physical Chemistry Chemical Physics* **2014,** *16* (41), 22687-22693.

54. Tu, C.-C.; Lin, L. Y., High efficiency photodetectors fabricated by electrostatic layer-by-layer self-assembly of CdTe quantum dots. *Applied Physics Letters* **2008,** *93* (16), 163107.

55. Park, H.; Yang, G.; Chun, S.; Kim, D.; Kim, J., CdTe microwire-based ultraviolet photodetectors aligned by a non-uniform electric field. *Applied Physics Letters* **2013,** *103* (5), 051906.

56. Song, X.; Li, L.; Qian, H.; Fang, N.; Ren, J., Highly efficient size separation of CdTe quantum dots by capillary gel electrophoresis using polymer solution as sieving medium. *Electrophoresis* **2006,** *27* (7), 1341-1346.

57. Rajh, T.; Micic, O. I.; Nozik, A. J., Synthesis and characterization of surface-modified colloidal cadmium telluride quantum dots. *The Journal of Physical Chemistry* **1993,** *97* (46), 11999-12003.

58. Wuister, S. F.; Swart, I.; van Driel, F.; Hickey, S. G.; de Mello Donegá, C., Highly luminescent water-soluble CdTe quantum dots. *Nano Letters* **2003,** *3* (4), 503-507.

59. Zhou, D.; Lin, M.; Chen, Z.; Sun, H.; Zhang, H.; Sun, H.; Yang, B., Simple synthesis of highly luminescent water-soluble CdTe quantum dots with controllable surface functionality. *Chemistry of Materials* **2011,** *23* (21), 4857-4862.

60. Zhang, H.; Wang, D.; Möhwald, H., Ligand-selective aqueous synthesis of one-dimensional CdTe nanostructures. *Angewandte Chemie International Edition* **2006,** *45* (5), 748-751.

61. Nie, W.; He, J.; Zhao, N.; Ji, X., A controllable synthesis of multi-armed CdTe nanorods. *Nanotechnology* **2006,** *17* (4), 1146.

62. Shieh, F.; Saunders, A. E.; Korgel, B. A., General shape control of colloidal CdS, CdSe, CdTe quantum rods and quantum rod heterostructures. *The Journal of Physical Chemistry B* **2005,** *109* (18), 8538-8542.

63. Liang, H.-W.; Liu, S.; Wu, Q.-S.; Yu, S.-H., An efficient templating approach for synthesis of highly uniform CdTe and PbTe nanowires. *Inorganic Chemistry* **2009,** *48* (11), 4927-4933.

64. Tang, B.; Niu, J.; Yu, C.; Zhuo, L.; Ge, J., Highly luminescent water-soluble CdTe nanowires as fluorescent probe to detect copper (II). *Chemical Communications* **2005,** (33), 4184-4186.

65. Lee, S. H.; Kim, Y. J.; Park, J., Shape evolution of ZnTe nanocrystals: nanoflowers, nanodots, and nanorods. *Chemistry of Materials* **2007,** *19* (19), 4670-4675.

66. Sun, J.; Wang, L.-W.; Buhro, W. E., Synthesis of cadmium telluride quantum wires and the similarity of their effective band gaps to those of equidiameter cadmium telluride quantum dots. *Journal of the American Chemical Society* **2008,** *130* (25), 7997-8005.

67. Kloper, V.; Osovsky, R.; Kolny-Olesiak, J.; Sashchiuk, A.; Lifshitz, E., The growth of colloidal cadmium telluride nanocrystal quantum dots in the presence of Cd^0 nanoparticles. *The Journal of Physical Chemistry C* **2007,** *111* (28), 10336-10341.

68. Hu, D.; Zhang, P.; Gong, P.; Lian, S.; Lu, Y.; Gao, D.; Cai, L., A fast synthesis of near-infrared emitting CdTe/CdSe quantum dots with small hydrodynamic diameter for in vivo imaging probes. *Nanoscale* **2011,** *3* (11), 4724-32.

69. Yang, Y. A.; Wu, H.; Williams, K. R.; Cao, Y. C., Synthesis of CdSe and CdTe nanocrystals without precursor injection. *Angewandte Chemie International Edition* **2005,** *44* (41), 6712-6715.

70. Zhang, J.; Jin, S.; Fry, H. C.; Peng, S.; Shevchenko, E.; Wiederrecht, G. P.; Rajh, T., Synthesis and characterization of wurtzite ZnTe nanorods with controllable aspect ratios. *Journal of the American Chemical Society* **2011,**

133 (39), 15324-7.

71. Ji, B.; Panfil, Y. E.; Banin, U., Heavy-metal-free fluorescent ZnTe/ZnSe nanodumbbells. *ACS Nano* **2017,** *11* (7), 7312-7320.

72. Sun, H.; Wang, F.; Buhro, W. E., Tellurium precursor for nanocrystal synthesis: tris(dimethylamino)phosphine telluride. *ACS Nano* **2018,** *12* (12), 12393-12400.

73. Pedetti, S.; Nadal, B.; Lhuillier, E.; Mahler, B.; Bouet, C. c.; Abécassis, B.; Xu, X.; Dubertret, B., Optimized synthesis of CdTe nanoplatelets and photoresponse of CdTe nanoplatelets films. *Chemistry of Materials* **2013,** *25* (12), 2455-2462.

74. Gammer, C.; Mangler, C.; Rentenberger, C.; Karnthaler, H., Quantitative local profile analysis of nanomaterials by electron diffraction. *Scripta Materialia* **2010,** *63* (3), 312-315.

75. Ruberu, T. P. A.; Albright, H. R.; Callis, B.; Ward, B.; Cisneros, J.; Fan, H.-J.; Vela, J., Molecular control of the nanoscale: effect of phosphine–chalcogenide reactivity on CdS–CdSe nanocrystal composition and morphology. *ACS Nano* **2012,** *6* (6), 5348-5359.

76. Cho, J. W.; Kim, H. S.; Kim, Y. J.; Jang, S. Y.; Park, J.; Kim, J.-G.; Kim, Y.-J.; Cha, E. H., Phase-tuned tetrapod-shaped CdTe nanocrystals by ligand effect. *Chemistry of Materials* **2008,** *20* (17), 5600-5609.

77. Yao, D.; Liu, Y.; Zhao, W.; Wei, H.; Luo, X.; Wu, Z.; Dong, C.; Zhang, H.; Yang, B., A totally phosphine-free synthesis of metal telluride nanocrystals by employing alkylamides to replace alkylphosphines for preparing highly reactive tellurium precursors. *Nanoscale* **2013,** *5* (20), 9593-9597.

78. McAfee, J. L.; Andreatta, J. R.; Sevcik, R. S.; Schultz, L. D., Equilibrium among potassium polytellurides in N, N-dimethylformamide solution. *Journal of Molecular Structure* **2012,** *1022*, 68-71.

79. Zhou, Y.; Jiang, R.; Wang, Y.; Rohrs, H. W.; Rath, N. P.; Buhro, W. E., Isolation of amine derivatives of $(ZnSe)_{34}$ and $(CdTe)_{34}$. Spectroscopic comparisons of the $(II–VI)_{13}$ and $(II–VI)_{34}$ magic-size nanoclusters. *Inorganic Chemistry* **2019,** *58*, 1815-1825.

80. Son, J. S.; Park, K.; Kwon, S. G.; Yang, J.; Choi, M. K.; Kim, J.; Yu, J. H.; Joo, J.; Hyeon, T., Dimension-controlled synthesis of CdS nanocrystals: From 0D quantum dots to 2D nanoplates. *Small* **2012,** *8* (15), 2394-2402.

81. Delikanli, S.; Yu, G.; Yeltik, A.; Bose, S.; Erdem, T.; Yu, J.; Erdem, O.; Sharma, M.; Sharma, V. K.; Quliyeva, U., Ultrathin highly luminescent two-monolayer colloidal CdSe nanoplatelets. *Advanced Functional Materials* **2019,** *29* (35), 1901028.

82. Park, H.; Chung, H.; Kim, W., Synthesis of ultrathin wurtzite ZnSe nanosheets. *Materials Letters* **2013,** *99*, 172-175.

83. Gong, J.; Li, L.; Xue, S.; Xie, P.; Hou, X.; Feng, H.; Wei, X.; Liu, Z.; Xu, Z.; Huang, J., The preparation and photocatalytic performance research of CdSe and wool ball-like GO/CdSe microspheres. *Journal of Alloys and Compounds* **2019,** *779*, 962-970.

84. Zhang, G.; Jiang, S.; Lin, Y.; Ren, W.; Cai, H.; Wu, Y.; Zhang, Q.; Pan, N.; Luo, Y.; Wang, X., Improving the photovoltaic performance of solid-state ZnO/CdTe core–shell nanorod array solar cells using a thin CdS interfacial layer. *Journal of Materials Chemistry A* **2014,** *2* (16), 5675-5681.

Every reasonable effort has been made to acknowledge the owners of copyright material. I would be pleased to hear from any copyright owner who has been omitted or incorrectly acknowledged.

Chapter 5 Conclusions and Outlook

The research presented in this PhD thesis was intented to investigate the synthesis, growth mechanism and optical properties of colloidal wurtzite ZTe (Z=Zn and Cd) nanoplatelets. Although there are intensive investigations on 2D zinc-blende or wurtzite CdSe nanocrystals in the literature, there are only a few of reports on the synthesis of 2D ZTe (Zn and Cd) nanocrystals. The synthesis of high-quality collodial 2D wurtzite ZTe (Z=Zn and Cd) nanocrystals is challenging because of the limited choice of tellurium precursor and the instability of 2D ZTe (Zn and Cd) nanocrystals. We found that 2D wurtzite ZnTe nanoplatelets are extremely vulnerable to air and moisture and are tend to undergo decomposition as they have a large portion of surface atoms which made the material characterization difficult. Therefore, we prepared the samples in a glove box for rigid oxygen- and moisture-free conditions which were usually required in the post-synthesis handling.

In charpter 3, we have successfully prepared 2D wurtzite ZnTe NPLs with a thickness of about 1.5 nm by using superhydride ($LiEt_3BH$) reduced tributylphosphine-Te (TBP-Te) as the tellurium precursor. Mechanistic studies including experimentally UV-vis absorption spectra as well as TEM morphological characterizations and theoretical DFT calculations reveal that the transition of metastable ZnTe F323 magic-sized nanoclusters (MSNCs) produces metastable ZnTe F398 MSNCs which then form wurtzite ZnTe NPLs via oriented attachment along [100] and [002] directions.

Inspired by the synthetic experience from colloidal 2D wurtzite ZnTe NPLs, we further tried to synthesize colloidal 2D wurtzite CdTe NPLs based on the synthetic method of colloidal 2D wurtzite ZnTe NPLs with some modifications in charpter 4. The growth temperature of wurtzite CdTe NPLs is around 120 ^oC, which is much lower than that (200 ^oC) of wurtzite ZnTe NPLs. The different growth temperature could result from the different formation energy between Cd-Te and Zn-Te bond. Interestingly, we found that the shape of 2D wurtzite CdTe nanoplatelets is controllable by simply tailoring tellurium precursor reactivity. Ribbon-, shield- and bullet-like 2D CdTe NPLs were prepared by a step-wise conversion from CdTe magic size nanoclusters (MSNCs) by using Te_3^{2-}, Te_2^{2-} and Te^{2-} polytellurides as tellurium precursor, respectively.

This research laid a foundation for the synthesis of colloidal wurtzite ZTe (Z=Zn and Cd) nanoplatelets. Due to the instability of colloidal wurtzite ZTe (Z=Zn and Cd) nanoplatelets that results in surface traps on the nanocrystals, no characteristic PL from 2D colloidal wurtzite ZTe (Z=Zn and Cd) nanoplatelets was detected. The possible approach to reduce the surface traps and increase the quantum yeild of characteristic PL emission from 2D colloidal wurtzite ZTe (Z=Zn and Cd) nanoplatelets is to grow an inorganic shell to eliminate the surface traps.

To summarize, the availability of the intriguing colloidal wurtzite ZTe (Z=Zn and Cd) nanoplatelets paves the way for further extending their properties of multiple-quantum well structures with a variety of potential applications in optoelectronics, sensors and detectors.

Appendix A: Def2-SVP Basis Set for Zn and Te in Gaussian-format

```
Zn    0
S  6  1.00
  82000.711629     .14210764000E-02
  12312.471777     .10891499487E-01
  2801.3944193     .54057188059E-01
  790.99424302     .18847463904
  257.56551079     .38346549346
  88.814933400     .29723794197
S  3  1.00
  171.86353716    -.11051849523
  20.302534785     .64607716984
  8.3464123068     .44220117322
S  3  1.00
  14.847536940    -.22705309278
  2.4495029507     .72433217935
  .99845821824     .44836495592
S  1  1.00
  .11891307937     1.0000000000
S  1  1.00
  .42297428760E-01  1.0000000000
P  5  1.00
  1071.5185372     .92767797235E-02
  252.69712152     .69541149434E-01
  80.100829126     .27156772564
  28.903393172     .53401355573
  10.768899879     .34501323446
P  3  1.00
  5.6446212530     .34129600164
```

2.1678291347 .56390521973

.80540898341 .23676109735

D 4 1.00

56.088939191 .29588869140E-01

15.751908917 .158725714045

5.3115812367 .379762291591

1.7737904917 .468989591719

D 1 1.00

.51975583665 .309071490776

P 1 1.00

.162455 1.000000

A. Schäfer, H. Horn, R. Ahlrichs; “Fully optimized contracted Gaussian basis sets for atoms Li to Kr”, J. Chem. Phys. 97, 2571 (1992).

****

Te 0

S 3 1.00

2.4738251440 .24373106576

1.5164659774 -.60050992723

.24617861660 .81317963772

S 1 1.00

.96587532924E-01 1.0000000000

P 4 1.00

2.3887340000 -.13002261391386

1.5277144816 .31729704779928

.37921156859 -.34274527164499

.16289707664 -.57386855562281

P 1 1.00

.64536787436E-01 1.0000000000

D 1 1.00

.237 1.000

K. Eichkorn, F. Weigend, O. Treutler, R. Ahlrichs, “Auxiliary basis sets for main row

atoms and transition metals and their use to approximate Coulomb potentials", Theor. Chem. Acc. 97, 119 (1997).

```
TE    0
TE-ECP    3    46
f POTENTIAL
 1
2      1.93927000          -17.86464100
s-f POTENTIAL
 3
2      2.92379400           50.08380500
2      1.15275400            1.96814000
2      1.93927000           17.86464100
p-f POTENTIAL
 3
2      2.60308600          119.82070200
2      0.98544800           -2.03904800
2      1.93927000           17.86464100
d-f POTENTIAL
 2
2      1.43501900           37.75721400
2      1.93927000           17.86464100
```

A. Bergner, M. Dolg, W. Kuechle, H. Stoll, H. Preuss, "Ab initio energy-adjusted pseudopotentials for elements of groups 13–17", Mol. Phys. 80, 1431 (1993).

Appendix B: Attribution Statements

Oriented Attachment Growth of Wurtzite ZnTe Nanoplatelets from Metastable Magic-Size Nanoclusters

Fei Wang, Minyi Zhang, Wei Chen, Shaghraf Javaid, Mark Buntine, Chunsen Li, and Guohua Jia

Contribution of Fei Wang to this research work:

To Whom It May Concern,

Guohua Jia and Chunsen Li conceived the project and supervised the research. Fei Wang performed all the chemical syntheses and conducted materials characterization and analysis including UV-Vis absorption spectra, NMR spectra and TEM images. The DFT calculations were conducted by Minyi Zhang and Chunsen Li. The preparation of this manuscript was primarily done by Fei Wang and Minyi Zhang. All authors revised this manusrcipt and gave valuable comments for better presentation.

Fei Wang

I, as a Co-Author, endorse that this level of contribution by the candidate indicated above is appropriate.

Minyi Zhang

Wei Chen

Shaghraf Javaid

Mark Buntine

Chunsen Li

Guohua Jia

Shape-controllable synthesis of two-dimensional wurtzite CdTe nanoplatelets by tailoring tellurium precursor reactivity

Fei Wang, Shaghraf Javaid, Wei Chen, Guohua Jia

Contribution of Fei Wang to this research work:

To Whom It May Concern,

Guohua Jia conceived the project and supervised the research. Fei Wang performed all the chemical syntheses and conducted all materials characterization and analysis including UV-Vis absorption spectra, TEM, and FT-IR absorption spectra. XRD and XPS data were collected by Shaghraf Javaid. The XRD data and XPS peak fittings were analyzed by Wei Chen and Fei Wang. The preparation of this manuscript was primarily done by Fei Wang and Guohua Jia. All authors revised this manusrcipt and shared their valuable comments for better presensation.

Fei Wang

I, as a Co-Author, endorse that this level of contribution by the candidate indicated above is appropriate.

Shaghraf Javaid

Wei Chen

Guohua Jia

List of published works

1. F. Wang, G. Jia, Y. Pang, Heavy-metal-free metal chalcogenide nanoplatelets, WO/2019/109143.
2. W. Chen, A. Karton, T. Hussian, S. Javaid, F. Wang, Y. Pang and G. Jia, *CrystEngComm*, 2019, **21**, 2955-2961.
3. W. Chen, X. Li, F. Wang, S. Javaid, Y. Pang, J. Chen, Z. Yin, S. Wang, Y. Li and G. Jia, *Small*, 2019, DOI: 10.1002/small.201902231, 1902231.
4. S. Javaid, X. Li, F. Wang, W. Chen, Y. Pang, S. Wang, G. Jia and F. Jones, J. *Mater. Chem. C*, 2019, **7**, 14517-14524.
5. S. Javaid, Y. Li, D. Chen, X. Xu, Y. Pang, W. Chen, F. Wang, Z. Shao, M. Saunders and J.-P. Veder, *J. Phys. Chem. C*, 2019, **123**, 10604-10613.
6. Y. Pang, M. Zhang, D. Chen, W. Chen, F. Wang, S. J. Anwar, M. Saunders, M. R. Rowles, L. Liu and S. Liu, *J.Phys. Chem. Lett.*, 2019, **10**, 3465-3471.
7. A. Wang, X. Hu, F. Wang, W. Chen, Y. Pang, S. Javaid, D. Chen, X. Li, L. Staaden and G. Jia, *Mater. Lett.*, 2019, **237**, 88-91.
8. J. Zhang, F. J. Rogers, N. Darwish, V. R. Gonçales, Y. B. Vogel, F. Wang, J. J. Gooding, M. C. R. Peiris, G. Jia and J.-P. Veder, *J. Am. Chem. Soc.*, 2019, **141**, 5863-5870.

Appendix C: Copyright Permissions

This PhD thesis contains no material which infringes the copyright of any other person(s). Any third-party copyright materials reproduced, where necessary, have been granted the permission from the copyright owners. Permission details are listed as follow:

Copyright permission for Scheme 1.1 and Figure 1.20 in Chapter 1

Copyright Clearance Center RightsLink®

Home | Account Info | Help

Title: Large-Scale Soft Colloidal Template Synthesis of 1.4 nm Thick CdSe Nanosheets

Author: Taeghwan Hyeon, Roald Hoffmann, Young Kuk, et al

Publication: Angewandte Chemie International Edition

Publisher: John Wiley and Sons

Date: Aug 26, 2009

Copyright © 2009 WILEY-VCH Verlag GmbH & Co. KGaA, Weinheim

Logged in as:
Fei Wang
Account #: 3001434560
LOGOUT

Order Completed

Thank you for your order.

This Agreement between Fei Wang ("You") and John Wiley and Sons ("John Wiley and Sons") consists of your license details and the terms and conditions provided by John Wiley and Sons and Copyright Clearance Center.

Your confirmation email will contain your order number for future reference.

printable details

License Number	4683430906982
License date	Oct 07, 2019
Licensed Content Publisher	John Wiley and Sons
Licensed Content Publication	Angewandte Chemie International Edition
Licensed Content Title	Large-Scale Soft Colloidal Template Synthesis of 1.4 nm Thick CdSe Nanosheets
Licensed Content Author	Taeghwan Hyeon, Roald Hoffmann, Young Kuk, et al
Licensed Content Date	Aug 26, 2009
Licensed Content Volume	48
Licensed Content Issue	37
Licensed Content Pages	4
Type of use	Dissertation/Thesis
Requestor type	University/Academic
Format	Print and electronic
Portion	Figure/table
Number of figures/tables	2
Original Wiley figure/table number(s)	Scheme 1, Figure 1
Will you be translating?	No
Title of your thesis / dissertation	Synthesis, Growth Mechanism and Optical Properties of Colloidal Wurtzite ZTe (Z=Zn, Cd) Nanoplatelets
Expected completion date	Dec 2019
Expected size (number of pages)	140
Requestor Location	Fei Wang Kent St, Bentley

	Perth, Western Australia 6102 Australia Attn:
Publisher Tax ID	EU826007151
Total	0.00 USD

Would you like to purchase the full text of this article? If so, please continue on to the content ordering system located here: Purchase PDF

If you click on the buttons below or close this window, you will not be able to return to the content ordering system.

[redacted]

Copyright permission for Figure 1.7 in Chapter 1

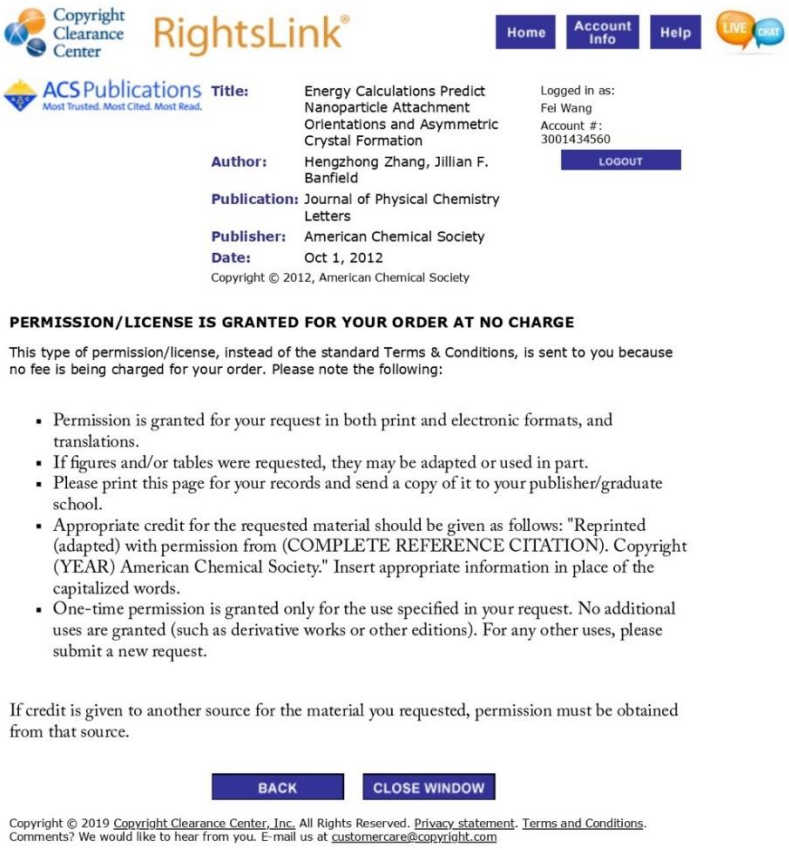

Copyright Clearance Center RightsLink®

Home | Account Info | Help | LIVE CHAT

ACS Publications
Most Trusted. Most Cited. Most Read.

Title: Energy Calculations Predict Nanoparticle Attachment Orientations and Asymmetric Crystal Formation

Author: Hengzhong Zhang, Jillian F. Banfield

Publication: Journal of Physical Chemistry Letters

Publisher: American Chemical Society

Date: Oct 1, 2012

Copyright © 2012, American Chemical Society

Logged in as:
Fei Wang
Account #:
3001434560

LOGOUT

PERMISSION/LICENSE IS GRANTED FOR YOUR ORDER AT NO CHARGE

This type of permission/license, instead of the standard Terms & Conditions, is sent to you because no fee is being charged for your order. Please note the following:

- Permission is granted for your request in both print and electronic formats, and translations.
- If figures and/or tables were requested, they may be adapted or used in part.
- Please print this page for your records and send a copy of it to your publisher/graduate school.
- Appropriate credit for the requested material should be given as follows: "Reprinted (adapted) with permission from (COMPLETE REFERENCE CITATION). Copyright (YEAR) American Chemical Society." Insert appropriate information in place of the capitalized words.
- One-time permission is granted only for the use specified in your request. No additional uses are granted (such as derivative works or other editions). For any other uses, please submit a new request.

If credit is given to another source for the material you requested, permission must be obtained from that source.

BACK | CLOSE WINDOW

Copyright © 2019 Copyright Clearance Center, Inc. All Rights Reserved. Privacy statement. Terms and Conditions.
Comments? We would like to hear from you. E-mail us at customercare@copyright.com

Copyright permission for Figure 1.8, Figure 1.24, and Figure 1.25 in Chapter 1

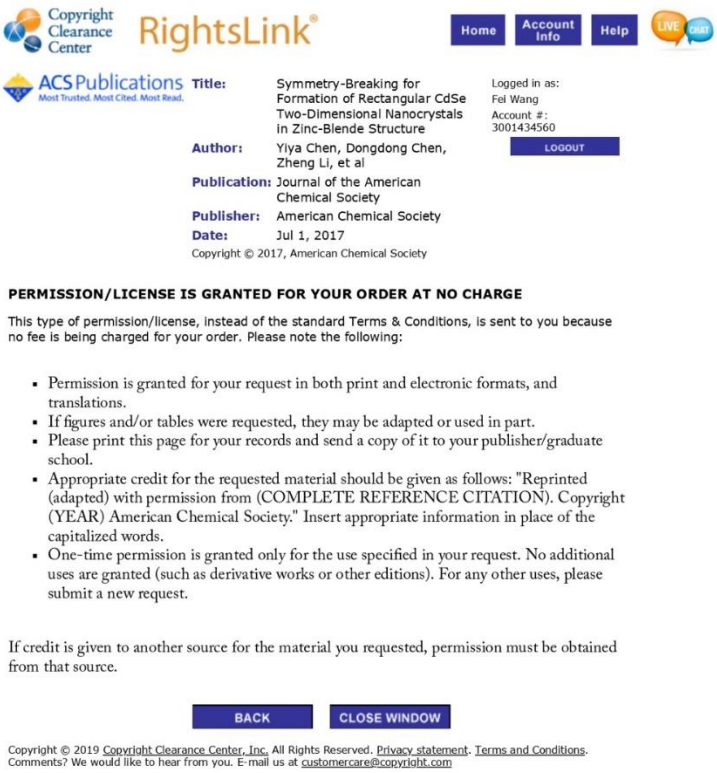

Copyright Clearance Center RightsLink®

Home | Account Info | Help | LIVE CHAT

ACS Publications
Most Trusted. Most Cited. Most Read.

Title:	Symmetry-Breaking for Formation of Rectangular CdSe Two-Dimensional Nanocrystals in Zinc-Blende Structure
Author:	Yiya Chen, Dongdong Chen, Zheng Li, et al
Publication:	Journal of the American Chemical Society
Publisher:	American Chemical Society
Date:	Jul 1, 2017

Logged in as:
Fei Wang
Account #:
3001434560
LOGOUT

Copyright © 2017, American Chemical Society

PERMISSION/LICENSE IS GRANTED FOR YOUR ORDER AT NO CHARGE

This type of permission/license, instead of the standard Terms & Conditions, is sent to you because no fee is being charged for your order. Please note the following:

- Permission is granted for your request in both print and electronic formats, and translations.
- If figures and/or tables were requested, they may be adapted or used in part.
- Please print this page for your records and send a copy of it to your publisher/graduate school.
- Appropriate credit for the requested material should be given as follows: "Reprinted (adapted) with permission from (COMPLETE REFERENCE CITATION). Copyright (YEAR) American Chemical Society." Insert appropriate information in place of the capitalized words.
- One-time permission is granted only for the use specified in your request. No additional uses are granted (such as derivative works or other editions). For any other uses, please submit a new request.

If credit is given to another source for the material you requested, permission must be obtained from that source.

BACK | CLOSE WINDOW

Copyright © 2019 Copyright Clearance Center, Inc. All Rights Reserved. Privacy statement. Terms and Conditions.
Comments? We would like to hear from you. E-mail us at customercare@copyright.com

Copyright permission for Scheme 1.2 in Chapter 1

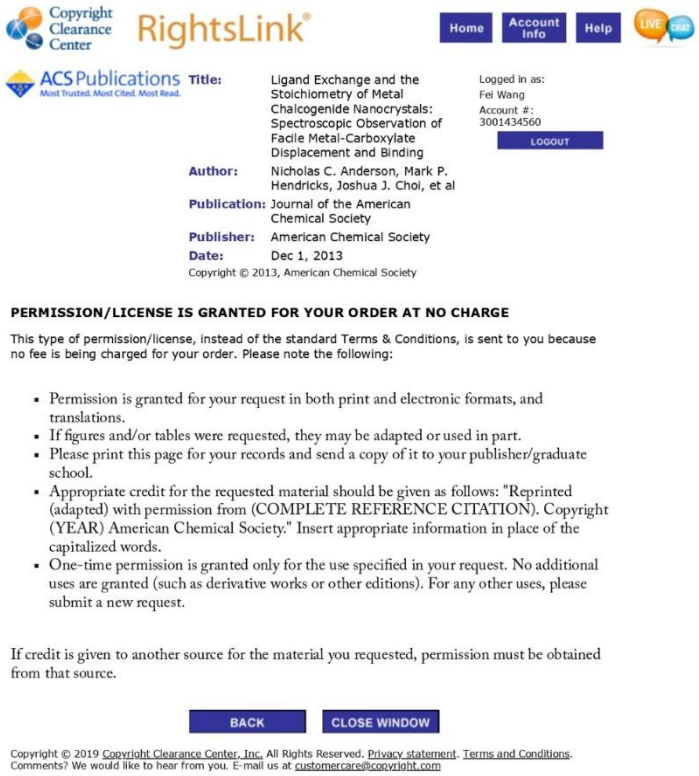

Copyright Clearance Center RightsLink®

Home | Account Info | Help | LIVE CHAT

ACS Publications
Most Trusted. Most Cited. Most Read.

Title:	Ligand Exchange and the Stoichiometry of Metal Chalcogenide Nanocrystals: Spectroscopic Observation of Facile Metal-Carboxylate Displacement and Binding
Author:	Nicholas C. Anderson, Mark P. Hendricks, Joshua J. Choi, et al
Publication:	Journal of the American Chemical Society
Publisher:	American Chemical Society
Date:	Dec 1, 2013

Logged in as:
Fei Wang
Account #:
3001434560
LOGOUT

Copyright © 2013, American Chemical Society

PERMISSION/LICENSE IS GRANTED FOR YOUR ORDER AT NO CHARGE

This type of permission/license, instead of the standard Terms & Conditions, is sent to you because no fee is being charged for your order. Please note the following:

- Permission is granted for your request in both print and electronic formats, and translations.
- If figures and/or tables were requested, they may be adapted or used in part.
- Please print this page for your records and send a copy of it to your publisher/graduate school.
- Appropriate credit for the requested material should be given as follows: "Reprinted (adapted) with permission from (COMPLETE REFERENCE CITATION). Copyright (YEAR) American Chemical Society." Insert appropriate information in place of the capitalized words.
- One-time permission is granted only for the use specified in your request. No additional uses are granted (such as derivative works or other editions). For any other uses, please submit a new request.

If credit is given to another source for the material you requested, permission must be obtained from that source.

BACK | CLOSE WINDOW

Copyright permission for Figure 1.15 in Chapter 1

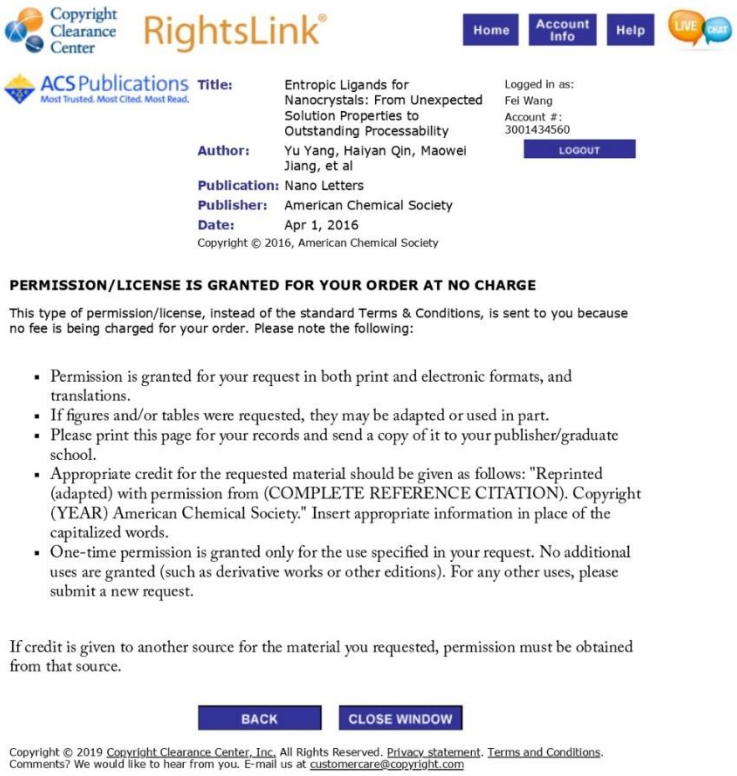

Copyright Clearance Center RightsLink®

Home | Account Info | Help | LIVE CHAT

ACS Publications
Most Trusted. Most Cited. Most Read.

Title:	Entropic Ligands for Nanocrystals: From Unexpected Solution Properties to Outstanding Processability	Logged in as: Fei Wang Account #: 3001434560 LOGOUT
Author:	Yu Yang, Haiyan Qin, Maowei Jiang, et al	
Publication:	Nano Letters	
Publisher:	American Chemical Society	
Date:	Apr 1, 2016	

Copyright © 2016, American Chemical Society

PERMISSION/LICENSE IS GRANTED FOR YOUR ORDER AT NO CHARGE

This type of permission/license, instead of the standard Terms & Conditions, is sent to you because no fee is being charged for your order. Please note the following:

- Permission is granted for your request in both print and electronic formats, and translations.
- If figures and/or tables were requested, they may be adapted or used in part.
- Please print this page for your records and send a copy of it to your publisher/graduate school.
- Appropriate credit for the requested material should be given as follows: "Reprinted (adapted) with permission from (COMPLETE REFERENCE CITATION). Copyright (YEAR) American Chemical Society." Insert appropriate information in place of the capitalized words.
- One-time permission is granted only for the use specified in your request. No additional uses are granted (such as derivative works or other editions). For any other uses, please submit a new request.

If credit is given to another source for the material you requested, permission must be obtained from that source.

BACK | CLOSE WINDOW

Copyright permission for Figure 1.16 in Chapter 1

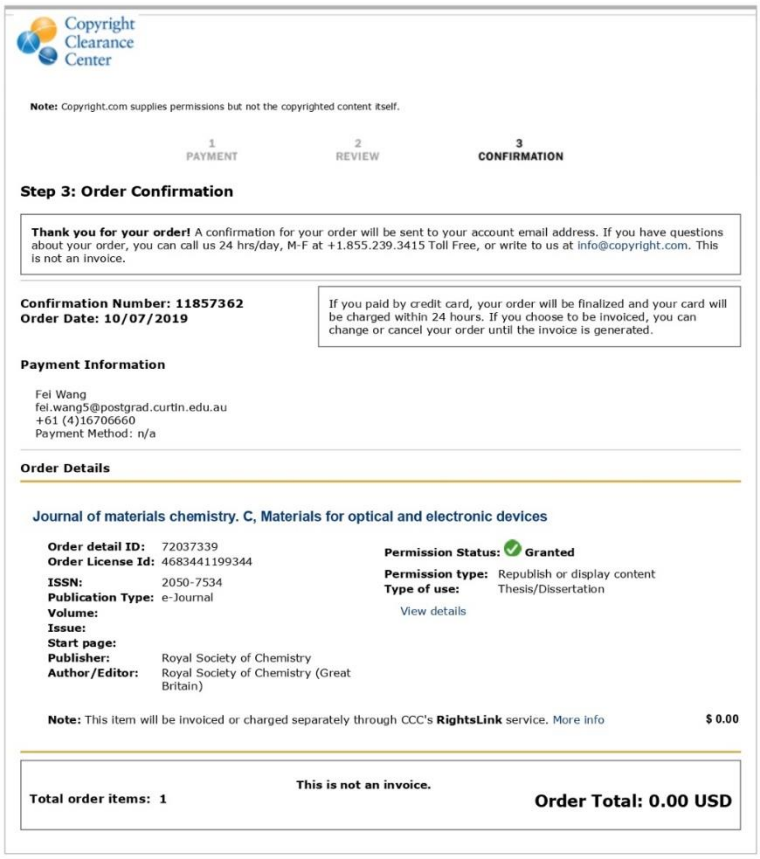

Copyright Clearance Center

Note: Copyright.com supplies permissions but not the copyrighted content itself.

1 PAYMENT 2 REVIEW **3 CONFIRMATION**

Step 3: Order Confirmation

Thank you for your order! A confirmation for your order will be sent to your account email address. If you have questions about your order, you can call us 24 hrs/day, M-F at +1.855.239.3415 Toll Free, or write to us at info@copyright.com. This is not an invoice.

Confirmation Number: 11857362
Order Date: 10/07/2019

If you paid by credit card, your order will be finalized and your card will be charged within 24 hours. If you choose to be invoiced, you can change or cancel your order until the invoice is generated.

Payment Information

Fei Wang
fei.wang5@postgrad.curtin.edu.au
+61 (4)16706660
Payment Method: n/a

Order Details

Journal of materials chemistry. C, Materials for optical and electronic devices

Order detail ID: 72037339
Order License Id: 4683441199344
ISSN: 2050-7534
Publication Type: e-Journal
Volume:
Issue:
Start page:
Publisher: Royal Society of Chemistry
Author/Editor: Royal Society of Chemistry (Great Britain)

Permission Status: Granted
Permission type: Republish or display content
Type of use: Thesis/Dissertation
View details

Note: This item will be invoiced or charged separately through CCC's **RightsLink** service. More info **$ 0.00**

This is not an invoice.

Total order items: 1 **Order Total: 0.00 USD**

Copyright permission for Figure 1.19 in Chapter 1

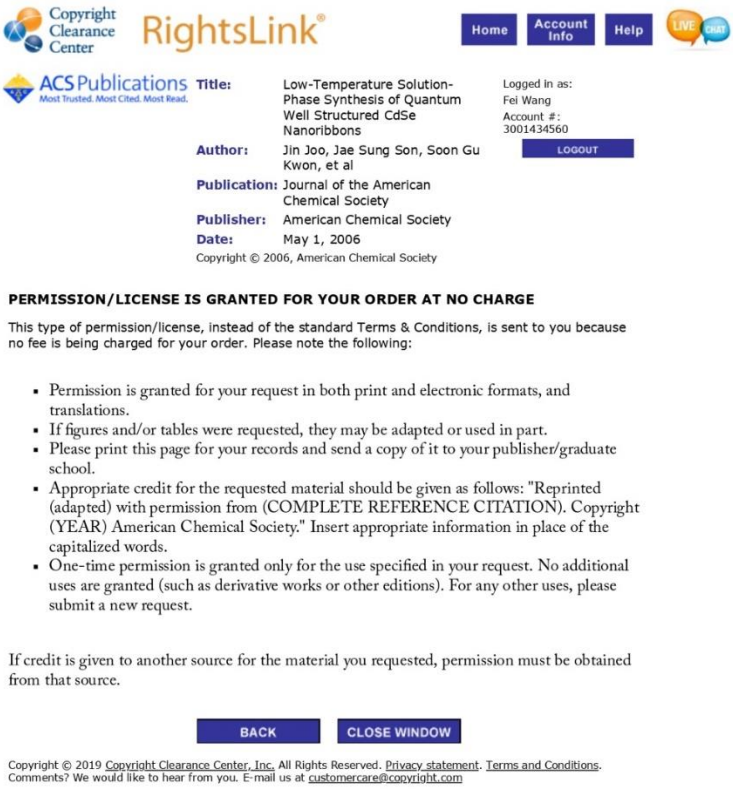

Copyright Clearance Center RightsLink®

Home | Account Info | Help | LIVE CHAT

ACS Publications
Most Trusted. Most Cited. Most Read.

Title:	Low-Temperature Solution-Phase Synthesis of Quantum Well Structured CdSe Nanoribbons	Logged in as: Fei Wang Account #: 3001434560 LOGOUT
Author:	Jin Joo, Jae Sung Son, Soon Gu Kwon, et al	
Publication:	Journal of the American Chemical Society	
Publisher:	American Chemical Society	
Date:	May 1, 2006	

Copyright © 2006, American Chemical Society

PERMISSION/LICENSE IS GRANTED FOR YOUR ORDER AT NO CHARGE

This type of permission/license, instead of the standard Terms & Conditions, is sent to you because no fee is being charged for your order. Please note the following:

- Permission is granted for your request in both print and electronic formats, and translations.
- If figures and/or tables were requested, they may be adapted or used in part.
- Please print this page for your records and send a copy of it to your publisher/graduate school.
- Appropriate credit for the requested material should be given as follows: "Reprinted (adapted) with permission from (COMPLETE REFERENCE CITATION). Copyright (YEAR) American Chemical Society." Insert appropriate information in place of the capitalized words.
- One-time permission is granted only for the use specified in your request. No additional uses are granted (such as derivative works or other editions). For any other uses, please submit a new request.

If credit is given to another source for the material you requested, permission must be obtained from that source.

BACK | CLOSE WINDOW

Copyright permission for Figure 1.21, Figure 1.22, and Figure 1.23 in Chapter 1

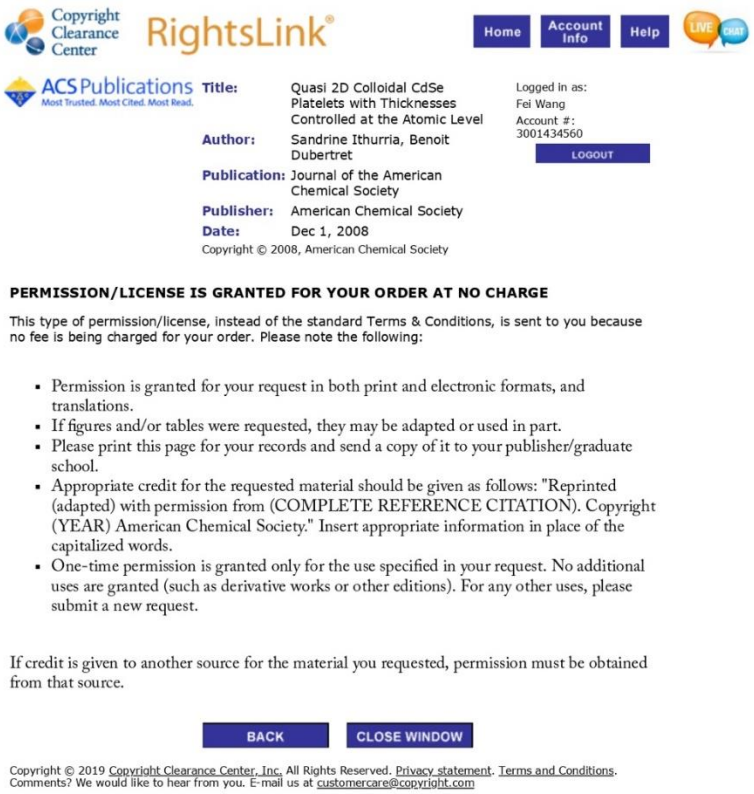

Copyright Clearance Center RightsLink®

Home | Account Info | Help | LIVE CHAT

ACS Publications
Most Trusted. Most Cited. Most Read.

Title:	Quasi 2D Colloidal CdSe Platelets with Thicknesses Controlled at the Atomic Level
Author:	Sandrine Ithurria, Benoit Dubertret
Publication:	Journal of the American Chemical Society
Publisher:	American Chemical Society
Date:	Dec 1, 2008

Copyright © 2008, American Chemical Society

Logged in as:
Fei Wang
Account #:
3001434560
LOGOUT

PERMISSION/LICENSE IS GRANTED FOR YOUR ORDER AT NO CHARGE

This type of permission/license, instead of the standard Terms & Conditions, is sent to you because no fee is being charged for your order. Please note the following:

- Permission is granted for your request in both print and electronic formats, and translations.
- If figures and/or tables were requested, they may be adapted or used in part.
- Please print this page for your records and send a copy of it to your publisher/graduate school.
- Appropriate credit for the requested material should be given as follows: "Reprinted (adapted) with permission from (COMPLETE REFERENCE CITATION). Copyright (YEAR) American Chemical Society." Insert appropriate information in place of the capitalized words.
- One-time permission is granted only for the use specified in your request. No additional uses are granted (such as derivative works or other editions). For any other uses, please submit a new request.

If credit is given to another source for the material you requested, permission must be obtained from that source.

BACK | CLOSE WINDOW

Copyright permission for Figure 1.26 in Chapter 1

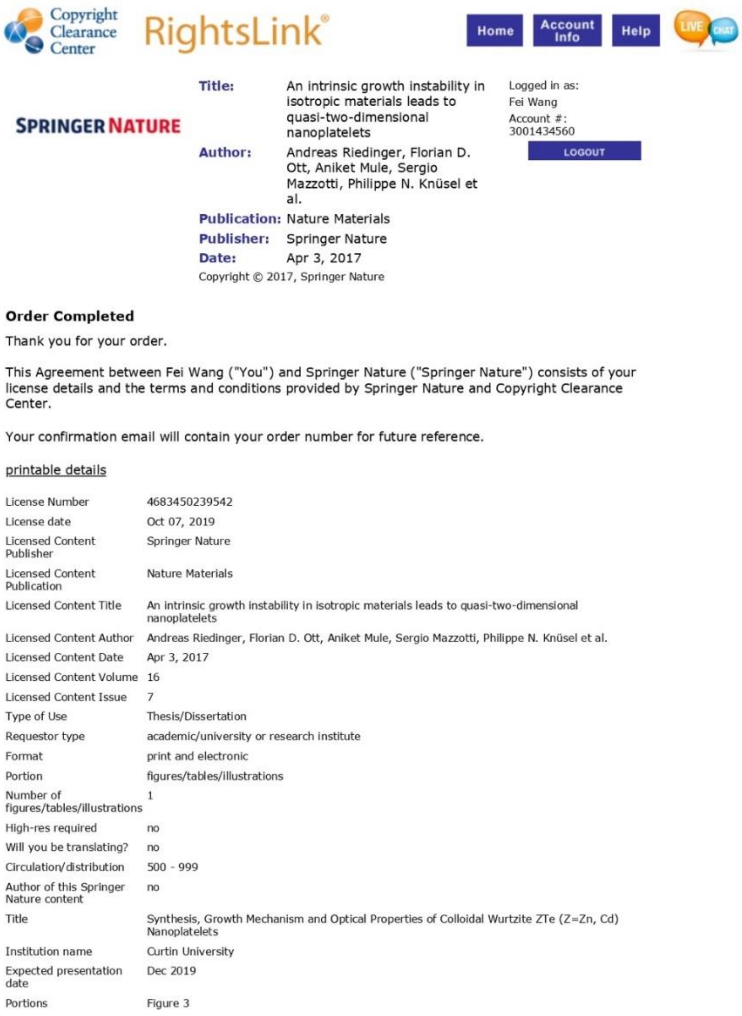

Copyright Clearance Center RightsLink®

Home | Account Info | Help | LIVE CHAT

SPRINGER NATURE

Title: An intrinsic growth instability in isotropic materials leads to quasi-two-dimensional nanoplatelets

Author: Andreas Riedinger, Florian D. Ott, Aniket Mule, Sergio Mazzotti, Philippe N. Knüsel et al.

Publication: Nature Materials

Publisher: Springer Nature

Date: Apr 3, 2017

Copyright © 2017, Springer Nature

Logged in as:
Fei Wang
Account #:
3001434560

LOGOUT

Order Completed

Thank you for your order.

This Agreement between Fei Wang ("You") and Springer Nature ("Springer Nature") consists of your license details and the terms and conditions provided by Springer Nature and Copyright Clearance Center.

Your confirmation email will contain your order number for future reference.

printable details

License Number	4683450239542
License date	Oct 07, 2019
Licensed Content Publisher	Springer Nature
Licensed Content Publication	Nature Materials
Licensed Content Title	An intrinsic growth instability in isotropic materials leads to quasi-two-dimensional nanoplatelets
Licensed Content Author	Andreas Riedinger, Florian D. Ott, Aniket Mule, Sergio Mazzotti, Philippe N. Knüsel et al.
Licensed Content Date	Apr 3, 2017
Licensed Content Volume	16
Licensed Content Issue	7
Type of Use	Thesis/Dissertation
Requestor type	academic/university or research institute
Format	print and electronic
Portion	figures/tables/illustrations
Number of figures/tables/illustrations	1
High-res required	no
Will you be translating?	no
Circulation/distribution	500 - 999
Author of this Springer Nature content	no
Title	Synthesis, Growth Mechanism and Optical Properties of Colloidal Wurtzite ZTe (Z=Zn, Cd) Nanoplatelets
Institution name	Curtin University
Expected presentation date	Dec 2019
Portions	Figure 3

Requestor Location	Fei Wang Kent St, Bentley Perth, Western Australia 6102 Australia Attn:
Total	0.00 USD

[redacted] [redacted]

Copyright permission for Figure 4.1, Figure 4.2 and Scheme 4.1 in Chapter 4

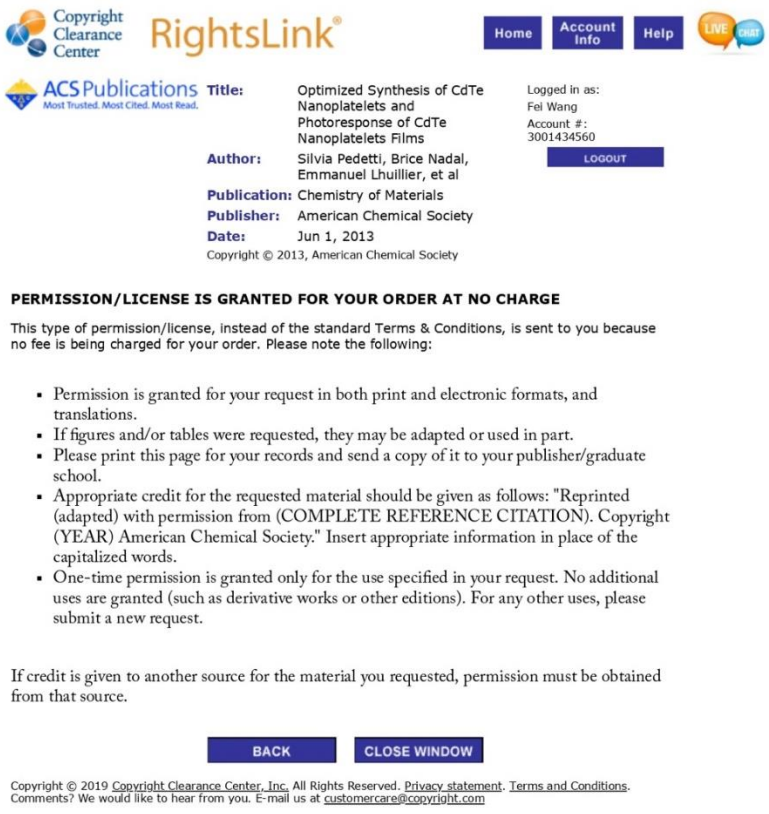

Copyright Clearance Center RightsLink®

Home | Account Info | Help | LIVE CHAT

ACS Publications Most Trusted. Most Cited. Most Read.

Title:	Optimized Synthesis of CdTe Nanoplatelets and Photoresponse of CdTe Nanoplatelets Films
Author:	Silvia Pedetti, Brice Nadal, Emmanuel Lhuillier, et al
Publication:	Chemistry of Materials
Publisher:	American Chemical Society
Date:	Jun 1, 2013

Copyright © 2013, American Chemical Society

Logged in as:
Fei Wang
Account #:
3001434560
LOGOUT

PERMISSION/LICENSE IS GRANTED FOR YOUR ORDER AT NO CHARGE

This type of permission/license, instead of the standard Terms & Conditions, is sent to you because no fee is being charged for your order. Please note the following:

- Permission is granted for your request in both print and electronic formats, and translations.
- If figures and/or tables were requested, they may be adapted or used in part.
- Please print this page for your records and send a copy of it to your publisher/graduate school.
- Appropriate credit for the requested material should be given as follows: "Reprinted (adapted) with permission from (COMPLETE REFERENCE CITATION). Copyright (YEAR) American Chemical Society." Insert appropriate information in place of the capitalized words.
- One-time permission is granted only for the use specified in your request. No additional uses are granted (such as derivative works or other editions). For any other uses, please submit a new request.

If credit is given to another source for the material you requested, permission must be obtained from that source.

BACK | CLOSE WINDOW

Copyright © 2019 Copyright Clearance Center, Inc. All Rights Reserved. Privacy statement. Terms and Conditions.
Comments? We would like to hear from you. E-mail us at customercare@copyright.com

Copyright permission for Scheme 4.2 in Chapter 4

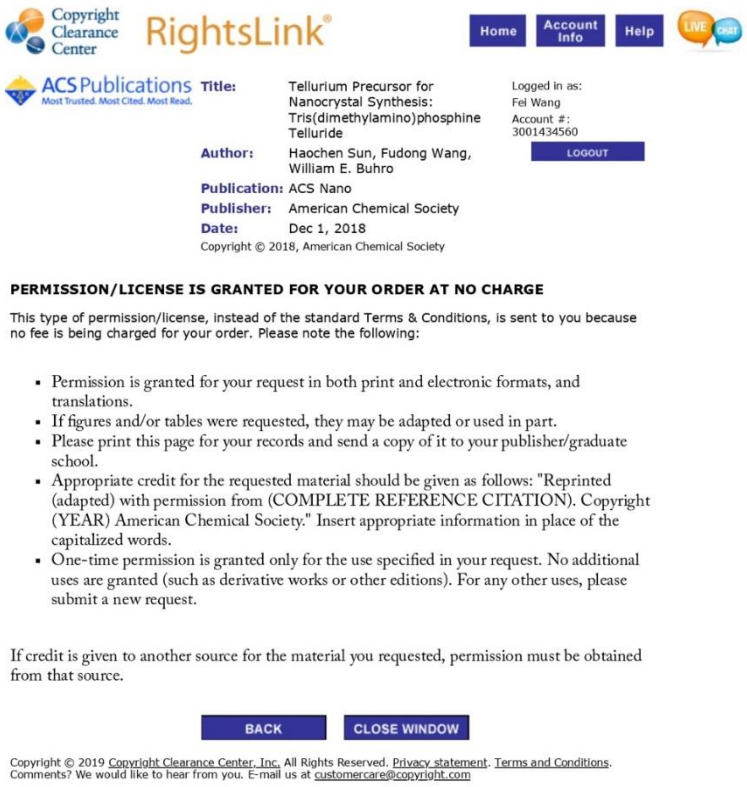

Copyright Clearance Center RightsLink®

Home | Account Info | Help | LIVE CHAT

ACS Publications
Most Trusted. Most Cited. Most Read.

Title:	Tellurium Precursor for Nanocrystal Synthesis: Tris(dimethylamino)phosphine Telluride
Author:	Haochen Sun, Fudong Wang, William E. Buhro
Publication:	ACS Nano
Publisher:	American Chemical Society
Date:	Dec 1, 2018

Logged in as:
Fei Wang
Account #:
3001434560
LOGOUT

Copyright © 2018, American Chemical Society

PERMISSION/LICENSE IS GRANTED FOR YOUR ORDER AT NO CHARGE

This type of permission/license, instead of the standard Terms & Conditions, is sent to you because no fee is being charged for your order. Please note the following:

- Permission is granted for your request in both print and electronic formats, and translations.
- If figures and/or tables were requested, they may be adapted or used in part.
- Please print this page for your records and send a copy of it to your publisher/graduate school.
- Appropriate credit for the requested material should be given as follows: "Reprinted (adapted) with permission from (COMPLETE REFERENCE CITATION). Copyright (YEAR) American Chemical Society." Insert appropriate information in place of the capitalized words.
- One-time permission is granted only for the use specified in your request. No additional uses are granted (such as derivative works or other editions). For any other uses, please submit a new request.

If credit is given to another source for the material you requested, permission must be obtained from that source.

BACK | CLOSE WINDOW

Copyright © 2019 Copyright Clearance Center, Inc. All Rights Reserved. Privacy statement. Terms and Conditions.
Comments? We would like to hear from you. E-mail us at customercare@copyright.com